KEK Proceedings 96-5
JHP-29
August 1996
H/M

KEK-PROC--96-5
JP9612242

Nuclear Physics and Fundamental Physics with Neutrons II

KEK, Tsukuba, March, 15 - 16, 1996

Edited by Y. Masuda

NATIONAL LABORATORY FOR
HIGH ENERGY PHYSICS

National Laboratory for High Energy Physics, 1996

KEK Reports are available from:

Technical Information & Library
National Laboratory for High Energy Physics
1-1 Oho, Tsukuba-shi
Ibaraki-ken, 305
JAPAN

Phone: 0298-64-5136
Telex: 3652-534 (Domestic)
(0)3652-534 (International)
Fax: 0298-64-4604
Cable: KEK OHO
E-mail: Library@kekvax.kek.jp (Internet Address)
Internet: http://www.kek.jp

Remark

Tokushi Shibata

Institute for Nuclear Study, University of Tokyo
3-2-1 Midori, Tanashi, Tokyo 188, Japan

I will not make a concluding remark of this workshop, because I am working in the different field these days and thus I think that I am not a proper person to make a concluding remark of this intensively discussed workshop. I would rather like make an important remark to promote the study of the fundamental physics using the neutron facility of JHP(N-arena).

We are thinking that the construction of JHP including accelerators and experimental facilities will probably starts in 1998. Therefore the detailed design are now under progress. This is true for the N-arena. The huge number of scientists working on various fields other than the fundamental physics such as the condensed matter, the life science, etc. are waiting for the experimental facilities in the N-arena. They request the various kinds of apparatuses and beam courses. Since the space and the budget for the N-arena are not enough to accommodate all the requirements, the serious discussion will be held to make decisions on what kind of facilities should be installed, what kind of requirement for the neutron beam should be fulfilled, etc.

The fundamental physics using low-energy neutrons can achieve very important and unique progress in physics, I think, therefore I strongly suggests that the all the users who are going to use the N-arena for studying the fundamental physics provide a list of requirements for the experimental apparatuses and the neutron beam. The number of scientists who are interested in study of the fundamental physics is much smaller than those who are interested in other fields. Therefore it is crucial that the all the scientists provide a clear requirements for the N-arena to carry out their experiments on the fundamental physics as soon as possible.

Finally on behalf of organizers of this workshop I wish to express of our cordial thanks to all the participants especially from abroad for attending this workshop and making it fruitful.

JHP-workshop on

"*Nuclear Physics and Fundamental Physics with Neutrons* II"

KEK-lecture hall, March 15_16, 1996

program agenda

March, 15

1. 9:45 am Opening (Y. Masuda)

H. Ikeda(KEK) 20 min.
"*JHP and neutron* "
Y. Yamazaki(KEK) 20 min.
"*JHP Accelarator*"

2. 10:30 am General (Y. Nagai)

V.K. Ignatovich(Dubna) 30 min.
"*Fundamental Neutron Physics Research in JINR (Dubna)*"

S.A. Werner(Missouri) 30 min.
"*Fundamental Physics with Neutron Interferometer* "

coffee (11:50 ~ 12:00)

3. 12:00 am Nuclear Astro-Physics (S. Kubono)

Y. Nagai(TIT) 30 min.
"*Nuclear Astrophysics Studied by the Neutron Capture Reaction*"
T. Shima(TIT) 20 min.
"*Plans for Studies of (alpha,n) Reactions*
Relevant to Astrophysics via Inverse Reactions"

Lunch 1:05 pm ~ Restrant " ***Zen*** "

4. 2:20 pm P, T symmetry violation and Neutrino Physics (I. Katayama)

K. Asahi(TIT) 20 min.
"*Spin-Polarized Nuclei as a Tool for Fundamental Physics*"
Y. Masuda(KEK) 30 min.
"*T-Violation in Neutron-Nucleus Interaction*"
M. Sakuda(KEK) 30 min.
"*Transition Radiation of the Neutrino Magnetic Moment*"

(4:30 pm ***tour to neutron experimental hall***)

5. 6:30 pm ***Welcome party*** at restrant " ***Zen*** "

March 16

6. 9:30 am **UCN** (T. Shibata)

S.J. Seestrom(Los Alamos) 30 min.
"*Progress Toward an Ulta-Cold Neutron Source at Los Alamos*"
H. Yoshiki(Ibaraki) 30 min.
"*Superthermal Ultracold Neutron Source*"
A.P. Serebrov(Gatchina) 30 min.
"*Cold and Ultra-Cold Neutrons in Fundamental Physics Research*"

coffee (11:30 ~ 11:40)

N. Akiyama(Tokyo) 30 min.
"*Confinement of Ultra-Cold Neutron in a Multiple Cusp Magnetic Field*"
E. Gravador(Ibaraki) 20 min
"*Construction of a Stable and Uniform Magnetic Field at 10 milli-Gauss for Neutron EDM Measurements*"
K. Sakai(TIT) 15 min.
"*Development of Polarized ^{3}He Filter for Polarized Neutron Experiment at KEK*"

Lunch 1:00 pm ~ Restrant " ***Zen*** "

7. 2:00 pm **Interferometry** (K. Morimoto)

A.I. Ioffe(Berlin) 30 min.
"*Fundamental Physics Research and Neutron Interferometry*"
R. Gaehler(Munich) 30 min.
"*VCN Interferometry*"

coffee (3:20 ~ 3:30)

T. Ebisawa(KURRI) 30 min.
"*Cold Neutron Interferometry Using Multilayer Mirrors*"
Y. Hasegawa(Wien) 30 min.
"*Perfect Crystal Interferometer and its Applications*"

concluding (T. Shibata)

CONTENTS

Interferometry

typeset using JPSJ.sty <ver.0.7e>

Fundamental Neutron Research in JINR (Dubna).

Vladimir K. IGNATOVICH*

Laboratory of neutron physics, JINR, 141980 Dubna Moscow reg., Russia.

(Received April 2, 1996)

A short review of fundamental neutron research, conducted in the nuclear department of the Laboratory of Neutron Physics of Joint Institute for Nuclear Research is presented.

KEYWORDS: ultracold neutrons, thermal neutrons, resonance neutrons, scattering, fission, review

§1. Introduction

For those who do not remember the initialism JINR, I remind that JINR is the Joint Institute for Nuclear Research. It is located 70 miles north of Moscow in a small town called Dubna on the bank of the Volga River. The Institute consists of many laboratories, which conduct research in many fields of science: from biology to high energy elementary particles. I shall tell only about one of them: The Frank Laboratory of Neutron Physics, where we have two pulsed reactors. Our main research tool is the neutron, but even here the research field is very broad. We use neutrons for solid state experiments, for radiation investigations, for technological purposes, but I shall limit myself only to the Nuclear Physics Departement. The head of the Department is Valeriy Nikolaevich Shvetsov (shv@nfsun1.jinr.dubna.su) who is an experimentalist dealing with ultracold neutrons (UCN). The deputy director of the Laboratory responsible for our departement, is Walter Il'ich Furman (furman@nfsun1.jinr.dubna.su), who is a theorist in the field of nuclear physics.

Concise information about our laboratory can be found in the world wide web (WWW) at:

http://nfdfn.jinr.dubna.su,

but there is insufficient detailed information about groups, their work and their goals. I myself started this www project about our laboratory, and my idea was to give some general information and then to arrange the pointers to working groups. The information about the groups should be provided by the groups themselves. But these people are very conservative, they were reluctant to think about anything else except their work so most cells of information about the groups remained the same as I provided originaly, and has not been updated. I suppose this situation will change with time, as people understand that the information about their work is the main factor for obtaining grants and some financial or moral support (it seems that the application for this support should be facilitated, because the information about the work, its proceedure and goals in that case will be alwas at hand for everybody) but at present we have not reached the ideal and all the information is provided in a centralized manner, published in an annual report and this report is then copied in the WWW.

Now I would like to give you information about the fundamental neutron research in our laboratory in such a way as it is seen and understood by me. Here is the list of the main topics I shall talk about:

1. IBR-30 booster.
2. The problem of (n,e)-interaction and the neutron polarizability.
3. (2γ)-cascades and the nonstatistical effects in nuclei.
4. Multiplicity of γ-quanta after neutron capture and determination of parameters of neutron resonances.
5. Subthreshold resonance neutron fission and the search of $(n,\gamma f)$ processes in ^{237}Np.
6. Delayed neutrons in neutron fission of ^{235}U and ^{234}U.
7. The mass and angular distribution of fission

* Present address: Research Reactor Institute Kyoto University Kumatori-cho, Senan-gan, Osaka 590-04, Japan.

products in (n,f) reaction at resonances.
8. (n,α) reaction with nuclei at the energy of 4-6 Mev.
9. Time reversal asymmetry investigations.
10. Ultracold neutrons (UCN).

The topic where I have made some contribution is at the bottom of the list, because I am afraid if I start with it, I shall waste all my time and shall not be able to talk about anything else.

§2. IBR-30 booster

The IBR-30 booster is an updated version of the first IBR pulsed reactor which became operational more than 35 years ago. This booster consists of the deep subcritical reactor and a linear electron accelerator (fig. 1). The reactor itself contains two boxes with fuel element (20 kg of Pu) and a rotating wheel between them with two 5 kg ^{235}U shells at the opposite ends of a diameter. Reactor is subcritical even if the uranium enters the space between boxes. To create the neutron burst the linear electron accelerator is attached to the reactor. It gives a pulse of electrons with energy 40 Mev and current 0.6 A preciselyat the time when the uranium is between the boxes. The electrons enter a tungsten target placed between fuel elements in one of the boxes, and because of photo-neutron reactions, create neutrons which are multiplied in the reactor with multiplication factor variable from 16 to 200. As a result we have a neutron pulse with peak power 25 MW and with the pulse width of 4 μs. The wheel inbetween boxes makes 50 rotations per second, so we have 100 pulses per second and the average power of the reactor is 10 kW.

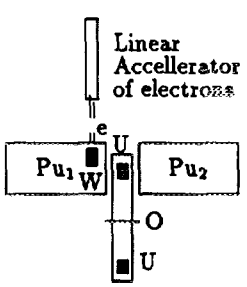

Fig. 1. Layout of the booster IBR-30

At present we are working on modernization of the booster (project IREN). The scheme of the booster will be nearly the same, but there will be no rotating wheel. The average power will be nearly the same, but the energy of electrons will be increased up to 200 Mev, its current up to 5 A, so the peak power will be one order of magnitude higher, but the multiplication factor will be decreased down to nearly 10 and as a result the pulse width will be only 0.4 μs.

There are 7 channels around our booster. The following experiments are conducted there in.

§3. The problem of (n,e) interaction and the neutron polarizability

{Yu.A.Alexandrov, A.B.Popov, G.S.Samosvat,
V.G.Nikolenko, L.Mitsyna
(mitsyna@nfsun1.jinr.dubna.su) T.Tret'yakova.}

Let us first formulate the problem of (n,e)-scattering. The amplitude a_{ne} of the neutron-electron scattering gives a contribution $Za_{ne}f(q)$ to the total scattering amplitude of neutrons on atoms, where Z is the charge of the atomic nucleus, (number of electrons) and $f(q)$ is a form-factor of the electron distribution in the atom (q is the momentum transfered). The amplitude a_{ne} was measured by many different experimentalists, and there is some discrepancy between their results. One group of physicists obtained the value:

$$a_{ne} = (-1.32 \pm 0.03)10^{-3}\text{fm}, \qquad (3.1)$$

and the other got a somewhat different result:

$$a_{ne} = (-1.59 \pm 0.04)10^{-3}\text{fm}. \qquad (3.2)$$

The discrepancy is considerably higher than the uncertainty of their magnitudes. So the first problem is to determine the source of such a discrepancy. Of course, this problem could be outside the interests of the broad scientific community, if it were not related to some contradiction of a significant scientific importance. And this is the second problem.

The (n,e)-scattering amplitude is related to the mean square charge radius of the neutron $< r^2 >$ by the equation:

$$< r^2 >= (3\hbar/mc\alpha)(a_{ne} - a_F),$$

where m is the neutron mass, α is the fine structure constant: $\alpha = e^2/\hbar c$, and a_F is the so called Foldy amplitude, which is a constant equal to $\mu_n \hbar\alpha/2mc = -1.46810^{-3}$ fm, where μ_n is the neutron anomalous magnetic moment in nuclear magnetons: $\mu_n = -1.91$. And it is this very constant that considerably spoils the life, because two results for a_{ne} give different signs for the mean square charge radius of the neutron. The present day picture of the neutron requires the negative sign for

$< r^2 >$.

Indeed, the magnitude $< r^2 >$ is defined as

$$< r^2 >= \int r^2 \rho(r) d^3 r,$$

where $\rho(r)$ is charge distribution inside the neutron. We are used to the image of the neutron as a compact proton (positive charge), surrounded by a diffuse cloud of negatively charged pions as shown in fig. 2.

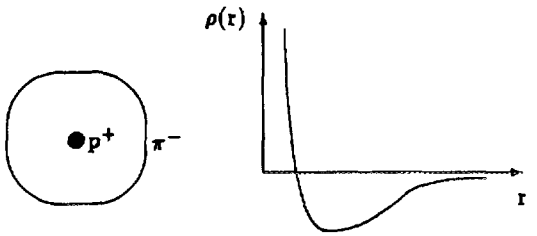

Fig. 2 The picture of the neutron and the charge distribution inside of it

Thus, the charge distribution must be of the form, shown in the right hand part of fig. 2, and it is evident that the integral of this charge distribution, multiplied by $< r^2 >$ must be negative. The result (3.2) supports this image, and the other one contradicts it. No model of elementary particles at present can give the positive sign of $< r^2 >$, but it is not a reason for rejection of the highly reliable result (3.1).

Let us look at the origin of this problem. We know that the neutron (its wave function ψ) is described by the Schrödinger (and even better, by the Dirac) equation. This equation generalized by Pauli can be represented in the form:

$$[\gamma^\mu (p_\mu - \frac{e}{c} A_\mu) + m + \mu_n \gamma^\mu \gamma^\nu F_{\mu\nu}]\psi = 0. \quad (3.3)$$

where A_μ is the electromagnetic potential, and $F_{\mu\nu}$ is the electromagnetic field. This equation is put down for a point particle with the charge e. The neutron has no charge, thus the term with A_μ can be omitted, but if we take into account, that the neutron has a structure with some distribution $\rho(r)$ of the charge inside it, we must keep this term, but expand $A_\mu(r)$ in power series around the n eutron's center:

$$A_\mu(r) = \sum (d^n A_\mu(r_0)/dr_i dr_j dr_k..) \times$$
$$\times (r_0 - r)_i (r_0 - r)_j .../n!$$

and integrate it with the factor $\rho(r)$.

In the lowest order it gives instead of $(e/c)A_\mu$ in the equation (3.3) another term: $(e/c)(\langle r^2 \rangle/6)\Box A_\mu = (e/c)(\langle r^2 \rangle/6) j_\mu$, where j_μ is the 4-current of the electromagnetic field source. In particular, if we neglect the motion of electrons in the atom the current j_μ is reduced to $j_0 = \rho_e$ — to the density distribution of electrons inside the atom, at which the neutron is scattered. Now the equation (3.3) can be represented in the form:

$$[\gamma^\mu p_\mu - \gamma^0 \frac{e}{6c} \langle r^2 \rangle \rho_e + m + \mu_n \gamma^\mu \gamma^\nu F_{\mu\nu}]\psi = 0. \quad (3.4)$$

You see here the neutron-electron interaction expressed in $\langle r^2 \rangle$ and the magnetic interaction via anomalous magnetic moment, but there is no Foldy interaction term. So, if you measure directly a_{ne}, you measure $\langle r^2 \rangle$, and because the $a_{ne} < 0$, it seems, no terrible contradiction exists between our image of the neutron and the experimental data. If so, we have only one problem of disagreement of two results, but it looks like a private problem of two groups, which is not very relevant to science itself.

It could be interpreted like this, if there were not one moment. It is well known that there exist some transformation S, devised by Foldy and Wouthuysen, which transforms 4-spinor ψ, into a two-spinor ϕ: $\exp(iS)\psi = \phi$.

This transformation is like a rigorous transition from a relativistic equation to a nonrelativistic one, and it seems to be very appropriate for such a massive and slow particle like thermal neutron. But after the transformation we get interaction with electrons (beside the usual magnetic term) of the type: $V = (< r^2 > + C a_F)$, which means, that the measured a_{ne} amplitude for the neutron must be compared with $a_F + (\alpha mc/\hbar)\langle r^2 \rangle$, and we return to the fundamental problem formulated above.

Now this problem could be formulated differently: What is the neutron we are dealing with? Is it a relativistic particle, satisfying the Dirac equation, or it is a nonrelativistic particle, satisfying the Schrodinger equation, which is not related to the relativistic one? At present we have no solution to this problem. It is like a deadlock of theoretical physics.

But let us see what our physicists have done, and what their plans are. First, it is necessary to tell, that number -1.59 was also obtained in our laboratory by the Alexandrov group (see, for example[1-3], and referencies therein). It was measured with the help of neutron diffraction on a single crystal of

isotope ^{186}W. During the last years the many endeavors were devoted to precise measurement of the dependence of the total cross section of ^{208}Pb on energy in the range of 0.1 eV - 30 keV. Such a measurement was undertaken with two goals: to obtain the a_{ne} and to measure the neutron polarizability α_n. The last one gives an interaction with electric field E equal to $V = \alpha_n E^2/2$, and this interaction leads to the scattering amplitude: Δa which is proportional to $-\alpha_n(1-C\sqrt{E})$. It means, that the dependence of the total scattering cross section on energy should be like one, shown qualitatively in fig. 3.

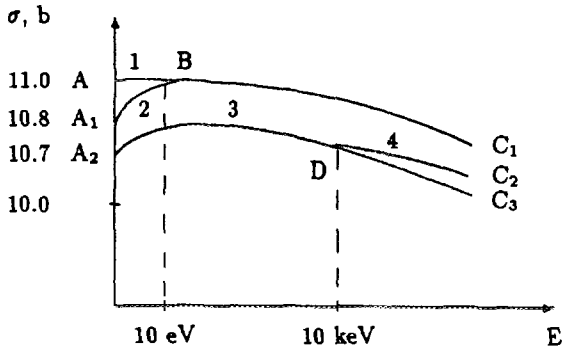

Fig. 3 The dependence of $\sigma_t(E)$ for scattering of neutrons on ^{208}Pb.

The curve 1 (ABC_1) shows the dependence of the cross section on energy, if there were no (n-e)-scattering and no polarizability. Curve 2 (A_1BC_1) shows the $\sigma(E)$ if we take into account only the contribution of (n-e)-scattering (this contribution becomes negligeable at the energy $E \approx$ 10eV). Curve 3 (A_2DC_3) shows the $\sigma(E)$ if we take into account also the contribution of polarizability, but discount the term, growing proportionally to $\sqrt{E}$. At last, curve 4 (A_2DC_2) shows the full contribution of (n-e)-scattering and of polarizability (the deviation from the curve 3 becomes seen at energies of order 30 keV).

The magnitudes, the experimentalists should hunt for, to be able to tell something about (n-e) scattering and polarizability, are represented by numbers $A_1A \sim$ 0.2 b, $A_2A_1 \sim$ 0.1 b and $C_3C_2 \sim$ 20 mb, which are very small in comparison with the total magnitude of cross section which is of the order of 10 b. Such measurements are very hard work.

At present the result of measurements in this way led to

$$a_{ne} = (-1.32 \pm 0.03)10^{-3} \quad \text{fm}$$

and for polarizability

$$\alpha_n = (0.0 \pm 0.5)10^{-3} \quad \text{fm}^3,$$

but strong negative resonance found recently makes the last one to be $\sim (0.7 \pm 1.7)10^{-3}$ fm^3.

We cite here only the results obtained with participation of our physicists. There are other figures. For instance, there is a result for polarizability obtained in Oak-Ridge: $\alpha_n = (1.71 \pm 0.24 \pm 0.43)10^{-3}$ fm^3, but detailed analysis performed in Dubna shows the systematic errors here to be $\sim 1 \cdot 10^{-3}$ fm^3.

The polarizability can be also measured differently by measuring angular distribution of the neutron scattering and its dependence on energy. The differential cross section of elastic scattering can be represented as

$$\sigma(\theta) = \sigma_0(1 + \omega(E)\cos(\theta))$$

where $\omega(E) = CE - D\sqrt{E}$ and D contains the contribution of α_n.

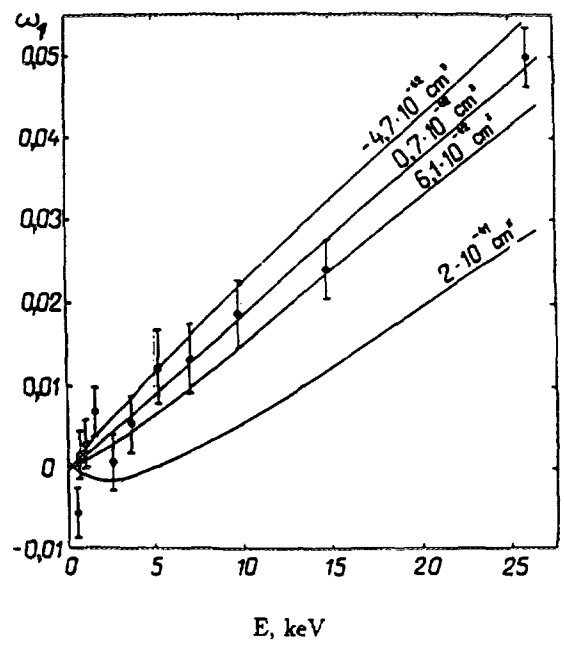

Fig. 4 The dependence of $\omega(E)$ for elastic scattering of neutrons on ^{208}Pb.

Fig. 4 show what the omega looks like for different α_n. Here also are shown the experimental

points. It is evident, that at present the experimental data does not give an opportunity to extract α_n. To reach higher sensitivity the spectrometer UGRA is being now installed in our laboratory. It contains a rotatable platform with 16 counters filled with 3He counters.

We are also planning to build some new installations to measure the angular asymmetry of the differential cross section and the energy dependence of this asymmetry and of the total scattering cross section on noble gazes like ^{136}Xe and ^{86}Kr. The expected behavior of the searched values is qualitatively represented in fig. 5, where R is the ratio

$$R = \frac{b_N^2 F_s(E,\theta_1) + 2b_N a_{ne} Z f(E,\theta_1)}{b_N^2 F_s(E,\theta_2) + 2b_N a_{ne} Z f(E,\theta_2)}$$

F_s is the formfactor due to velocity distribution of the gas atoms, f is the atomic formfactor and b_N is the nuclear scattering amplitude. Two angles $\theta_{1,2}$ are chosen in such a way as to get the largest effect. The depth of the dip on both curves is of the order 10^{-2}. It is not very spectacular and requires a lot of devotion of physicists to their work and devices.

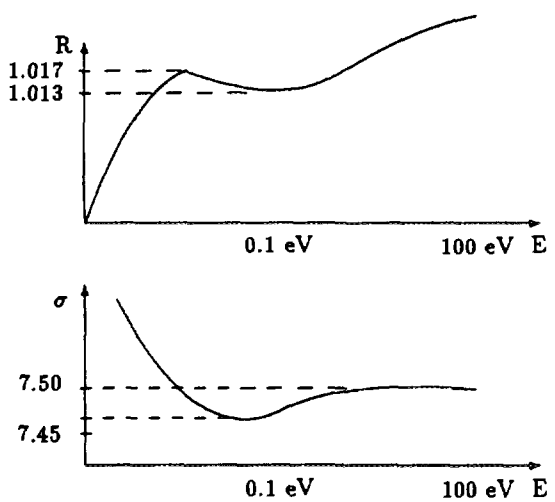

Fig. 5 The form of the dependence of $R(E)$ and $\sigma(E)$ for neutron scattering on ^{136}Xe or ^{86}Kr

§4. (2γ)-Cascades and the nonstatistical effects in nuclei

{A.M.Sukhovoy (suchovoj@nfsun1.jinr.dubna.su), V.A.Khitrov, Yu.V.Voinov, S.Boneva, E.Vasilieva}

The experiment on the study of 2-γ cascade could be explained as follows. Suppose that a nucleus with mass A captures a slow neutron (see fig. 6). After that it jumps to the compound state E_c with the excitation energy equal to B_n — the bound energy of the neutron in the resulted nucleus $A+1$. Then the nucleus emits two γ-quanta and rests in some final excited state E_f. It is evident, that the summed energy of two quanta $E_{2t} = \gamma_1 + \gamma_2$ should be equal to $B_n - E_f$ because we can neglect kinetic energy of the incident neutron.

The levels E_f are the discrete ones, thus E_{2t} also should have the discrete magnitudes. Let us look, as example for the case, when the final state corresponds to the first excited state of the nucleus. The E_{2t} has a given magnitude, represented by the segment AC on the right hand side of fig. 6. But it is a sum of two values γ_1 and γ_2. These two values are also not continuous and can have only discrete magnitudes, because after emission of the 1-st quanta the nucleus is at some intermediate state E_i (point B on the segment), which is a discrete one too. For every such E_i there is an intensity of radiation that fires one of the detectors. If we could discriminate between the first quantum and the second one, we could find a spectrum shown above the segment AC. Here the different points B_i mark the energy AB_i of the first quanta and the vertical axis denotes the intensity of transition to the intermediate level E_i.

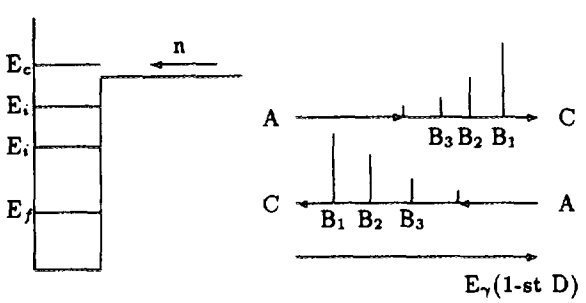

Fig. 6 Capture of a neutron, emission of two γ-quanta via intermediate level E_i, the final state of the nucleus E_f and the spectrum for different E_i, measured in the experiment.

In the experiment there are two detectors near the sample, that count γ-quanta, and we do not know which of them is the first. If the first quanta were measured only by 1-st detector then the spectrum would be looking as is shown at the segment AC where the length AB_1, for example, measures the energy, delivered in the 1-st detector, length B_1C measures the energy delivered in the second detector, and the height of the bar at the point B_1

shows the intensity of such a cascade.

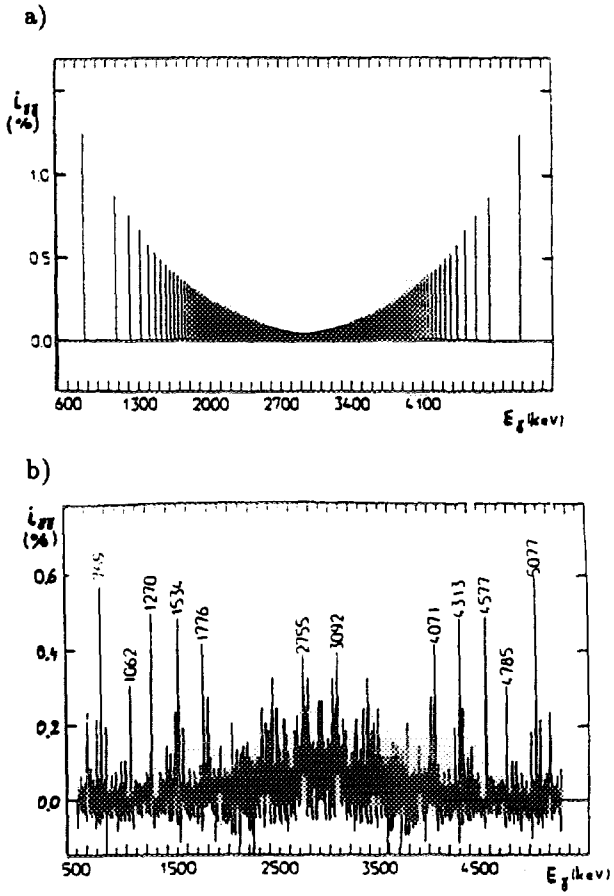

Fig. 7 The spectrum of the 2γ cascade with the given total energy E_{2t} a) calculated for ^{163}Dy (E_f = 422 keV) and b) the measured one for ^{162}Dy (E_{2t} = 5.848 MeV).

But the first quanta can be detected by the 2-nd detector. If the 2-nd detector always measured the first quanta, the spectrum would look like on the segment CA. Here CB_1, for example, is the energy delivered in the 1-st detector, and B_1A is the energy delivered in the 2-nd one. Since the first quanta is measured randomly by both detectors we are to add two spectra shown on the right hand side of fig. 6. As a result we obtain the symmetrical spectrum shown on fig. 7, where the horizontal axis denotes the energy delivered in the 1-st detector. In fig. 7 you see two spectra: one is calculated according to the statistical model (fig. 7a), and the other (fig. 7b) is the measured one. The very important part of the experiment, beside the sample and two Ge(Li) detectors, is a very sophisticated computer program, that analyzes the total energy delivered by two quanta in the two detectors and builds the spectrum. For some nuclei this spectrum happened to be very similar to the calculated one, but for others, as the one demonstrated in fig. 7b, there is a great discrepancy.

Having all these spectra you can find positions of the intermediate levels, their density and the intensity of transitions to them. And we can compare the experimental results with theoretical models. The most widely used is the statistical model of compound states.

The result of calculations along this model for the case of ^{163}Dy is shown in fig. 7a. The agreement with the experiment (results of which are not shown here) is good in this case. We see, that the intensity steadily decreases with the increasing of the transition energy toward the middle, but the density of levels increases.

Such an agreement is not always good. For instance, the spectrum, shown in fig. 7b for ^{162}Dy shows increasing of intensities toward the middle. It is a clear discrepancy with the statistical theory. There are many other discrepancies. For instance, in the range of excitation energies between 2 and 3 Mev for ^{198}Au the density of states with resolved transitions is a constant and is not exponentially growing, as is predicted by statistical models. These experiments give a wealth of information about distribution of levels, intensities of transitions, great enhancement of E2 transitions (more than the order of magnitude), the observation of equidistant excitations, the presence of some correlations between intensities of 2γ cascades and neutron widths and many more. So I am glad to present here some short account about these experiments to attract your attention to the productive work of these physicists (See[4])

§5. Multiplicity of γ-quanta after neutron capture and determination of parameters of neutron resonances

{G.Georgiev (georgiev@nfsun1.jinr.dubna.su) and N.Panajotova}

Now I want to introduce to you the work of our Bulgarian group. Their experiment is performed on a spectrometer called ROMASHKA, which can be translated as DAISY. Spectrometer is placed at the distance of 502 m from the IBR-30 booster and is designed to measure the number of gamma quanta emitted after neutron capture at neutron

resonances, and to determine the resonance parameters. The data was recorded into two-dimensional TOF vs multiplicity spectra. The detector consists of 16 NaJ(Tl) crystals placed like petals of a flower around the sample. The total volume of the scintillator is 36 liters.

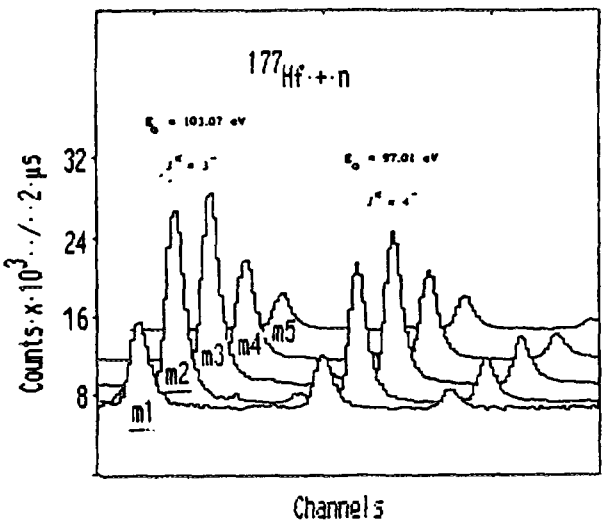

Fig. 8 The time-of-flight spectrum with coincidence of different number of the γ quanta after neutron capture.

Fig. 8 shows time of flight spectrum for different number of coincidences of detectors in the case of ^{177}Hf. We see here two sets of resonances with J=3 and J=4. It is reasonable to think, that resonances with larger J will emit larger number of gamma-quanta. So you can find a probability distribution of multiplicities for every resonance:

$$P(k, E_i) = S(k, E_i) / \sum_{k=1}^{6} S(k, E_i) \qquad (5.1)$$

where $S(k, E_i)$ is the integral under the peak with multiplicity k in the resonance E_i, and the upper limit in the sum is put equal to 6, because usually no coincidences with larger number of gamma quanta were observed. You can find the mean multiplicity by means of the distribution P:

$$\langle k(E_i) \rangle = \sum_{k=1}^{6} k P(k, E_i) \qquad (5.2)$$

This parameter helps you to identify spin of resonances, but it is more spectacular to use the magnitude

$$R(E_i) = [S(1, E_i) + S(2, E_i)] / [\sum_{k=3}^{6} S(k, E_i)], \quad (5.3)$$

which is also very sensitive to spin of resonance. It is larger for lower spin and lower for higher spin.

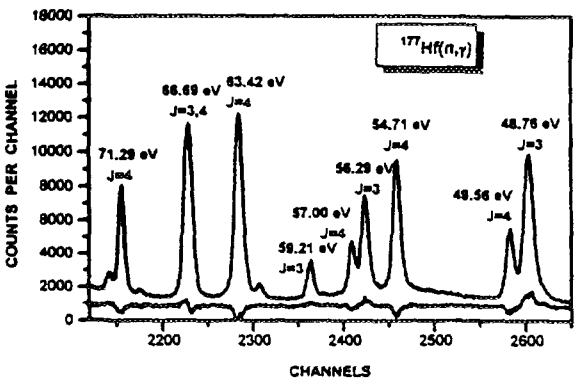

Fig. 9 The spectrum of coincidences with an arbitrary number of γ quanta for resonances with different spins. The lower curve is the graph (5.4).

Now you can average this magnitude over all the resonances and get some magnitude $\langle R \rangle$. With this magnitude you look at the combination

$$Q(E) = [N(1, E) + N(2, E)] - \langle R \rangle [\sum_{k=4}^{6} N(k, E)] \qquad (5.4)$$

in every channel of time of flight spectrum. Here $N(k,E)$ means the count in channel E with multiplicity of quanta equal to k. If this magnitude is positive, you have spin J=3, if negative, the spin of the resonance is 4.

Fig. 9 shows how it works for ^{177}Hf. But it is not the full story, this approach helps you to resolve some resonances that are not resolved in time of flight spectrum. Look, for instance at fig. 10. Here the resonance of ^{177}Hf is presented which can be found in BNL as a single resonance with J=3. But the present approach shows that this resonance is an unresolved double resonance. It is indicated by the behavior of the function $R(J, E)$ inside this resonance. This effect seems to be very spectacular. and it was well checked on resonances, that are unresolved here, but are resolved in BNL.

This group identified many new resonances in ^{148}Sm, ^{119}Sn and many others. I cannot give the tables of all the resonances here, but you can find

them in the publication[5)]

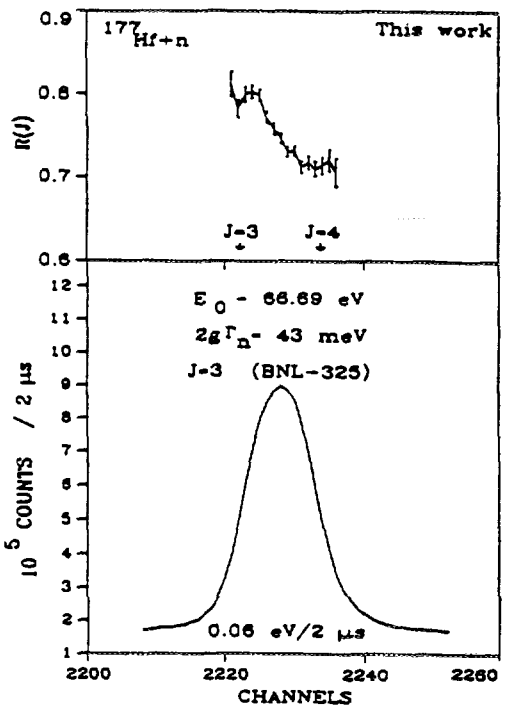

Fig. 10 The unresolved resonance. The behavior of the value 5.3 shows that it consists of two resonances with different spins.

§6. Subthreshold fission, (n,γ f) and delayed neutrons

{E.Dermendjiev, Yu.S.Zamyatnin, I.Ruskov (ruskov@nfsun1.jinr.dubna.su), S.B.Borzakov, V.Yu.Konovalov}

Subthreshold fission is especially interesting in the case of two hump barriers of nuclear potential. In this case the resonances for reaction (n,f) have a cluster structure shown in fig. 11. This structure is explained by the interference phenomena inside the barrier. The cluster can be considered as a broad resonance, related to a level in the second potential well, and the narrow peaks or troughs are related to the levels in the first well. The interference between these levels can enhance or suppress fission.

The goal of physicists was to look for reaction (n,γf), which means that before the fission a gamma quantum is emitted. In the experiment the fission chamber, surrounded by a liquid scintillation detector (LSD) was placed at a distance of 60 m from the reactor core. The LSD contained 6 sections and allowed them to count 2 and more quanta in coincidence. The experimentalists looked for coincidence of $i \geq 3$ gamma-quanta and fission.

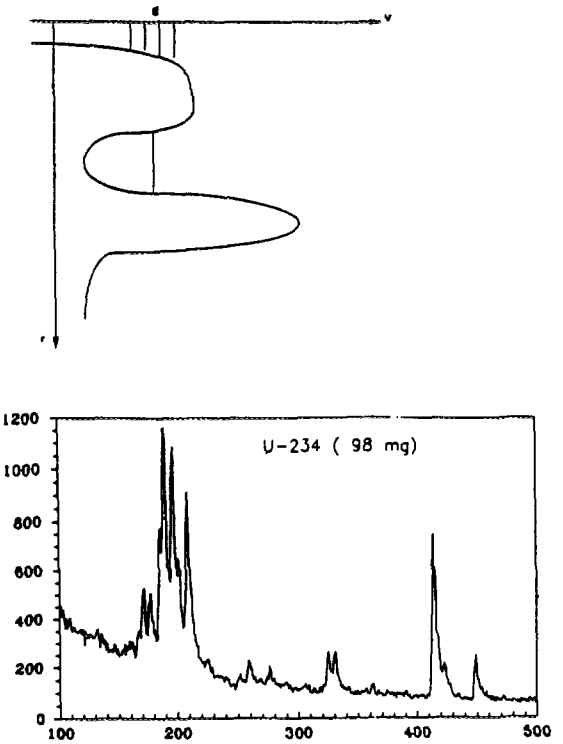

Fig. 11 The cluster structure of the fission resonances in ^{234}U.

It was expected that the ratio R:

$$R = (\sum_{i=3}^{6} N_{fi})/N_f,$$

where N_{if} means the number of coincidences with i-quanta registered simultaneously with fission, and N_f the total number of fissions with any number of gamma quanta, represents the probability of emission of prefission quanta. The probability of γ emission should be larger when the fission process is slow or the fission width Γ_f is small.

In the experiment 1.5 g of neptunium was used in a 6-section fission chamber. The results of measurements for ^{237}Np are shown in fig. 12. (The results are accepted for publication in Russian journal Nuclear Physics and will be published also in the English version of it.)

On the vertical axis the magnitude of R is shown related to R at the resonance 40 meV. Though the uncertainties are pretty large, some linear correlation between probability of emission prefission quantum and a reciprocal fission width $1/\Gamma_f$ can

be seen.

The left side of the set of the pictures is related to resonances near or below 10 eV. The right hand side is related to resonances in the region of the cluster centered at 40 eV. The three lines of pictures were obtained at three different thresholds for registration of γ quanta, which helps to estimate what the energy of prefission quantum was.

It follows from these measurements that

1. In weak resonanses below 10 eV the width $\Gamma_{\gamma,f} \approx \Gamma_f$, which means that almost every act of fission is accompanied by γ emission.
2. In weak resonances in the claster at 40 eV the $\Gamma_{\gamma,f} > 5\,\mu$eV, which means that there is some enhancement of prefission radiation. This can be interpreted as the emission of γ-quanta in the second potential well.
3. The energy of γ-quanta in weak resonances is larger than 0.6 MeV.

In parallel to these measurements with Np the experiments on delayed neutrons were conducted at another reactor: IBR-2. The goal was to look in the millisecond range of time at the delayed neutrons after fission of ^{233}U and ^{235}U by thermal neutrons. Usually the delayed neutrons were studied in the time range of several seconds after fission. Measurements in the milliseconds range has shown that delayed neutrons are also emitted with exponential decrease there.

§7. The mass and angular distribution of fission products in (n,f) reaction at resonances.

{W.I.Furman, N.Gundorin, Yu.Kopach
(kopach@nf.jinr.dubna.su), S.Telezhnikov,
A.B.Popov}

One of the interesting questions in nuclear physics is how the fission proceeds. Study of fission with resonance neutrons may help elucidate the picture. The fission can be described by a potential energy which is represented by a surface in the space of deformation parameters. This surface contains valleys along which the system proceeds toward fission and these valleys are called Broza channels. These broza channels characterize mass distribution of fission fragments.

It can be presented differently with the help of R-matrix theory, taking into account the angular momentum combinations of neutron and the nucleus spins and projection of angular momenta on deformation axis. In that case you are dealing with Bohr channels and can describe the angular distribution of fission fragments. The question is: how the Broza's channels interconnected with the Bohr's ones.

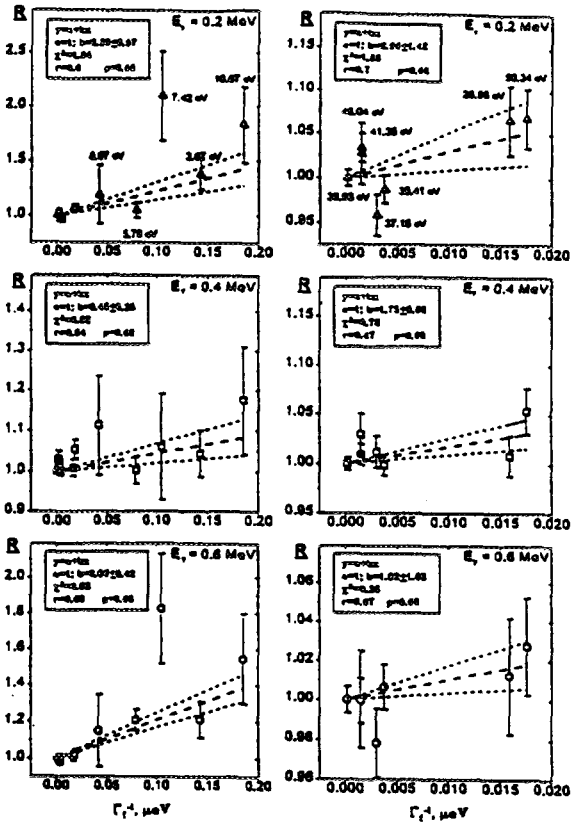

Fig. 12 The search of a linear correlation between the probability of γ-quantum emission and the reciprocal fission width.

In our laboratory both angular and mass distribution are studied. For mass distribution a method of identification of fission fragments by their γ-rays portrait is used. There are two fission chambers with ^{235}U (10 g) and ^{239}Pu (1.5 g). These fission chambers are used as a trigger for measuring the γ quanta with Ge(Li) detectors in coincidence with fission. Usually it is impossible to get mass distribution in Pu fission because of high background of α particles. Here the α particles do not represent a background, because fission fragments are identified by characteristic γ radiation. But at present the obtained result (variation of mass distribution from resonance to resonance) is not very good because of poor efficiency of detectors and time of

flight resolution. It will be improved soon. The efficiency will be increased by anti-Compton shielding with a big BGO detector, and the time-of-flight resolution will be improved after IREN starts to operate.

For studying of Bohr channels the angular distribution of fission fragments, represented in the form

$$d\sigma_{nf}(\Omega) = \sigma_0(E)[1 + A_2(E)P_2(\cos\theta)]$$

was measured, and the dependence of $A_2(E)$ on energy was determined. The experiment was performed with aligned U nuclei. The result is represented in fig. 13.

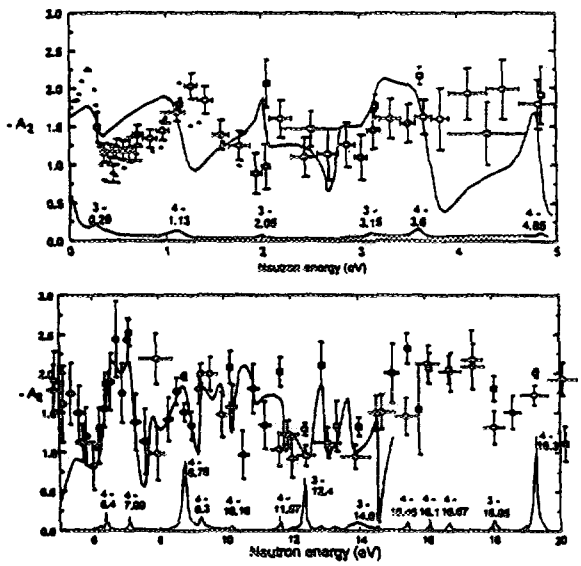

Fig.13 An energy dependence of fission fragment angular distribution coefficient A_2 from resonance neutron induced fission of ^{235}U aligned target. The last results obtained in our laboratory are represented by black triangles. Solid curve is the result of R-matrix multilevel two fission channel calculation. The curve in the lower part of the picture is the fission cross section in arbitrary units.

In the picture, besides the experimental points obtained at different times two solid curves are shown. The one drawn along the experimental points was calculated with the help of multilevel R-matrix theory with two fission channels but without accounting for interference between resonances with different spins. The agreement is not very fascinating, which points out to the necessity of accounting for the interference. A new approach to handle all that is now under development.

§8. (n,α) Reaction with nuclei at the energy of 4-6 Mev

{Yu.M.Gledenov (gledenof@nf.jinr.dubna.su), Yu.P.Popov}

This work was performed together with Chinese physicists[6]. The goal was to measure the total cross section and the angular distribution of α-particles in the reaction (n,α) in the energy range, where it has not yet been well investigated. The neutrons with energies 4-6 Mev were produced in the reaction d(d,n)^{3}He in the Van de Graaf ion source. The results were obtained and reported. It seems to me that the most interesting aspect in these experiments is the methodical part — the construction and performance of the ionization chamber with grids. Fig. 14 shows the scheme of the chamber and fig. 15 shows the amplitude signal generated by α-particle after (n,α) reaction on anode and cathode in forward angle (upper spectrum) and in backward angle (lower spectrum, which at the given geometry represents background). The anode signal characterizes the energy of the α-particle, and the cathode signal characterizes the angle of the particle flight with respect to the cathode normal. The cathode with the sample can be rotated, and after its rotation by 180^O the left part part of the chamber (see fig. 14) registers the particles going backward, and the right part of the chamber gives a signal that characterizes the background.

The group measured (n,α) reaction with ^{36}Ar, ^{40}Ca, ^{54}Fe, ^{58}Ni and ^{64}Zn. The results show that the angular distribution is symmetrical with respect to the angle 90°, which means, that the reaction (nα) at these energies goes through the formation of a compound state.

§9. Around time-parity violation.

{V.P.Alfimenkov, V.V.Novitskiy, L.B.Pikelner, Yu.D.Mareev, V.R.Skoy (skoy@nf.jinr.dubna.su)}

The search for time symmetry violation has become a very popular topic at present. Some time ago there was a discussion about what is better to measure: the triple fold correlation $\sigma[\boldsymbol{kI}]$, or the five-fold correlation $\sigma[\boldsymbol{kI}](\boldsymbol{kI})$. Some arguments were advanced in favor of 5-fold correlation. The most appropriate substance to seek it was Ho, and some experiments on depolarization of neutrons in

Ho were performed in our laboratory. Now it is understood, that because the 5-fold correlation does not violate space symmetry, we cannot hope to get the enhancement of effect similar to the one, observed in p-resonances of La. For that reason it is not further discussed. Nevertheless the experiments on depolarization in Ho have their own value.

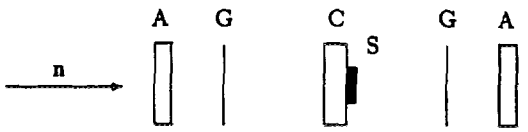

Fig. 14. Construction of ionization chamber. A is anode; G is grid; C is cathode, S is sample; n is the neutron beam.

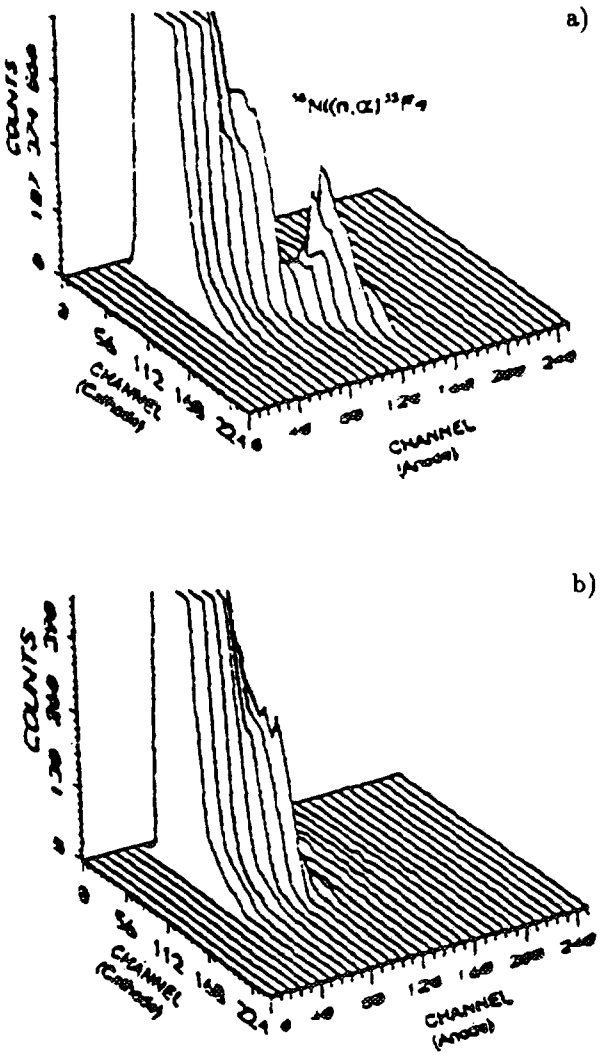

Fig. 15. Two-dimensional amplitude spectrum on cathode and anode a) in the right (fig. 14) and b) in the left (fig. 14) chambers. The horisontal axises show the height of the signal amplitude measured on cathode (the left axis) and anode (the right one).

The experiments were performed on a well known spectrometer POLYANA. Its arrangement is shown in fig. 16. A wealth of experimental data was obtained here. The depolarization was measured at different temperatures, when the sample was in a paramagnetic or ferromagnetic state, at different orientation of c-axis of the single crystal with respect to the neutron beam direction, and at different external fields. Part of the data is published[7]. Another one is being prepared for publication, but because they are related rather to the field of solid state physics than to nuclear physics, I shall not discuss them further.

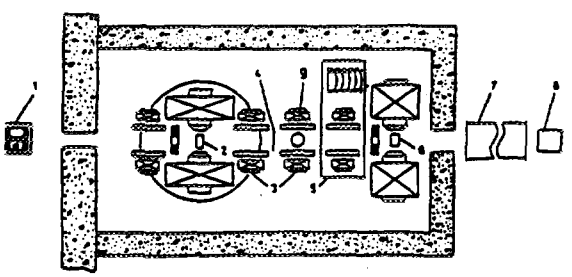

Fig.16 Experimental arrangement of the POLYANA spectrometer[7] — neutron polarizer, holmium single crystal, dysprosium analyzer, and neutron detector: 1 — IBR-30 source, 2 — dynamically polarized proton target, 3 — neutron polarization guide field magnets, 4 — current sheet, 5 — interchangeable magnets of the guide field, 6 — polarized Dysprosium target, 7 — neutron guides, 8 — n4 eutron detector, 9 — holmium crystal in cryostat.

The experiments to search time symmetry violation are now only in project. In fig. 17 the scheme of the proposed experiment is shown, Here we see the rotatable platform with the polarizer and sample. In the experiment the transmission of the sample will be measured for different spin orientation of polarized neutrons (please note that there is no analyzer of polarization). Then the platform will be turned to 180° and the polarization induced by sample transmission will be measured. The role of analyzer is played by the same device that was the polarizer in first round of the experiment. It

was shown[8] that in such a case no false effects due to disalignment of polarizer and analyzer appear. Some false effect appears here, but its magnitude will be determined by the precision of the rotation. Our country has developed the technology that permits a very precise control of the rotation angle.

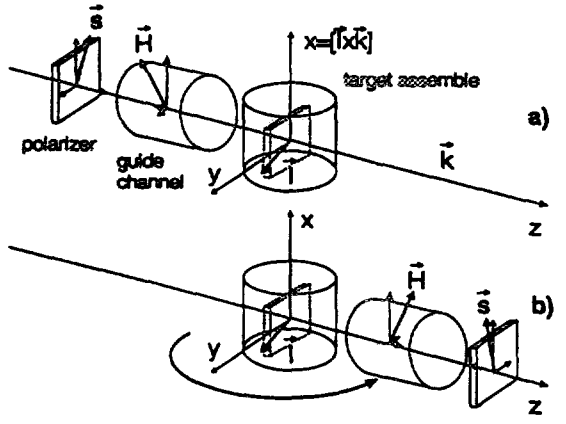

Fig. 17 Geometry of proposed time-reversal invariance experiment.

§10. UCN

{V.G.Nekhaev, V.N.Shvetsov (shv@nf.jinr.dubna.su), A.V.Strelkov.}

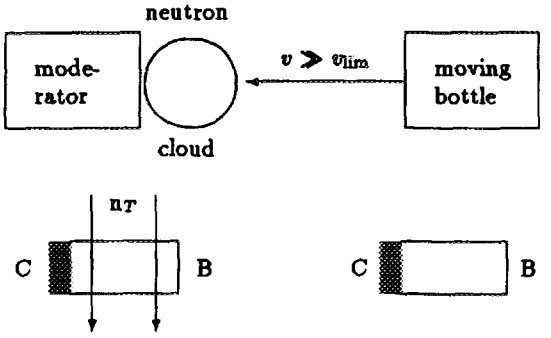

Fig. 18 The idea of the experiment for accumulating a record UCN density in a closed bottle. It is possible to prepare a UCN cloud and to shoot a bottle upon it, as shown in the top, or it is possible to attach to the bottle B a convertor C and shoot it through the shower of thermal neutrons n_t, as shown in the bottom.

For those who forgot what the UCN are, I remind you that these are the neutrons with small velocities $v \leq v_{lim}$, that can be totally reflected from a majority of substances at any angle of incidence, so they can be stored in closed vessels. The limiting velocity for them v_{lim} is of order 5 m/s. The problem of UCN is that their losses at single collision with the wall can be two order of magnitude higher than is predicted by theory.

There are two types of experiments that are being conducted now (I shall not tell here about the neutron life-time measurements).

Scheme of one experiment is shown in fig. 18. The goal is to get a record amount of neutrons in the bottle. Here you see a cloud of UCN, and a hermetically closed bottle without doors approaching this cloud at a high speed. If the velocity v of the bottle is considerably higher of the v_{lim}, all the UCN in the cloud enter the bottle through its walls. The next step is to stop the bottle immediately when the cloud becomes inside it.

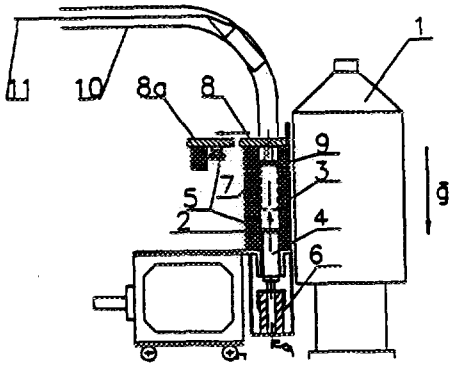

Fig.19 The arrangement of the real experiment for accumulation of the record UCN density inside the bottle. 1— reactor BIGR; 2 — moderator; 3 — BC_4; 4 — the bottle; 5 — the convertor; 6 — shooting device; 7, 9 — stopping system; 8 — the door of the reactor hall; 10 — the bottle guide; 11 — the system of guiding the bottle to the experimental hall.

But how to get such a cloud? In the experiment this problem is solved with the help of a convertor (polyethylene) attached to the bottle. In that case it is enough to shoot the bottle into the thermal beam shower. The thermal neutrons create UCN cloud inside the convertor, and this cloud enters the bottle.

The real arrangement of the experiment shown in fig. 19 was prepared at Arzamas reactor BIGR, which has a GW power in the pulse of width about 1.5 ms. The bottle shot in pulse time acquires a velocity of about 75 m/s at the length of 2 cm, flies 20 cm and then is stopped at the length of 5 cm. The maximum density of UCN inside the bottle is

expected to reach 10^5 n/cm^3.

This experiment is at the last stage of preparation. Now physicists are looking at the influence of moving objects on the behavior of the reactor.

Another experiment is devoted to searching of a solution to the problem of anomalous UCN losses. The goal is to see for heating of UCN up to those small energies that were not yet checked up. I shall not tell much about it because one of the participants of our conference, Dr. Serebrov, is directly involved in it and is the rghtful person to discuss its details. I shall only show the scheme of it (fig. 20). There you see a barrel on the left, which is fed with neutrons from neutron guide and is connected with the storage bottle on the right. The barrel is closed by polyethylene piston, which determines the upper energy of UCN in the barrel and in the bottle. Above the bottle there is a detector with variable efficiency (variable pressure of gas inside it). At low gas pressure the detector sees only the neutrons of very small energies.

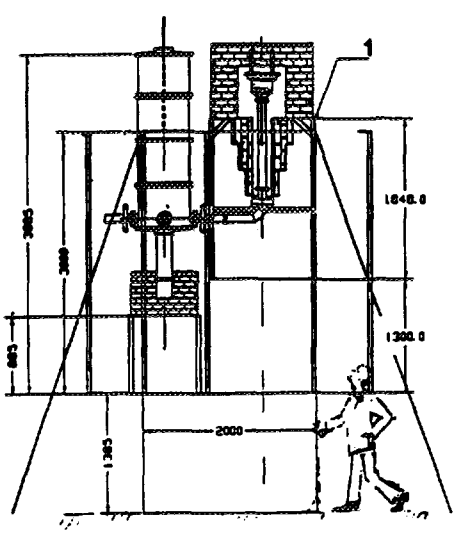

Fig.20 Layout of the experiment for search of UCN upscattering to low energies.

§11. Some projects

Here I was talking mainly about experiments conducted in our laboratory. But if you look at our entry in WWW, you will see some topics that I have not yet discussed. You will find here the works of A.I.Frank group (frank@nf.jinr.dubna.su). They consider, for example, a possibility to construct an interferometer similar to the well known three crystalline one but which acts not in space but in time. These investigations are related to ultracold neutrons and they have not yet reached the final stage.

In a different stage is the work of Yu.N. Pokotilovskiy (pokot@nf.jinr.dubna.su) group. This group is now ready to start their experiments with ultracold neutrons to study penetration depth of them in substance in the process of total reflection, their accumulation in bottles at pulsed sources with deuterium convertors and many others. They are also considering the possibility of direct measurement of neutron-neutron scattering at BIGR reactor in Arzamass-16.

I have not mentioned anything about theoretical works of W.I.Furman (furman@nf.dubna.su), about fission, and G.G.Bunatyan, whose favorite topic is Cloudy Bag Model. I had no opportunity to discuss them and I was even unable to do that.

And I told nothing about my own work. I did not do that because I strongly restricted myself in that respect from the very beginning of this lecture.

Acknowledgments

Prof. Masuda invited this report for the conference and I would like to express my heartfelt gratitude to him for the great honor and for the pleasure this opportunity gave to me to present the report before so many famous physicists. The invitation by prof. Masuda came to me together with the invitation by Prof. Utsuro to visit Japan, and I would like to express my deep gratitude to him and to Japanese government for the opportunity to see this beautiful country and to work with its kind and ingenious people. I would like also to express my gratitude to my friends and coworkers in the Laboratory of Neutron Physics in Dubna, who were very patient with my stupid questions, shared with me their knowledge and helped me to prepare this report. I would like also to express my permanent gratitude to I.Carron for his assistance.

1) Yu.A.Alexandrov, *Phys.Rev.* C **49** (1994) R2295
2) L.Köster et al, *Phys. Rev.* C **51** (1995) n. 5
3) G.S. Samosvat, *Particles and Nuclei* **26** (1995) n. 6
4) S.T.Boneva, V.A.Khitrov, A.M.Sukhovoj, A.V.Voinov, *Nucl. Phys.* A **589** (1995) 293
5) G.P.Georgiev, Yu.V.Grigor'ev, N.G.Panajotova et al, *Nucl. Phys.* A **565** (1993) 643
6) Tang Guo-yu et al, *Chinese J. Nucl. Phys.* **17** (1995) 45
7) V.P.Alfimenkov et al, *Nucl.Instr.Meth.* **A352** (1995) 592
8) V.R.Skoy. in: VII school on neutron physics, v.1, 97, Dubna, 1995.

FUNDAMENTAL PHYSICS WITH THE NEUTRON INTERFEROMETER

Samuel A. Werner
Physics Department and Research Reactor Center
University of Missouri-Columbia
Columbia, MO, 65211, USA

The perfect-silicon-crystal neutron interferometer has provided us with a very sophisticated didactic device to investigate fundamental quantum mechanical phenomena occurring over macroscopic distances. For example, we have used this device to observe the change of sign of a Fermion wave function due to precession through 360 degrees in a magnetic field, gravitationally-induced quantum interference, and the phase shift of a neutron due to the rotation of the Earth (Sagnac Effect). Experiments related to the topological Aharonov-Bohm (AB) Effects have attracted considerable interest. In particular, we have observed the phase shift due to a neutron diffracting around a charged electrode, as predicted by Aharonov and Casher in 1984. We have also observed the Scalar AB Effect for the first time by neutron interferometry, and recently achieved a clear separation of dynamical and geometric (Berry's) phases.

This work is supported by the Physics Division, National Science Foundation. Grant number #9024608.

For KEK Workshop, Tsukuba, JAPAN, March 15, 1996

SHORT LIST OF NEUTRON INTERFEROMETRY EXPERIMENTS AT MISSOURI (1975-1996)

- **Measurement of Gravitationally-Induced Quantum Interference (1975,1980,1988,1993,1996).**
- **Observation of the Change of Sign of the Wave Function of a Fermion due to Precession of 360 Degrees in a Magnetic Field (1975).**
- **Observation of the Effect of the Earth's Rotation on the Q.M. Phase of the Neutron (Sagnac Effect, 1980).**
- **Measurement of the Longitudinal Coherence Length of a Neutron Beam (1983).**
- **Detection of the Topological Aharonov-Casher Phase Shift (1989).**
- **Observation of the Phase Echo Effect (1991).**
- **Observation of the Scalar Aharonov-Bohm Effect (1993).**
- **Separation of (Berry's) Geometrical Phase and the Dynamical Phase by Polarized Neutron Interferometry (1995).**

Recent Review Paper:
"Gravitational, Rotational and Topological Quantum Phase Shifts in Neutron Interferometry"
S.A.Werner, Class. Quantum Grav. 11, A207-A226 (1994).

Neutron Interferometry Experiments (1974-1996)

- First Test of Perfect Si-Crystal Interferometer with Neutrons: Vienna (1974)
- Observation of Gravitationally-Induced Quantum Interference: Michigan, Missouri (1975
- 1980, 1988, 1993, 1996).
- Observation of the Change of Sign of the Wave Function of a Fermion due to Precession of 360° in a Magnetic Field: Michigan, Vienna-Grenoble (1975, 1978)
- Observation of the Effect of the Earth's Rotation on the Quantum Mechanical Phase of the Neutron (Sagnac Effect): Missouri (1980)
- Measurement of the Energy-dependent Scattering Length of Sm-149 in the Vicinity of a Thermal Nuclear Resonance: Missouri (1982)
- Charge Dependence of the Four-Body Nuclear Interaction in (n-^{3}He versus n-^{3}H): Vienna-Grenoble (1979, 1985)
- Search for Nonlinear Terms in the Schrödinger Equation: MIT (1981)
- Search for the Aharonov-Bohm Effect for Neutrons with a Magnetized-Single-Crystal-of-Fe-inside Interferometer: MIT (1981)
- Measurement of the Longitudinal Coherence Length of a Neutron Beam: Missouri (1983)
- Observation of the Coherent Superposition of Spin States ("Wigner Phenomenon") with Both Static and RF Spin Flippers: Vienna-Grenoble (1983, 1984)
- Neutron Interferometric Search for Quaternions in Quantum Mechanics: Missouri (1984)
- Sagnac Effect Using a Laboratory Turntable—Shows Phase Shift due to Rotation Is Linear in ω: MIT (1984)
- Observation of Acceleration-Induced Quantum Interference: Dortmund-Grenoble (1984)
- Experiment on the Null-Fizeau Effect (Stationary Boundaries) for Thermal Neutrons in Moving Matter: Missouri-Melbourne (1985)
- Observation of the Neutron Fizeau Effect with Moving Boundaries of Moving Matter: Dortmund-Grenoble (1985)
- Double-RF Coil Experiment—Analogue of the Magnetic Josephson Experiment: Vienna-Grenoble (1986)
- Precision Measurement of the Bound-Coherent Neutron Scattering Lengths of U-235, U-238, V, Eu, Gd, Th, Kr, H, D, Si, Bi, etc.: Vienna-Grenoble, Missouri (1975-1993)
- Observation of a Motion-induced Phase Shift of Neutron de Broglie Waves Passing through Matter near a Nuclear Resonance (Sm-149): Missouri-Melbourne (1988)
- Observation of Stochastic versus Deterministic Absorption of the Neutron Wave Function: Vienna-Grenoble (1984, 1987, 1990)
- Observation of the Topological Aharonov-Casher Phase Shift: Missouri-Melbourne (1989)
- Test of Possible Nonergodic Memory Effects: Vienna-Grenoble (1989)
- Observation of the Effects of Spectral Filtering in Neutron Interferometry: Missouri-Vienna (1991)
- Counting Statistics Experiments—Particle Number/Phase Uncertainty: Vienna (1990, 1992)
- Observation of the Neutron Phase Echo Effect: Missouri-Vienna (1991)
- Coherence Effects in Time-of-Flight Neutron Interferometry: Missouri-Vienna (1992)
- Observation of the Scalar Aharonov-Bohm Effect: Missouri-Melbourne (1992, 1993)
- Spectral Modulation and Squeezed States in Neutron Interferometry: Missouri-Vienna (1994)
- Observation of Multiphoton Exchange Amplitudes by Interferometry: Vienna-Missouri (1995)
- Experimental separation of geometric (Berry) and dynamical phases by neutron interferometry: BARC-Missouri-Vienna (1996)

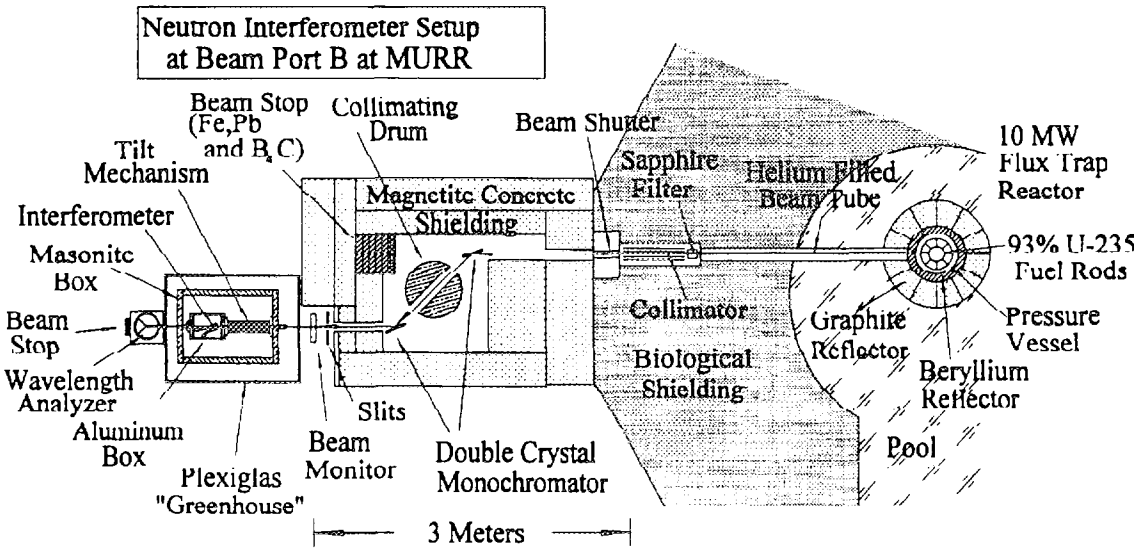
Neutron Interferometer Setup
at Beam Port B at MURR
Beam Stop
(Fe,Pb
and B4C)
Collimating
Drum
Beam Shutter
Tilt
Mechanism
Sapphire
Filter
Helium Filled
Beam Tube
10 MW
Flux Trap
Reactor
Magnetite Concrete
Shielding
Interferometer
Masonite
Box
93% U-235
Fuel Rods
Collimator
Graphite
Reflector
Pressure
Vessel
Beam
Stop
Biological
Shielding
Beryllium
Reflector
Wavelength
Analyzer
Slits
Aluminum
Box
Beam
Monitor
Double Crystal
Monochromator
Pool
Plexiglas
"Greenhouse"
3 Meters

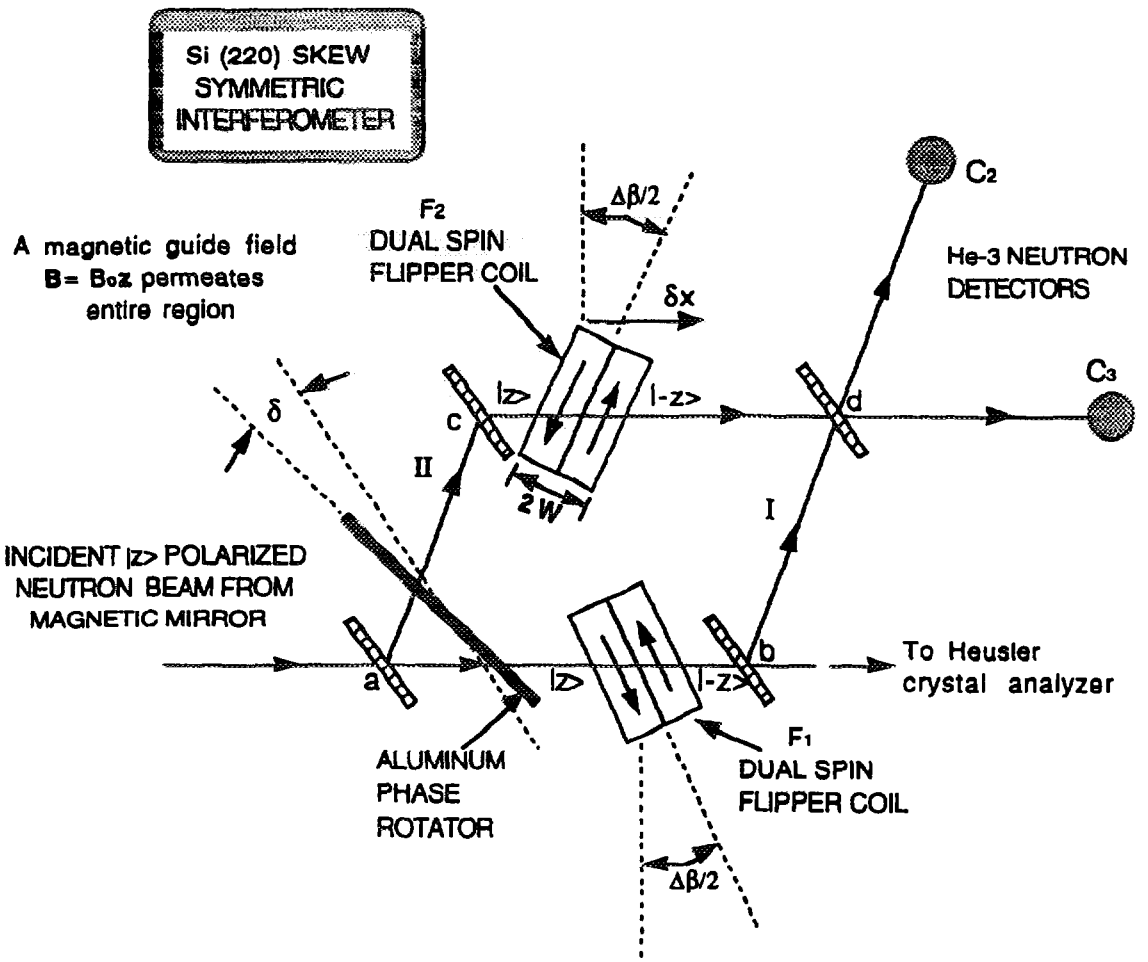

Schematic diagram of the experiment demarcating geometric and dynamical phases. A uniform guide field B_0z from a pair of Helmholtz coils is applied over the Si(220) skew symmetric interferometer. A relative rotation $\delta\beta$ between the identical dual-flippers F_1 and F_2 produces a pure geometric phase Φ_G, predicted to be equal to $\delta\beta$, for incident neutron polarized in the z-direction; their relative translation δx results in a pure dynamical phase Φ_D proportional to δx. (A.G.Wagh, et al. submitted to Phys. Rev. Lett. Feb.1,1996. Experiment done at MURR.)

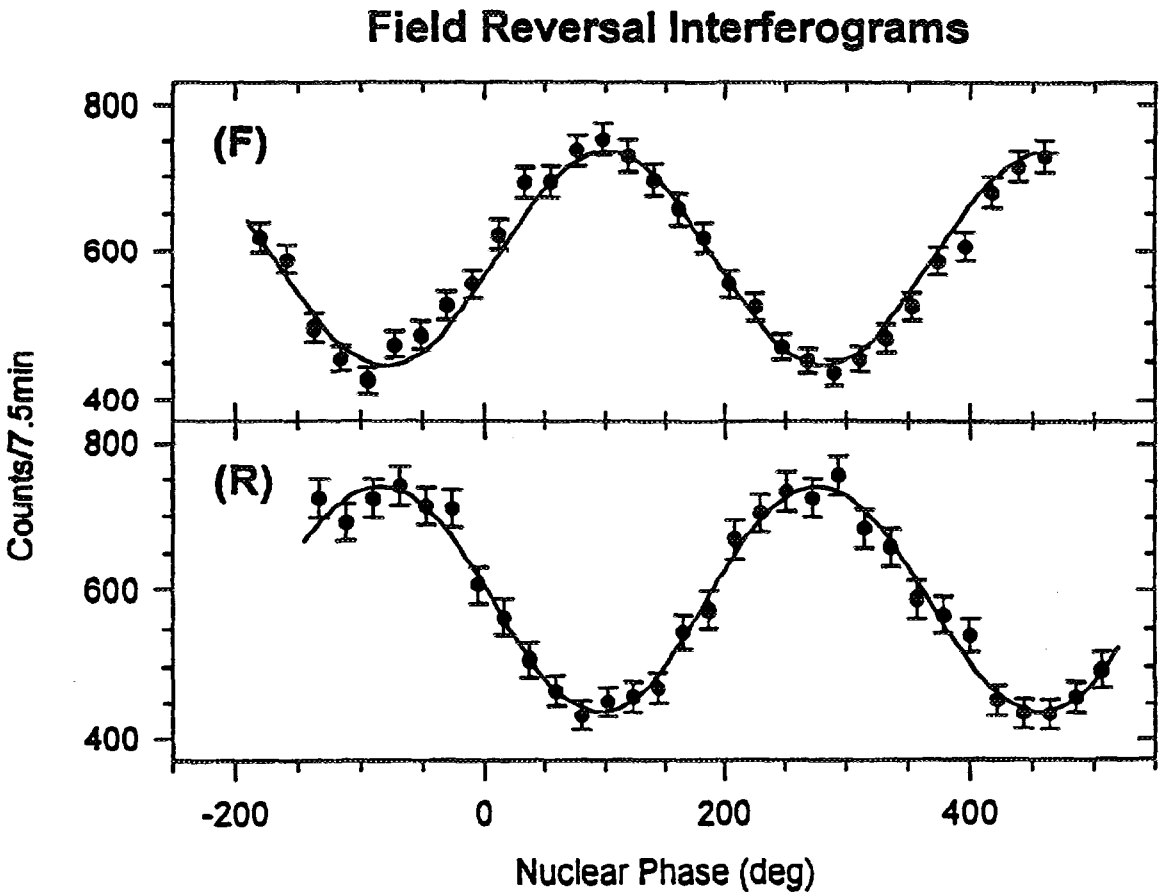
Field Reversal Interferograms
(F)
(R)
800
600
400
800
600
400
Counts/7.5min
-200
0
200
400
Nuclear Phase (deg)

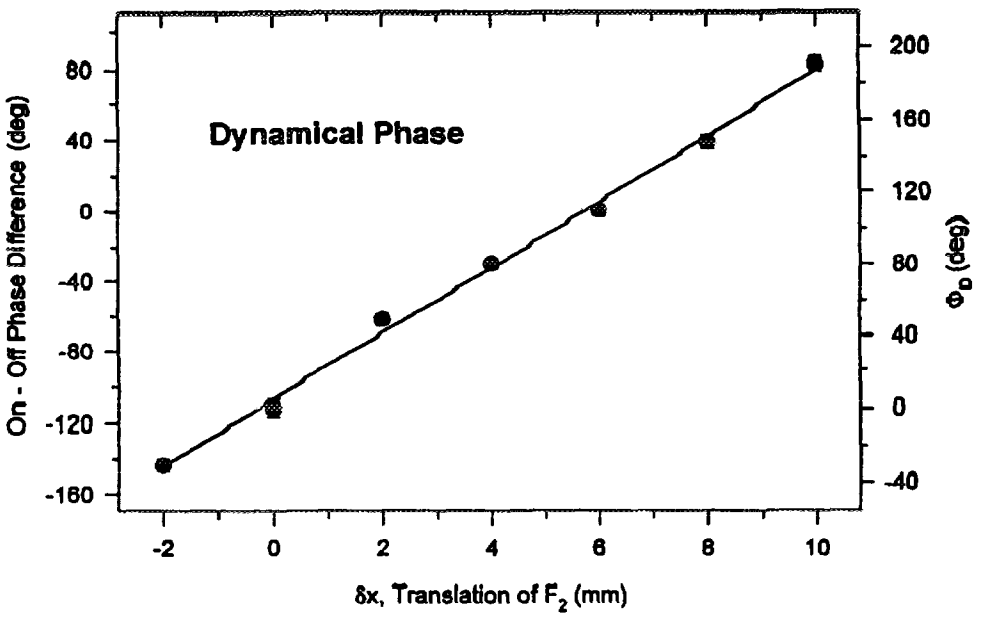
Dynamical Phase
On - Off Phase Difference (deg)
80
40
0
-40
-80
-120
-160
200
160
120
80
40
0
-40
Φ_D (deg)
-2
0
2
4
6
8
10
δx, Translation of F_2 (mm)

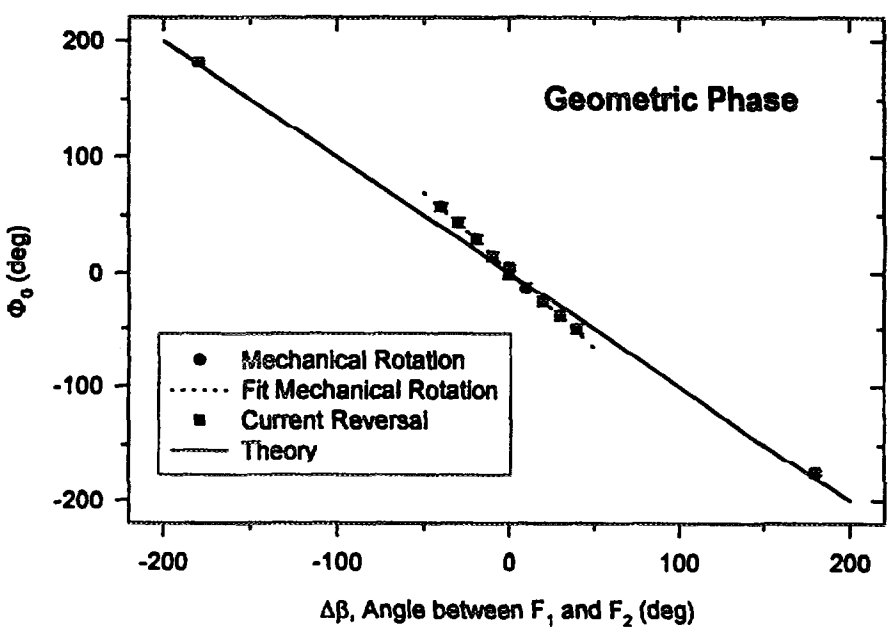
Geometric Phase
Φ_G (deg)
200
100
0
-100
-200
Mechanical Rotation
Fit Mechanical Rotation
Current Reversal
Theory
-200
-100
0
100
200
Δβ, Angle between F_1 and F_2 (deg)

Nuclear astrophysics studied by neutron capture reactions

Y.Nagai, T.Shima, T.Kikuchi, T.Kii, T.Kobayashi, T.Baba, F.Okazaki,
T.S.Suzuki, H.Sato M.Igashira[+], & T.Ohsaki[+]
Department of Applied Physics, [+]Research Laboratory for Nuclear Reactors,
Tokyo Institute of Technology, O-okayama,Meguro,Tokyo 152,Japan

Abstract:

Models of the stellar evolution and nucleosynthesis in stars is necessary to investigate the record of the Big Bang. The observed abundances of various elements in stars could be used to construct the models. Since the heavier elements than iron are considered to be synthesized by the neutron capture reaction of a nucleus in stars, it is necessary to measure the reaction cross section at stellar temperature to estimate quantitatively the production yield of these elements. To this purpose pulsed keV neutrons from the JHP spallation source would be very useful.

In order to reveal the record of the Big Bang it is necessary to construct the models of the chemical evolution of the Galaxy, which could be made by constructing the models of it's composition.[1)] Therefore, it is quite important to construct the models of the stellar evolution and nucleosynthesis. The observed abundances of various elements in stars have been playing an important role to construct the models of the stellar evolution.[2)] Those elements heavier than iron are considered to be synthesized by the two neutron capture reactions of rapid-(r) and slow-(s) processes in stars at stellar temperature of around 10^8 K, which corresponds to the neutron kinetic energy between 10 and 300 keV.[3)] Here, although the astrophysical site of the r-process remains as an open problem to be solved,[4)] that of the s-process is claimed to be the He-burning shell of an asmyptotic giant branch star.[5)] The neutrons from the $^{13}C(\alpha,n)^{16}O$ and $^{22}Ne(\alpha,n)^{25}Mg$ reactions are considered as the neutron source for the s-process isotopes, and pre-existing Fe (seed nucleus) reacts with these neutrons, producing the heavier elements. Therefore, it is necessary to measure the neutron capture cross sections of various nuclei at stellar temperature to know the production yields of s-process isotopes. One of our recent work on the neutron capture reaction of a nucleus is discussed below.

Recently, a lot of efforts are being paid to look for the s-process isotopes in less evolved old stars by the Hubble telescope etc.. It is quite natural to know the abundances of the s-process isotopes for low metallicity (ie., less evolved old) stars to construct models of the chemical evolution of the Galaxy.[1] In order to construct the models of the evolution of the s-isotopes in these stars, abundant light nuclei, such as ^{12}C, ^{16}O and ^{20}Ne, have been claimed to play an important role as a possible neutron poison.[2] Namely, in these stars, the abundance of the Fe seed nucleus decreases, however, those of the light nuclei remain the same. Therefore, if the neutron capture cross sections of these light nuclei would be large, the yields of heavier s-isotopes decrease. The number of neutrons captured per initial Fe is estimated as a function of metallicity as shown in fig.1, where the assumption was made for the capture cross section of the light nuclei.[2] It is seen clearly that no significant s-isotopes can be produced at metallicity below 10^{-2}. Thus, it is quite important to measure the neutron capture cross section of these light nuclei.

As for the primordial nucleosynthesis, a standard big-bang model of cosmology is well known to explain nicely the observed abundances of the light elements, up to ^{7}Li.[6] Recently an inhomogeneous big-bang model has been proposed as an alternative model of the standard one,[7] and thus it is important to study both the standard big-bang model and the inhomogeneous model in detail by determining the primordial abundance of the light elements and by measuring precise nuclear reaction rates, which concern the primordial nucleosynthesis. The p(n,γ)d reaction is one of the most important reactions in the primordial nucleosynthesis. However, it has not ever been measured directly at astrophysically relevant energies.

Recently, we have measured the cross sections of the $^{12}C(n,\gamma)^{13}C$, $^{16}O(n,\gamma)^{17}O$, and p(n,γ)d reactions. It should be noted that the capture cross sections of these nuclei have not been studied well.

The experiment was carried out by using pulsed neutrons in the neutron energies between 10 and 300 keV. The neutrons were produced by a $^{7}Li(p,n)^{7}Be$ reaction by using a bunched proton beam, provided from the 3.2MV Pelletron Accelerator of the Research Laboratory for Nuclear Reactors at the Tokyo Institute of Technology. Samples of polyethylene, carbon, enriched $^{7}Li_2O$, and a gold (Au) were used. Au was used for normalization of the cross section, since the capture cross section of Au has been well known.[8] Prompt γ-rays from a

capture state were detected by an anti-Compton NaI(Tl) spectrometer.[9] The time-of-flight (TOF) spectrum was measured by the NaI(Tl) spectrometer in order to obtain the background subtracted (net) γ-ray spectrum. A typical net γ-ray spectrum from a capture state of the $^{16}O(n,\gamma)^{17}O$ reaction is shown in fig.2. The absolute cross section of ^{16}O was obtained by comparing their γ-ray intensities with that of Au and it is obtained as $\sigma(E)=1.0/(E)^{1/2} + 3.80(38)(E)^{1/2}$. The energy dependence of the second term indicates that the keV neutrons are captured dominantly by a p-wave. Thus, the Maxwellian-averaged capture cross section at the temperature of 30 keV was obtained as 38(4) μb, which is 170 times larger than the previously reported value of 0.2(1) μb.[10]

In these studies we have successfully measured the small cross sections of proton, ^{12}C and ^{16}O in the neutron energies between 10 and 300 keV. The cross sections of the p(n,γ)d reaction are in good agreement with the newly calculated theoretical values.[11] The present result of the large reaction rate of the $^{16}O(n,\gamma)^{17}O$ reaction has important implications for nucleosynthesis theory of s-process, especially in metal deficient massive stars as a very important neutron poison. As for the inhomogeneous big-bang models, the present result favors the production of intermediate-heavy mass nuclei. The large capture cross section obtained here can be explained by a non-resonant p-wave capture,[12] which was found also in the $^{12}C(n,\gamma)^{13}C$ reaction.[13] Recently, the very interesting theoretical calculations based on the direct radiative capture model have been carried out by Otsuka, Ishihara et al., Mohr, and Mengoni et al..[14] Our results on ^{12}C and ^{16}O are in good agreement with the calculated values.

As discussed above, the measurement of the neutron capture cross section of various nuclei is necessary to the nucleosynthesis theory. To this purpose the pulsed keV neutrons together with the prompt γ-ray detetction method enables us to derive the small cross section accurately. The intensity of the pulsed neutrons from the JHP spallation source is about 500 times stronger than that from our accelerator, and thus the project will open the new possibility to measure the cross section on rare abundant elements. JHP N-arena would be very interesting new environment also for studying nuclear astrophysics.

References

1) J.C.Wheeler, C.Sneden & J.W.Truran, Ann.Rev.Astron.Astrophys. 27(1989)279

2) N.Prantzos, M.Hashimoto, & K.Nomoto, Astron. & Astrophys. 234(1990)211

3) E.M.Burbidge, G.R.Burbidge, W.A.Fowler & F.Hoyle, Rev.Mod.Phys. 29(1957)547

4) G.J.Mathews & J.J.Cowan, Nature 345(1990)491

5) I.Iben, Astrophys.J.196(1975)525

6) P.J.E.Peebles, Phys. Rev. Lett., 16 (1966) 410, H.Sato, Prog. Theor. Phys, 38(1967)1083, R.V.Wagoner, W.A.Fowler, & F.Hoyle, ApJ, 148 (1967) 3

7) J.H.Applegate, C.J.Hogan, & R.J.Scherrer, Phys.Rev.D35 (1987) 1151, T.Kajino, G.J.Mathews, & G.M.Fuller, ApJ,364 (1990) 7

8) R.L.Macklin, & H.Gibbons, Phys. Rev.159 (1967) 1007, ENDF/B-V data file for 197Au (MAT=1379). 1979, evaluated by S.F.Mughabghab

9) M.Igashira, H.Kitazawa, & N.Yamamuro, Nucl. Instr. Meth.A245 (1986) 432

10) B.J.Allen, & R.L.Macklin, Phys.Rev.C3(1971)1737

11) T.S.Suzuki, Y.Nagai, T.Shima, T.Kikuchi, H.Sato, T.Kii, & M.Igashira, ApJ, 439 (1995) L59

12) M.Igashira, Y.Nagai, K.Masuda, T.Ohsaki, & H.Kitazawa, ApJ,441(1995)L89

13) Y.Nagai, M.Igashira, K.Takeda, N.Mukai, S.Motoyama, F.Uesawa, H.Kitazawa, & T.Fukuda, ApJ, 372 (1991) 683, T.Ohsaki, Y.Nagai, M.Igashira, T.Shima, K.Takeda, S.Seino, & T.Irie, ApJ, 422 (1994) 912

14) T.Otsuka, M.Ishihara, N.Fukunishi,T.Nakamura, & M.Yokoyama, Phys. Rev. C49(1994) R2289, A.Mengoni, T.Otsuka & M.Ishihara, Phys. Rev. C52(1995)R2334

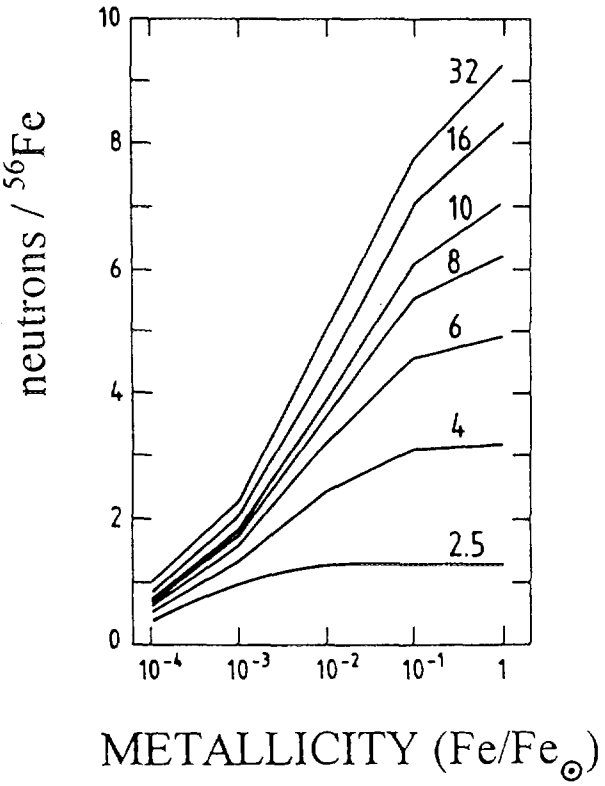

Fig.1. Calculated number of neutrons captured per initial Fe as a function of metallicity.[2)]

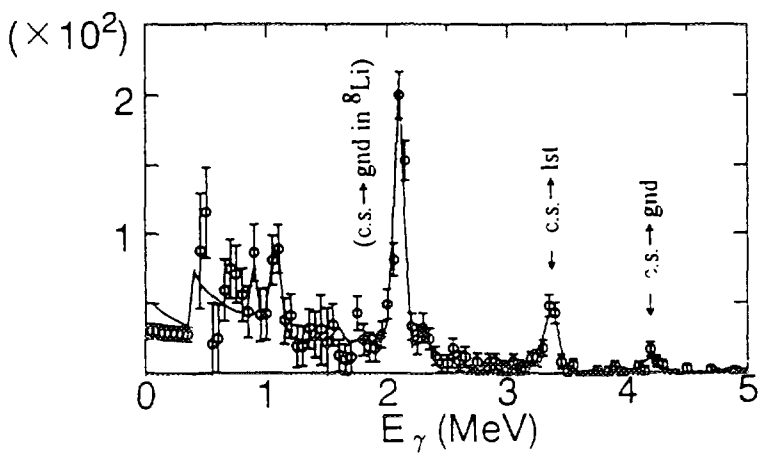

Fig.2. Net γ-ray spectrum from the ^{16}O(n,γ)^{17}O reaction at the average neutron energy of 40 keV.[12)]

PLANS FOR STUDIES OF (α,n) REACTIONS RELEVANT TO ASTROPHYSICS VIA INVERSE REACTIONS

T. Shima, Y. Nagai, T. Kii, T. Kikuchi, T. Baba, T. Kobayashi and F. Okazaki
Department of Applied Physics, Tokyo Institute of Technology,
2-12-1 O-okayama, Meguro-ku, Tokyo, Japan

(α,n) reactions in the keV energy region play important roles in astrophysical nucleosynthesis.

In the primodial nucleosynthesis, it has been pointed out that a fluctuation of the baryon density distribution could be formed if the QCD phase transition from quark-gluon plasma to hadron gas occured by first order[1]. In that case the space was separated into the high density proton-rich zones and the low density neutron-rich ones, and in the neutron-rich zones nucleosynthesis could proceed beyond the mass gap at $A = 8$ via the reaction chains such as

^{1}H(n,γ)^{2}H(n,γ)^{3}H(d,n) ^{4}He(t,γ)^{7}Li(n,γ)^{8}Li(α,n) ^{11}B(n,γ)^{12}B(e$^{-}\nu$)^{12}C(n,γ)
^{13}C(n,γ)^{14}C(n,γ)^{15}C .....,

and so on[2-4]. In the above nuclear reactions, the ^{8}Li(α,n)^{11}B reaction plays quite crucial role, because it can break through the mass gap at $A = 8$.

(α,n) reactions of some light nuclei are also important as neutron sources for slow neutron capture process (s-process) of nucleosynthesis in stars[5,6]. In low-mass and intermediate-mass ($M < 10M_{\odot}$) stars, neutrons are supposed to be supplied mainly by the ^{13}C(α,n)^{16}O reaction. On the other hand, the ^{22}Ne(α,n)^{25}Mg reaction is a candidate of the neutron source in massive stars with $M \geq 10M_{\odot}$. And the contribution of the ^{18}O(α,n)^{21}Ne reaction to s-process in massive stars is still unknown.

Since the temperatures of the above astrophysical sites correspond to the energy range of between a few ten and a few hundred keV, accurate data of the (α,n) reaction cross sections in the energy range are required for investigating nucleosynthesis. In order to measuere these cross sections, not only direct (α,n) reactions but also inverse (n,α) reactions can be studied. In the following we would like to show experimental designs for studying several (α,n) reactions of astrophysical importance.

(1) *^{8}Li(α,n)^{11}B*

So far the ^{8}Li(α,n)^{11}B reaction has been studied in the center-of-mass energy ($E(CM)$) regions down to 0.63 MeV and 0.38 MeV, by measuring the direct reaction[7,8] and the

inverse one[9], respectively, as shown in Fig. 1.

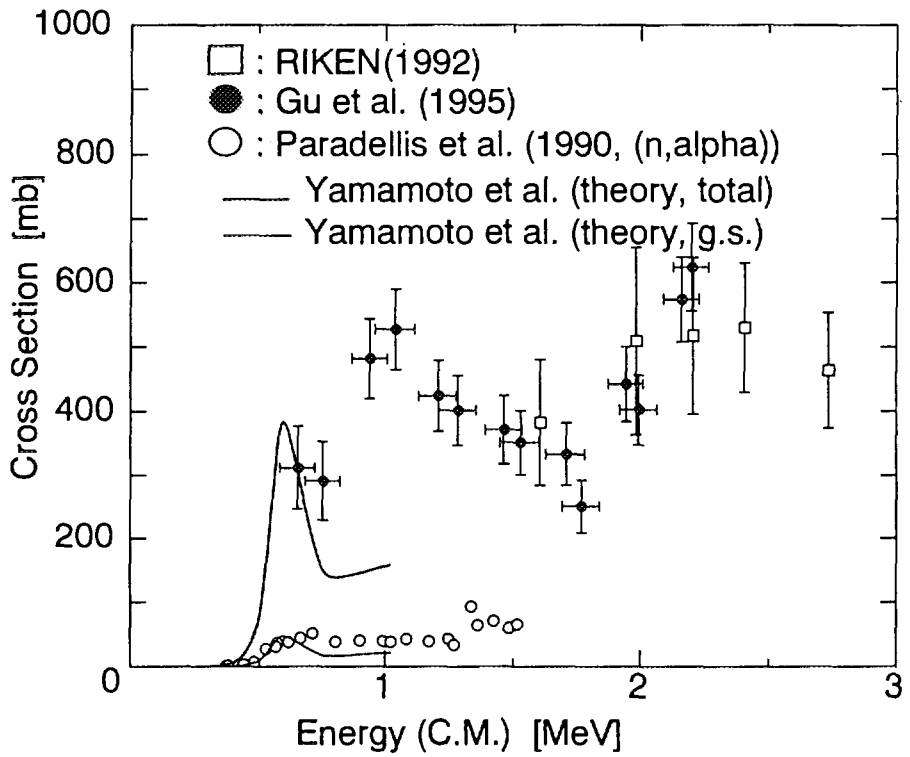

Fig. 1. ^{8}Li(α,n)^{11}B reaction cross sections from ref. 7 (open squares), ref. 8 (filled circles) and ref. 9 (open circles). Thick and thin lines are theoretical ones from ref. 10.

The energy region relevant to the primodial nucleosynthesis is, however, still lower than that studied by the previous experiments. So the cross section in the energy region of interest has been estimated by extrapolating the data with the use of theoretical models. Recently Yamamoto et al.[10] successfully reproduced the ratio between the total cross section $\sigma(\alpha,n)_{total}$ and the cross section $\sigma(\alpha,n)_{g.s.}$ for the transition from the capture state to the ground state of the produced ^{11}B nucleus theoretically, as indicated in Fig. 1. And we can expect that if the data of the cross section $\sigma(\alpha,n)_{g.s.}$ are determined accurately in the lower energy region, the total cross section $\sigma(\alpha,n)_{total}$ will be evaluated reliably by using theoretical models. $\sigma(\alpha,n)_{g.s.}$ can be determined with the data of the inverse ^{11}B(n,α)^{8}Li reaction by assuming the principle of detailed balance. The most remarkable advantage of the inverse measurement is that ^{11}B is stable and easily used as a target, in contrast to ^{8}Li ($T_{1/2}$ = 0.84 sec).

In order to determine $\sigma(\alpha,n)_{g.s.}$ in the range of $E(CM)$ = 0.28~0.38 MeV by using the inverse reaction, a neutron beam in the energy range of $E_n(lab)$ = 7.54~7.65 MeV is required, since $E_n(lab)$ is related to the corresponding $E(CM)$ by Eq. 1 :

$$E_n(lab) = 12/11 \times (E(CM) + Q). \quad (1)$$

Here $Q(= 6.631$ MeV) is the Q-value of the ^{8}Li(α,n)^{11}B reaction, and a factor 12/11 is a correction for the transformation from the center-of-mass system to the laboratory one. Since the cross section in this energy range is expected to be less than about 10 μb[9] (see Fig. 2), a high-intensity neutron beam and a high-sensitivity detector are needed.

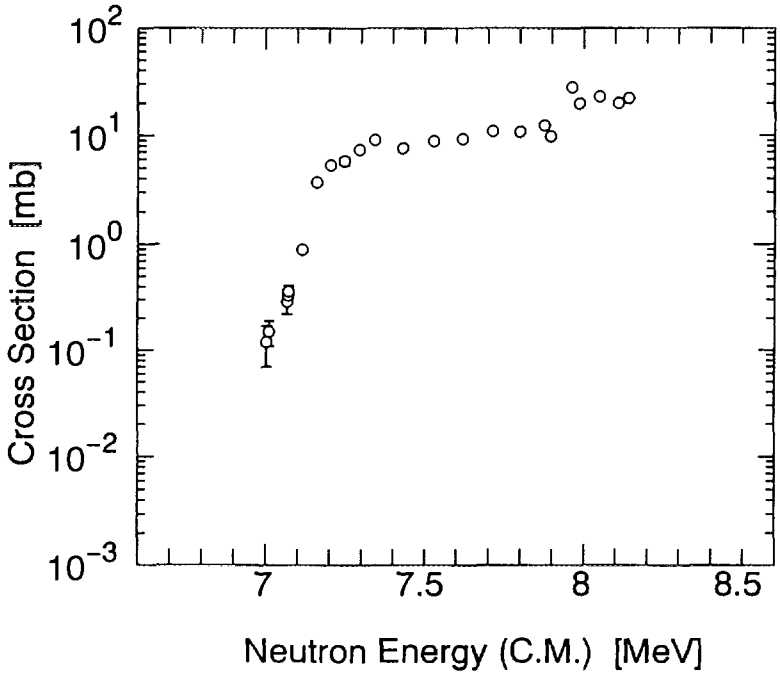

Fig. 2. ^{11}B(n,α)^{8}Li reaction cross sections from ref. 9.

In our plan we will use a spallation neutron source, which is planned to be constructed in the N-arena of the Japan Hadron Project (JHP). And for the detector we will employ a time projection chamber (TPC) filled with an operational gas of natural BF_3. The experimental setup is schematically shown in Fig. 3.

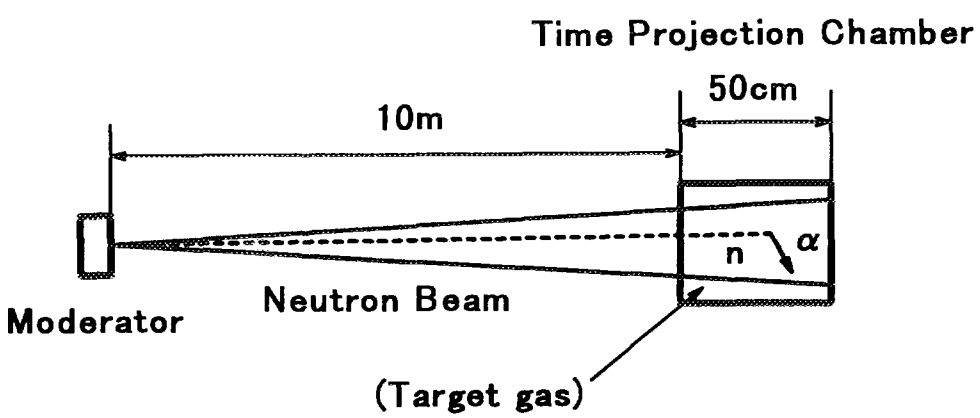

Fig. 3. Schematic drawing of the experimental set up for the ^{11}B(n,α)^{8}Li reaction measurement.

An MeV neutron beam is introduced into the effective region of the TPC, where the BF_3 gas is contained. This method has following merits :

- We can use a large amount of the target as thick as a few ten cm in order to get a good statistics, because the neutrons are not stopped by the electromagnetic interaction.
- Since the natural boron in the operational gas contains ^{11}B with the isotopic abundance of 80.1%, it can act as an active target, and therefore an acceptance of the solid angle of about 4π srad and a detection efficiency ε of almost 100% are expected for the α particles from the $^{11}B(n,\alpha)^8Li$ reaction events.
- Since the cross section of the $^{10}B(n,\alpha)^7Li$ reaction is well known[11] and large enough ($\sim$0.1 b), the $^{10}B(n,\alpha)^7Li$ reaction events can be used to determine the incident neutron intensity and for calibration of the detection efficiency of the TPC.
- The total energies and the shapes of the tracks of the emitted α particles can be measured, and those informations are quite useful to obtain an extremely high selectivity between the true (n,α) events and the background ones.

The neutron flux ϕ_n at the position of the detector is estimated with Eq. 2 :

$$\phi_n = I_n \times S(mod) \times \Omega \times \Delta E_n, \tag{2}$$

where I_n, $S(mod)$ and Ω are the neutron intensity on the surface of a neutron moderator, the surface area of the moderator and the solid angle of the BF_3 gas target viewed by the moderator, respectively. In the case of the neutron source in the N-arena, I_n is expected to be 5×10^4 n$\cdot$cm$^{-2}\cdot$sec$^{-1}\cdot$eV^{-1} $\cdot$srad^{-1} in the range of $E_n(lab)$ = 7.65$\sim$7.76 MeV, and $S(mod)$ will be 100 cm^2. Ω will be 10^{-4} srad for a gas target with an area of the cross section of 100 cm^2 placed 10 m distant from the moderator, for example. To determine $E_n(lab)$ in each events, the time-of-flight (TOF) method is not favorable, because the time width of the neutron pulse will be 100 nsec in the planned neutron source, and the corresponding energy range will be from 5.3 to 11.6 MeV for the neutron flight length of 10 m and the mean neutron energy of 7.5 MeV, which is too wide for the present purpose. Therefore $E_n(lab)$ should be determined by observing the energies E_α and $E_{^8Li}$ of the emitted α particles and the residual ^{8}Li nuclei, respectively. For $E_n(lab)$ from 7.65 to 7.76 MeV, E_α spreads between 0.187 and 0.253 MeV, and $E_{^8Li}$ spreads between 0.093 and 0.127 MeV. Since the resolutions for E_α and $E_{^8Li}$ are about 10$\sim$20 keV, ΔE_n can be set as 50 keV. Thus ϕ_n is estimated as 2.5×10^7 n/sec. If we use a TPC with a length of 50 cm and a gas pressure of 760 torr, the target thickness D is 1.1×10^{-3} atoms/b. The counting rate $R(n,\alpha)$ of the $^{11}B(n,\alpha)^8Li$ reaction is given by Eq. 3 :

$$R(n,\alpha) = \varepsilon \times D \times \sigma(n,\alpha) \times \phi_n. \tag{3}$$

In the present case R is expected to be 0.03$\sim$0.3 counts/sec, depending on $\sigma(n,\alpha)$, which seems to be enough to make a significant experiment. To estimate the statistical accuracy, we have to know the counting rate of the background events in the real

measurement. In principle, The most dangerous events are charged particle emitting reactions caused by neutrons in the active region of the TPC. The ^{19}F(n,d)^{18}O (Q = -5.768 MeV) and ^{19}F(n,t)^{18}O (Q = -7.557 MeV) reactions may be serious, because the energies of the emitted deuterons or tritons are close to that of the α particles produced by the ^{11}B(n,α)^{8}Li reaction. These background events can be discriminated from the true ones by comparing track lengths and energies of the emitted charged particles.

(2) $^{13}C(\alpha,n)^{16}O$

The ^{13}C(α,n)^{16}O reaction cross section is quite uncertain at the temperature of the site of s-process, i.e. in the energy range of $E(CM) \leq 0.1$ MeV, since the effect of the sub-threshold resonance at $E(CM)$ = -2 keV is still unknown. Until now experimental study of the reaction has been done only by Kunz et al[12]. in the energy range of $E(CM) \geq 0.28$ MeV. Their result suggests that the contribution of the sub-threshold resonance to the total cross section is much larger than that estimated by Caughlan and Fowler[13], which is generally adopted, and the ^{13}C(α,n)^{16}O reaction rate may be underestimated by a factor of about ten. Since the efficiency of stellar nucleosynthesis by s-procees is strongly dependent on the cross section, the ambiguity with a factor ten is quite unsatisfactory, and much accurate experimental data are required. However, the cross section is expected to be as small as about a few pb even in the energy range of $E(CM) = 0.23\sim0.24$ MeV, which corresponds to the neutron energy range of $E_n(lab) = 2.598\sim2.609$ MeV in the inverse ^{16}O(n,α)^{13}C reaction. So it is not practicable to determine the ^{13}C(α,n)^{16}O cross section by measuring the ^{16}O(n,α)^{13}C cross section in the region of $E(CM) \leq 0.25$ MeV. But yet it is possible to determine the contribution from the sub-threshold resonance by measuring the cross section at $E(CM) = 0.3\sim0.4$ MeV accurately, where the data given by Kunz et al. contain experimental errors of 50$\sim$100%, and are not accurate enough. The energy region of $E(CM) = 0.3\sim0.4$ MeV corresponds to the neutron energy range of $E_n(lab) = 2.673\sim2.779$ MeV, and in this range the neutron intensity I_n is expected to be 10^5 n$\cdot$cm$^{-2}\cdot$sec$^{-1}\cdot$eV$^{-1}\cdot$srad^{-1}. If we set a TPC with the cross section of the effective region of 2500 cm^2 at a distance of 10 m from the neutron source, the neutron flux ϕ_n will be 2.5×10^9 n/sec in the above range of $E_n(lab)$ at the position of the TPC. For the ^{16}O target we will use a CO_2 gas with a pressure of 7600 torr and a thickness of 100 cm. So the ^{16}O target thickness will be 0.054 atoms/b. Since the average cross section in the above energy range is estimated to be about 160 pb, the counting rate of the ^{16}O(n,α)^{13}C reaction events is expected to be $\sim$0.02 cps.

(3) $^{18}O(\alpha,n)^{21}Ne$

The ^{18}O(α,n)^{21}Ne reaction is also one of the candidates of neutron sources for s-process, because ^{18}O is produced very efficiently by the ^{14}N(α,n)^{18}F(β^+)^{18}O reactions at the early stage of the helium burning phase. The reaction rate at stellar energy has been studied by a few groups. Bair and Haas measured the cross section at $E(CM)$ =

0.818 MeV, and by using the data, they estimated the cross section at $E(CM) = 0.740$ MeV to be 140 nb[14]. But the data obtained by Kunz et al.[12] at the same energy was 8 nb, which is quite inconsistent with the value given by Bair and Haas. Furthermore, the result by Kunz et al. is smaller by about a factor of ten than the values estimated by Caughlan and Fowler[13] for the temperature below 10^9K. In order to measure the cross section at stellar energy by means of the inverse reaction measurement, a keV energy neutron beam is neccesary, because the ^{21}Ne(n,α)^{18}O reaction is exothermic (Q = +0.696 MeV). Since the ^{21}Ne(n,α)^{18}O cross section is expected to be as small as 1$\sim$10 nb in the keV region[12], use of an enriched ^{21}Ne target gas is favored to obtain sufficient statistics. And in order to reduce loss of the enriched gas, a gas leakage rate of the TPC should be minimized.

In summary, to study the (α,n) reactions of astrophysical importance, measurements of the inverse (n,α) reactions are useful, and they will play complementaly roles in the research of nucleosynthesis together with the direct measurements, which are also planned in the exotic-nuclei arena of the JHP project. In the inverse measurements, a high-intensity fast neutron beam and a time projection chamber with an active gas target will be promising tools. Such a neutron beam is expected to be available in the planned N-arena facility. And a new TPC with a reduced gas leakage rate is now under development in our laboratory. It will allow us to measure expensive enriched target gases.

Ackowledmgent

We would like to thank Professors M. Hashimoto, T. Kajino and S. Kubono for fruitful discussions.

References

1. J.H. Applegate and C.J. Hogan, *Phys. Rev.* **D31** (1985) 3037
2. J.H. Applegate, C.J. Hogan and R.J. Scherrer, *Phys. Rev.* **D35** (1987) 1151
3. T. Kajino, G.J. Mathews and G.M. Fuller, *Astrophys. J.* **364** (1990) 7
4. L.H. Kawano et al., *Astrophys. J.* **372** (1991) 1
5. A.G.W. Cameron, *Phys. Rev.* **93** (1954) 932
6. I. Iben Jr., *Astrophys. J.* **196** (1975) 525, 549
7. R.N. Boyd et al., *Phys. Rev. Lett.* **68**, 1283 (1992)
8. X. Gu et al., *Phys. Lett.* **B343** 31 (1995)
9. T. Paradellis et al., *Z. Phus.* **A337** 211 (1990)
10. Y. Yamamoto et al., to be appeared in *Proc. of Workshop on Science of Unstable Nuclear Beam '95* (JHP-Supplement-17).
11. ENDF/B-VI, data file for ^{10}B, 1991, evaluated by G. Hale and P.G. Young
12. R. Kunz et al., *Proc. of the 4th Int. Conf. on Applications of Nuclear Techniques ("Neutrons and their Applications")*, Crete, Greece, June 1994
13. G.R. Caughlan and W.A. Fowler, *Atomic Data and Nuclear Data Tables* **40** 283 (1988)

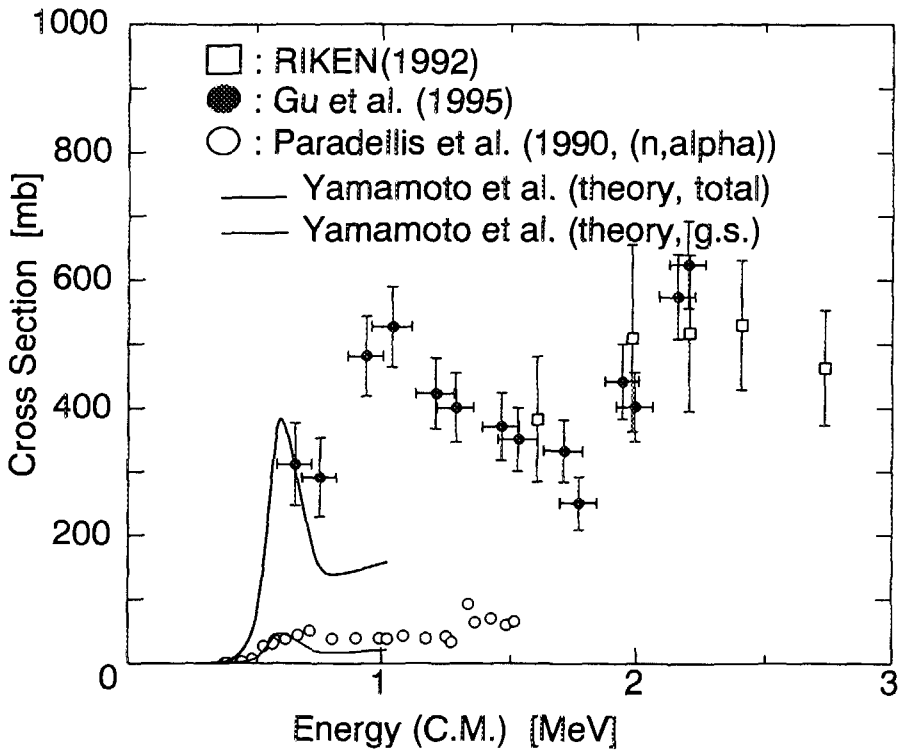
□ : RIKEN(1992)
● : Gu et al. (1995)
○ : Paradellis et al. (1990, (n,alpha))
Yamamoto et al. (theory, total)
Yamamoto et al. (theory, g.s.)
Cross Section [mb]
Energy (C.M.) [MeV]
0
200
400
600
800
1000
1
2
3

Fig. 1

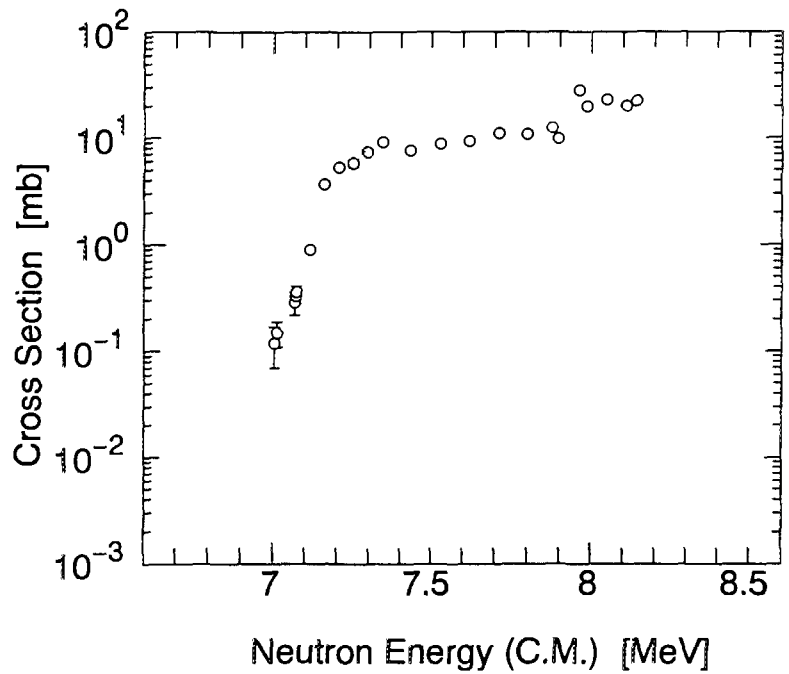
Cross Section [mb]
Neutron Energy (C.M.) [MeV]
10^{2}
10^{1}
10^{0}
10^{-1}
10^{-2}
10^{-3}
7
7.5
8
8.5

Fig. 2

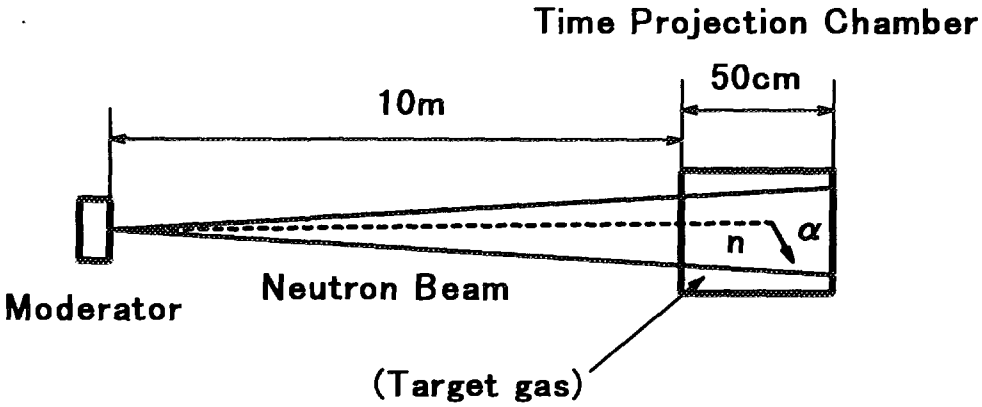
Time Projection Chamber
50cm
10m
n
α
Moderator
Neutron Beam
(Target gas)

Fig. 3

T-violation in neutron optics

Y. Masuda

National Laboratory for High Energy Physics
1-1 Oho, Tsukuba-shi, Ibaraki-ken, 305 Japan

Experimental method to detect a T-odd correlation term in neutron propagation through a nuclear target is discussed. The correlation term is between the neutron spin, neutron momentum and nuclear spin.

I Introduction

In 1964, Michel suggested the neutron spin rotates under the nucleon-nucleon (N-N) weak interaction. He estimated the rotation angle in terms of the Fermi coupling-constant. The rotation angle was too small, 5.8×10^{-9} rad/cm for a bismuth target, to be measured. In 1977, Forte suggested the P-violating effect is largely enhanced via neutron-nucleus resonance.[2] The first experiment was carried out on neutron propagation through a nuclear target in cold neutron region.[3] Indeed, very large P-violating rotation up to 4×10^{-5} rad/cm was observed for a ^{117}Sn target. Sushkov and Flambaum suggested the P-violating effect is particularly enhanced in the p-wave compound-nucleus-resonance: parity mixing between s- and p-wave resonances is largely enhanced because of very small level-spacing and large suppression for the p-wave state by the nuclear centrifugal-barrier compared with the s-wave state.[4] Bunakov and Gudkov suggested a similar enhancement mechanism.[5] In the meantime, a very large P-violating asymmetry up to 10% was found in the p-wave resonance of ^{139}La at Dubna, KEK and Los Alamos.[6,7,8] The P-violating effect is a neutron-helicity, namely $\boldsymbol{s}\cdot\boldsymbol{k}$ dependent cross-section. $\boldsymbol{s}$ is the neutron spin and $\boldsymbol{k}$ the neutron momentum.

In 1982, Stodolsky suggested similar enhancement in the T-violating effect as in the P-violating effect. The T-violating effect arises from a $\boldsymbol{s}\cdot(\boldsymbol{k}\times\boldsymbol{I})$ dependent neutron-scattering amplitude, which is odd term under time reversal.[10] $\boldsymbol{I}$ is the target-nucleus spin. The correlation term induces neutron-spin rotation around the axis of $\boldsymbol{k}\times\boldsymbol{I}$ and $\boldsymbol{s}\cdot(\boldsymbol{k}\times\boldsymbol{I})$ dependent neutron-attenuation. Kabir also pointed out the importance of the T-violation experiment on neutron forward-scattering, since the experiment is free from final-state interactions, which are serious problem in the correlation experiments of the decay processes.[11] Bunakov and Gudkov showed the same enhancement for the T-violating effect in the p-wave resonance as for the P-violation effect. They also suggested the nuclear wave-function uncertainty is greatly reduced in the ratio of the T-violating to P-violating effect.[12] Herczeg discussed CP-violating nucleon-nucleon interactions in terms of nucleon-meson coupling.[13] He showed the T-violation experiment on neutron forward-scattering is compared with neutron EDM values via CP-violating meson-coupling constant.

II T-violating scattering amplitude

The neutron propagation through matter is treated as a neutron-optical phenomena. The neutron-optical phenomena is discussed in terms of the neutron-scattering amplitude $f(k, k')$, which is generally represented in terms of t matrix as

$$f(k, k') = -(1/4\pi)(2M/\hbar^2)(2\pi)^3 \langle k'\, m'|\, t\, |k\, m\rangle \quad (1)$$

$$t = V + V(1/(E-H_0+i\varepsilon))V + V(1/(E-H_0+i\varepsilon))V(1/(E-H_0+i\varepsilon))V + ... \quad (2)$$

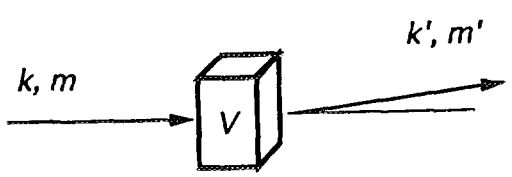

Fig. 1 Neutron scattering by potential V

Here, H_0 is a Hamiltonian for a free-particle state, V is a potential in matter, M is the neutron reduced-mass and m is the neutron-spin state. $|k\, m\rangle$ and

$|k' m'>$ are free-particle states. For polarized-neutron propagation through a polarized-nuclear target, t is represented in terms of Pauli-spin matrices as

$$\begin{aligned} t &= F_0' + F_1' \sigma_x + F_2' \sigma_y + F_3' \sigma_z. \\ &= F_0 + F_1 P_I \sigma \cdot \hat{I} + F_2 P_I \sigma \cdot (\hat{k} \times \hat{I}) + F_3 \sigma \cdot \hat{k}. \end{aligned} \tag{3}$$

Here, we assume the nuclear spin is along x, the neutron momentum along z. P_I is the nuclear polarization. The coefficients F_i (i = 0, 1, 2, 3) are functions of k. The expression of the t matrix is a general form for a spin 1/2 particle. The third term in Eq. (3) is the T-violating term, which is free from final-state interactions, since the initial and final states of the t matrix are the same free-particle state. The coefficients F_i are related to the forward-scattering amplitude $f(0)$,[14]

$$f(0) = A' + B' P_I \sigma \cdot \hat{I} + D' P_I \sigma \cdot (\hat{k} \times \hat{I}) + C' \sigma \cdot \hat{k}. \tag{4}$$

A' is the coherent scattering amplitude and B' is the spin-incoherent scattering amplitude which come from the strong interaction. C' is the weak interaction term. D' is a T-violating term. The scattering amplitude is related to the neutron refractive-index n in matter as

$$n = 1 + (\lambda/k) \rho f(0). \tag{5}$$

λ is the neutron wave-length and ρ is the number density of scatterer. The neutron phase-shift ϕ after propagation through matter is represented in terms of the refractive index as

$$\phi = (n - 1)kl . \tag{6}$$

l is the propagation length in matter. The spin-dependent scattering-amplitudes A', B', C' and D' in Eq. (4) induce spin-dependent phase-shift,

$$(\phi_0, \phi_1, \phi_2, \phi_3) = (\lambda l \rho A', \lambda l \rho B', \lambda l \rho D', \lambda l \rho C'). \tag{7}$$

The t matrix is represented in terms of the phase shifts as

$$t = \exp(i\phi). \tag{8}$$

$$F_0 = \exp(i\phi_0) \cos b , \tag{9}$$

$$F_j = \exp(i\phi_0)\ i(\sin b/b\ )\phi_j,\ (j = 1, 2, 3) \quad (10)$$

$$b = \sqrt{(\phi_1)^2+(\phi_2)^2+(\phi_3)^2}\ . \quad (11)$$

The spin-dependent phase-shifts give rise to neutron-spin rotation around j axes via real parts and spin-dependent attenuation via imaginary parts.

The neutron-optical phenomena is also discussed in terms of a time-evolution operator $u(t, 0) = \exp(-iH_{eff}t/\hbar)$.[15] H_{eff} is an effective Hamiltonian, which has spin dependence. The time-evolution operator corresponds to the t matrix which is shown in Eq. (8). In the neutron propagation, the time t is related to the neutron propagation-length l and the neutron momentum k. Therefore, the effective Hamiltonian H_{eff} is represented in terms of the spin-dependent phase-shift.

III Measure of T-violation

In 1984, Heckle proposed to measure a T-violating neutron-spin rotation in a polarized ^{129}Xe target,[16] since ^{129}Xe nuclei can be polarized by an optical pumping.[17] However, no large P-violation effect was observed at KEK.[18] In 1986, Stodolsky showed the fake effect of other correlation terms, the strong- and weak-interaction terms in Eq. (3) and (4) is very large in the

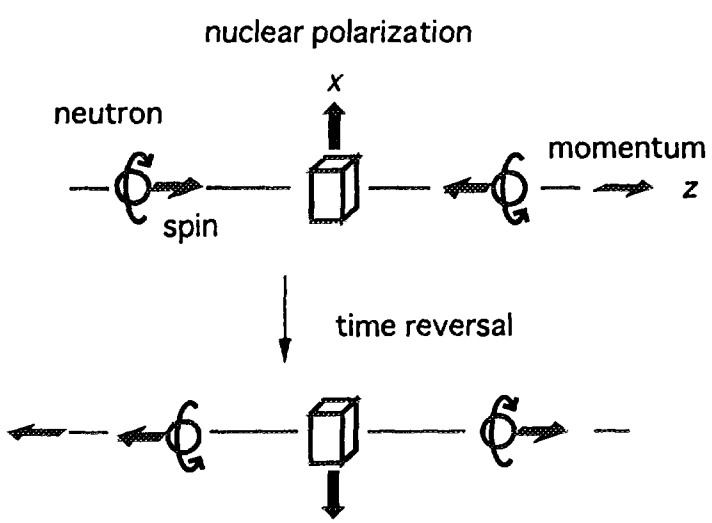

Fig. 2 Spin-flip difference as a measure of T-violation

rotation experiment.[14] He proposed to measure a difference between neutron-spin flips from forward to backward and vice versa upon propagation through the target polarized along the transverse direction (x axis). The two spin-flip processes are time-reversed processes for each other, if the rate of irreversible neutron-absorption is same for the two processes as in the exact alignment shown in Fig. 2, where the incident-neutron polarization and analyzer polarization are antiparallel and both are along the z axis, and the target nuclear spin is along the x axis. Kabir proposed to compare the neutron polarization P with asymmetry A. Following their proposal, experimental possibility was examined at KEK and Los Alamos.[19,20]

In the Stodolsky's and Kabir's proposals, the exact alignment between the neutron spin, neutron momentum and nuclear spin is assumed. However, Lamoreaux and Golub pointed out we can not exclude small misalignment in polarizer, analyzer and target nuclear polarizations in a real experiment.[15] The polarizer, analyzer and target nuclear polarizations are represented as

$$P_O = P_O(\varepsilon_x, \varepsilon_y, 1), \tag{12}$$
$$P_a = P_a(\xi_x, \xi_y, 1), \tag{13}$$
$$P_I = P_I(1, \delta_y, \delta_z). \tag{14}$$

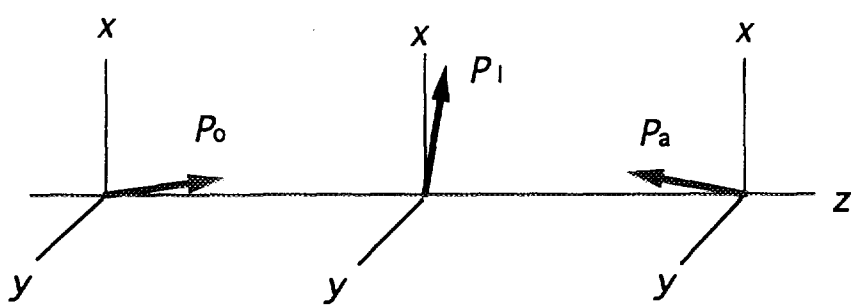

Fig. 3 Misalignments of polarizer, analyzer and target nuclear polarizations

including mixing angles ε, ξ and δ due to the misalignment. (Fig. 3) The difference of spin-flip probabilities is obtained in terms of a density operator and a projection operator,

$$\rho(P_O, \varepsilon_x, \varepsilon_y) = 1/2 \cdot (1 + P_O \cdot \sigma), \tag{15}$$
$$P(P_a, \xi_x, \xi_y) = 1/2 \cdot (1 + P_a \cdot \sigma) \tag{16}$$

and the t matrix. The misalignment of the target-nucleus polarization affects the t matrix through the spin-dependent phase-shift ϕ_i as

$$(\phi_1', \phi_2', \phi_3') = (\phi_1 P_I,\ \delta_y \phi_1 P_I + \phi_2 P_I,\ \delta_z \phi_1 P_I + \phi_3). \tag{17}$$

As a result, the difference of spin-flip probabilities is represented as

$$\begin{aligned}
&R_{+-} - R_{-+} \\
&= \mathrm{Tr}(t\rho(P_o, \varepsilon_x, \varepsilon_y)t\dagger P(-P_a, \xi_x, \xi_y)) - \mathrm{Tr}(t\rho(-P_o, \varepsilon_x, \varepsilon_y)t\dagger P(P_a, \xi_x, \xi_y)) \\
&= \exp(-2\mathrm{Im}(\phi_0)) \\
&\{[2\varepsilon_x P_o - 2\xi_x P_a + 2\varepsilon_y P_o \delta_y - 2\xi_y P_a \delta_y + 2(P_o - P_a)\delta_z] P_I \\
&\qquad \mathrm{Im}[\cos b\ (\sin b/b\ )^*\ \phi_1^*] \\
&\qquad + 2(P_o - P_a)\ \mathrm{Im}[\cos b\ (\sin b/b\ )^*\ \phi_3^*] \\
&+[2\varepsilon_x P_o \delta_y + 2\xi_x P_a \delta_y - 2\varepsilon_y P_o - 2\xi_y P_a] P_I \mathrm{Im}[(\sin b/b)(\sin b/b)^*\ \phi_1 \phi_3^*] \\
&\qquad + 2(P_o + P_a) P_I^2\ \mathrm{Im}[(\sin b/b)(\sin b/b)^*\ \phi_1 \phi_2^*]\ \}.
\end{aligned} \tag{18}$$

Here, $\mathrm{Re}(\phi_1)$ is dominant in b. The $\mathrm{Re}(\phi_1)$ comprises a real magnetic field and a pseudo-magnetic field. In order to increase the sensitivity for the effect of the T-violating term, the neutron spin should be controlled so as to rotate from forward to backward or vice versa. (The neutron-spin manipulation is discussed in chapter IV.) Therefore, the value of $\mathrm{Re}(\phi_1)$ is $\pi/2$ and

$$b = \pi/2 + \delta. \tag{19}$$

$\sin b$ is in the order of 1 and $\cos b$ is in the order of δ. $\mathrm{Re}(\phi_1)\cdot\mathrm{Im}(\phi_3)$ and $\mathrm{Re}(\phi_1)\cdot\mathrm{Im}(\phi_2)$ terms are dominant in the third and fourth term in Eq. (18), respectively, since

$$\mathrm{Im}(\phi_3) \gg \mathrm{Re}(\phi_3) \tag{20}$$
$$\mathrm{Re}(\phi_1) \gg \mathrm{Im}(\phi_1) \tag{21}$$

in the p-wave resonance of ^{139}La at E_n = 0.734 eV. Masuda proposed to reverse the neutron-spin rotation in the target in order to eliminate the misalignment effect.[21] (see Fig. 4) The first and second misalignment terms in Eq. (18) are canceled, since the sign of the $\mathrm{Re}(\phi_1)$ is reversed upon reversing the neutron-spin rotation. The nuclear-polarization reversal cancels the third misalignment term. But, rotation under stray field in the space between the

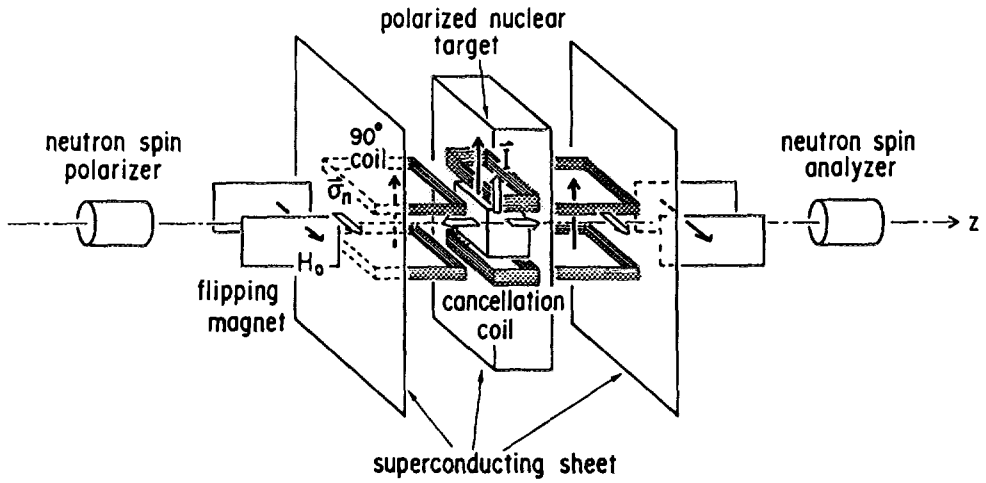

Fig. 4 Experimental scheme of rotation asymmetry

superconducting wall and polarized target gives rise to another misalignment effect. The stray-field effect remains, since the magnetic field is reversed upon the polarization reversal.[20] A 0.1-micron spacing in a 1-kG field gives rise to the misalignment effect which correspond to the error of the ratio of T-violating to P-violating term as

$$\delta\eta \sim 1.5\times10^{-4}. \tag{22}$$

Bowman and Masuda suggested further cancellation for the third term is possible by a 180° rotation of the apparatus around the nuclear polarization. Bowman also suggested a target-inhomogeneity effect is also canceled by the apparatus rotation.

Serebrov proposed to use a ratio of the asymmetry to polarization X,[22]

$$X = A/P\ . \tag{23}$$

This proposal is an extension of the polarization-asymmetry theorem of Kabir. The asymmetry and polarization are represented as

$$A = (R_+ - R_-)/(R_+ + R_-), \tag{24}$$

$$R_+ = R_{++} + R_{+-} = \mathrm{Tr}(t\rho(P_0, \varepsilon_x, \varepsilon_y)t\dagger), \tag{25}$$

$$R_- = R_{-+} + R_{--} = \mathrm{Tr}(t\rho(-P_0, \varepsilon_x, \varepsilon_y)t\dagger), \tag{26}$$

$$R_+ - R_- = \exp(-2\mathrm{Im}(\phi_0))$$
$$\{[2\varepsilon_x P_0 + 2\varepsilon_y P_0\delta_y + 2P_0\delta_z]P_I\,\mathrm{Im}[\cos b\ (\sin b/b\ )^*\ \phi_1^*]$$
$$+ 2P_0\ \mathrm{Im}[\cos b\ (\sin b/b\ )^*\ \phi_3^*]$$

$$+ [2\varepsilon_x P_o \delta_y - 2\varepsilon_y P_o] P_I \, \mathrm{Im}[(\sin b/b)(\sin b/b)^* \, \phi_1 \phi_3^*]$$
$$+ 2P_o \, P_I^2 \, \mathrm{Im}[(\sin b/b)(\sin b/b)^* \, \phi_1 \phi_2^*] \; \}, \tag{27}$$

$$P = (R_{0+} - R_{0-})/(R_{0+} + R_{0-}), \tag{28}$$

$$R_{0+} = R_{++} + R_{-+} = \mathrm{Tr}(P(P_a, \xi_x, \xi_y) tt\dagger), \tag{29}$$

$$R_{0-} = R_{+-} + R_{--} = \mathrm{Tr}(P(-P_a, \xi_x, \xi_y) tt\dagger), \tag{30}$$

$$R_{0+} - R_{0-} = \exp(-2\mathrm{Im}(\phi_0))$$
$$\{[2\xi_x P_a + 2\xi_y P_a \delta_y + 2P_a \delta_z] P_I \, \mathrm{Im}[\cos b \; (\sin b/b)^* \, \phi_1^*]$$
$$+ 2P_a \; \mathrm{Im}[\cos b \; (\sin b/b)^* \, \phi_3^*]$$
$$+ [-2\xi_x P_a \delta_y + 2\xi_y P_a] P_I \, \mathrm{Im}[(\sin b/b)(\sin b/b)^* \, \phi_1 \phi_3^*]$$
$$- 2P_a \, P_I^2 \, \mathrm{Im}[(\sin b/b)(\sin b/b)^* \, \phi_1 \phi_2^*] \; \}, \tag{31}$$

The ratio X is

$$X \cong P_o/P_a \; [\; 1 +$$
$$\{[2(\varepsilon_x - \xi_x) + 2(\varepsilon_y - \xi_y)\delta_y] P_I \, \mathrm{Im}[\cos b \; (\sin b/b)^* \, \phi_1^*]$$
$$+ [2(\varepsilon_x + \xi_x P)\delta_y - 2(\varepsilon_y + \xi_y)] P_I \, \mathrm{Im}[(\sin b/b)(\sin b/b)^* \, \phi_1 \phi_3^*]$$
$$4P_I^2 \, \mathrm{Im}[(\sin b/b)(\sin b/b)^* \, \phi_1 \phi_2^*] \tag{32}$$

The second and third terms in Eq. (32) are misalignment terms, which might be canceled by the polarization reversal. However, the effect of the stray field is also remained. We should also be careful to the following two problems in addition to the stray field. We need to measure transition probabilities between neutron-spin states as shown in Eq. (25,26,29,30). The polarizer and analyzer differences $(R_+ - R_-)$ and $(R_{0+} - R_{0-})$ have suppression factor b as shown in Eq. (27) and (31). The error of the ratio is largely enhanced from the statistical error of the neutron counting for the spin-state transition. Therefore, the sensitivity to detect the T-violating term is greatly reduced. The stability of the polarizer and analyzer polarization is quite important, since the fluctuation of the ratio P_o/P_a directly contributes to the error of the ratio X.

Skoy also extended the polarization-asymmetry theorem.[23] He proposed to use the same polarization device for the analyzer as for the polarizer by rotating the polarization device around the axis of $\boldsymbol{k} \times \boldsymbol{I}$. The analyzer polarization becomes

$$\boldsymbol{P}_a = (-\varepsilon_x P_o, \varepsilon_y P_o, -P_o). \tag{33}$$

The sum of the polarizer and analyzer differences, which are represented in Eq. (27) and (31), cancels almost all misalignment terms except the effect of the stray field as

$$(R_+ - R_-) + (R_{0+} - R_{0-}) = \exp(-2\mathrm{Im}(\phi_0))$$
$$\{ \; 4\varepsilon_y P_o \delta_y P_I \, \mathrm{Im}[\cos b \; (\sin b/b)^* \, \phi_1^*]$$

$$+ 4\varepsilon_x P_0 \delta_y P_I \ \mathrm{Im}[(\sin b/b)(\sin b/b)^* \ \phi_1 \phi_3^*]$$
$$+ 4 P_0 P_I^2 \ \mathrm{Im}[(\sin b/b)(\sin b/b)^* \ \phi_1 \phi_2^*] \ \}. \qquad (34)$$

In this experiment, we should take care of the misalignment of the rotation axis in addition to the effect of the stray field, since the cancellation in the sum assumes the same misalignment-parameters for the analyzer as for the polarizer. Although the setting of the rotation axis is accurate, the misalignment parameter has a different value due to the error of the nuclear polarization direction. He also proposed to take a ratio $\{(R_+ - R_-) + (R_{0+} - R_{0-})\}$ / $\{(R_+ - R_-) - (R_{0+} - R_{0-})\}$ to eliminate the suppression factor b. However the error is enhanced in the ratio, if the value of b is small.

The accuracy of the ratio of the T-violating to P-violating effect, η is limited by the misalignment between the neutron spin, neutron momentum and nuclear spin. The present limit corresponds to the accuracy of the neutron EDM of 10^{-25} cm. A new method is required to improve the limit of the T-violation. The apparatus rotation may give a solution.

[1] F.C. Michel, Phys. Rev. B133(1964)329.
[2] M. Forte, "Fundamental Physics with Reactor Neutron and Neutrino", ed. T. Egidy, Institute of Physics, Conference Series 42(1978)86.
[3] M. Forte et al., Phys. Rev. Lett. 45(1980)2088.
[4] O.P. Sushkov and V.V. Flambaum, Sov. Phys. Usp. 25(1982)1.
[5] V.E. Bunakov and V.P. Gudkov, Nucl. Phys. A401(1983)93.
[6] V.P. Alfimenkov et al., Nucl. Phys. A398(1983)93.
[7] Y. Masuda et al., Nucl. Phys. A504(1989)269.
[8] C.D. Bowman, J.D. Bowman and V.W. Yuan, Phys. Rev. C39(1989)1721.
[9] Y. Masuda, "Weak and electromagnetic interactions in nuclei", ed. H. Ejiri, T. Kishimoto and T. Sato, World Scientific (1995)58; K. Sakai et al., to be published.
[10] L. Stodolsky, Nucl. Phys. B197(1982)213.
[11] P.K. Kabir, Phys. Rev. Lett. 60(1988)686; Phys. Rev. D25(1982)25;
[12] V.E. Bunakov and V.P. Gudkov, Z. Phys. A308(1982)363.
[13] P. Herczeg, Hyperfine Interactions 75(1992)127.
[14] L. Stodolsky, Physics Lett. B172(1986)5.
[15] S.K. Lamoreaux and R. Golub, Phys. Rev. D50(1994)5632.
[16] E.G. Adelberger, J. Phys Soc. Jpn 54(1985)Suppl. I, 6.
[17] N.D. Bhaskar, W. Happer and T. McClelland, Phys. Rev. Lett. 49(1982)25.

[18] Y. Masuda et al., Nucl. Phys. A478(1988)737c.
[19] J.D. Bowman, "Tests of Time Reversal Invariance in Neutron Physics" World Scientific (1987)121.
[20] Y. Masuda et al., Hyp. Int. 74(1992)149.
[21] Y. Masuda, "Dark Matter in Cosmology, Clock and Tests of Fundamental Laws" Editions Frontieres(1995)605.
[22] A.P. Serebrov, JETP Lett. 58(1993)14.
[23] V.R. Skoy to be published in Proc. VII School on Neutron Physics in Ratmino, 1995.

T-VIOLATION AND NEUTRON OPTICS EXPERIMENTS

A.P.Serebrov

St.Petersburg Nuclear Physics Institute, 188350 Gatchina, Russia

(Received)

KEYWORDS: T-violation, neutron optics, ultracold neutrons

Neutron optics give the possibility to test T-violation, being in fact the method of comparison between the forward and backward reactions. This possibility arises due to the neutrons spin, when the neutron helicity in initial state and in the final state are opposite. The probabilities of processes with changing of helicity will be differed from each other only at T-violation. Neutron helicity can be changed by two ways: 1) changing of spin direction at the forward scattering; 2) changing momentum direction (backscattering) at the same spin direction. The both cases are shown in Fig.1, where the first one correspond to spin-flipp at the transmission, the second one correspond to the backscattering. The right part of picture can be transformed from the left one by means of time-reversal operation and rotation.

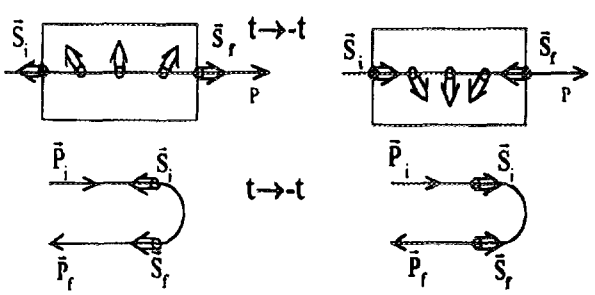

Fig. 1. The processes with the changing of neutron helicity at the forward scattering and the back scattering

The first case was discussed many times in relation with possible experiment searching for T-violation in transmission of polarized neutrons though the polarized target[1-3]. The second case is the subject of our consideration.

As it is well known P- and T-violating processes can be significantly increased near by p-wave compound nuclear resonances due to mixing of the states with opposite parity. The amplitudes of P,T-violating process can be written in the following form:

$$f_1^{P,T} = \frac{i\lambda < w > \vec{S}[\vec{P} \times \vec{I}]}{(E - E_s + i\Gamma_{s/2})(E - E_p + i\Gamma_{p/2})}, \quad (1)$$

$$f_2^{P,T} = \frac{i\lambda < w > (\vec{S}\vec{q})}{(E - E_s + i\Gamma_{s/2})(E - E_p + i\Gamma_{p/2})}. \quad (2)$$

Formula (1) describes the spin-flipp process, formula (2) - backscattering process. Both amplitudes are proportional to T-violating parameter $-i\lambda$, matrix element of weak interaction - $< w >$ and resonance factor defined by parameters of s-wave resonance and p-wave resonance - their energy positions (E_s, E_p) and widths (Γ_s, Γ_p), whereas the forms of correlations are distinguished, $\vec{S}$ - neutron spin, $\vec{P} = \vec{P}_i + \vec{P}_f$, $\vec{q} = \vec{P}_f - \vec{P}_i$, where $\vec{P}_i$ and $\vec{P}_f$ are initial and final neutron momentum, I - nuclear polarization.

It should be mentioned that the polarized nuclear target is not required at the search for T-violating amplitude $f_2^{P,T}(\vec{S}\vec{q}$ -correlation), what is rather attractive experimentally. However, there are the same kind of problems for $(\vec{S}\vec{q})$ - correlation like for $\vec{S}[P \times I]$ - correlation because of other correlations: $\vec{S}(\vec{P}_i + \vec{P}_f)$- correlation caused by weak interaction and $\vec{S}[\vec{P}_i \times \vec{P}_f]$ - correlation, caused by strong interaction. These tree correlations are at right angles to each other as shown in Fig.2.

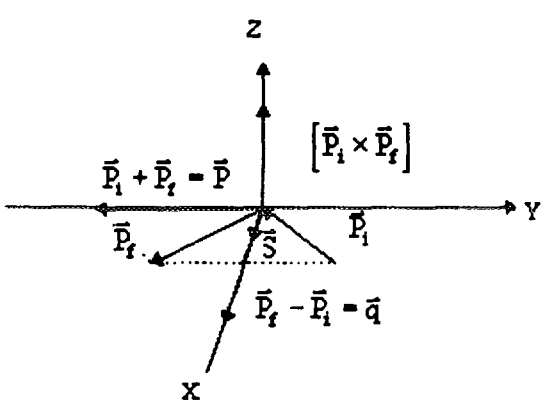

Fig. 2. Vector diagram of the scattering process

Any deviations of the vector of neutron polarization from the direction of $\vec{q}$ -vector will cause the false effects. Fortunately the direction of neutron polarization can be oriented with rather high accuracy, namely with accuracy of homogeneity of magnetic field at the target position, for instance, $10^{-4} \div 10^{-5}$ rad. If the crystal is chose as the target, the direction of transfer momen-

tum $\vec{q}$ can be oriented with accuracy of crystal mosaic ($10^{-4} \div 10^{-5}$rad). At the changing of direction of polarization (direction of magnetic field) with respect to vector $\vec{q}$ it is possible to extract effect of T-violation *due to $\vec{S}\vec{q}$- correlation. There is very important circumstance* that energy dependence of correlations is different. T-violating amplitude has factor $i\lambda$, therefore energy dependence of real part of T-violating correlation corresponde to energy dependence of imaginary part of P-violating correlation and vice versa.

Below the three possible scheme of neutron optics experiments to search T-violation will be considered.

I. The crystal of ^{139}La or its compounds can be the object for T-violation experiment because of possibility of resonance enhancement near by the p-wave resonance 0.74 eV.

The influence of T-violating ($\vec{S}\vec{q}$)- amplitude for dynamic diffraction on the perfect crystal is the question which should be considered specially. However, the simplest experimental scheme can be proposed for mosaic crystals, when extinct length and thickness of single crystal in the sample are the same order of magnitude. This scheme is shown in Fig.3.

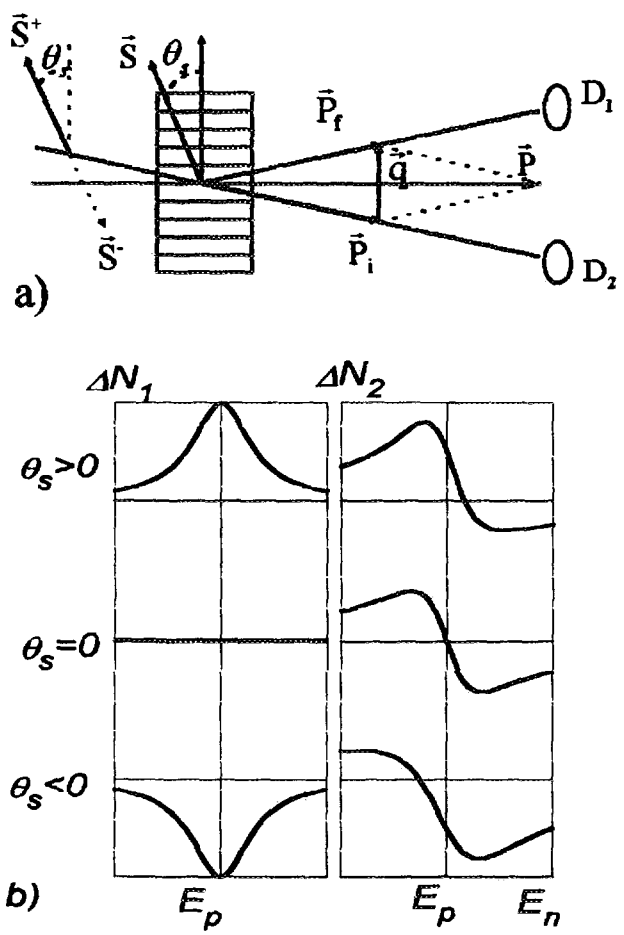

Fig. 3. Experiment to search T-violation in the Bragg scattering; a) experimental scheme: D_1 - detector, D_2 - monitor; b) energy dependences of experimental effects ΔN; ΔN_1 – when P-violation only, ΔN_2 – when P-violation and T-violation

The counting rate of the detector D_1 (reflected beam) is measured at the changing of sign of neutron beam polarization. The vector of polarization and normal vector to crystal planes should be parallel. Deviation between *the vector of neutron polarization and the normal vector* to crystal planes brings $\vec{S}(\vec{P}_i + \vec{P}_f)$ - effect which change the sign when the changing sign of deviation. Energy dependence and changing of its form are shown in Fig.3b, left part. If T-violating effect exists the distortion of left picture will arise as shown in Fig.3b, right part. Firstly, the energy dependence changes the sign at the resonance energy when $\Theta_s \simeq 0$, secondly, there are deviation from symmetrical form for p-violating effect at the $\Theta_s \neq 0$. Unfortunately, $\vec{S}[\vec{P}_i \times \vec{P}_f]$ - correlation has the same energy dependence near the resonance as the T-violating $\vec{S}\vec{q}$ - correlation, therefore only high precision in the orientation of neutron polarization (guiding magnetic field) with respect to normal vector to the crystal planes could help to solve this problem.

The descripsion of expected effects was done analyzing the energy dependence of imaginary part of T-violating amplitude which define the transmission effect, the contribution of real part of amplitude was considered as the small correction.

II. *Let us consider the possibility to search* T-violation in neutron optics experiments by means of interferometers based on the perfect crystal. The classic scheme of interferometer developed by spin-flippers to work with polarized beam are shown in the Fig.4. Simultaneous switching on (of) the flippers F_1, F_3 or F_2, F_4 allow us to change the sign $\vec{S}\vec{q}$ - correlation between upper and lower interferometer branches. Flipper F_0 can be used to change the sign of observed effect.

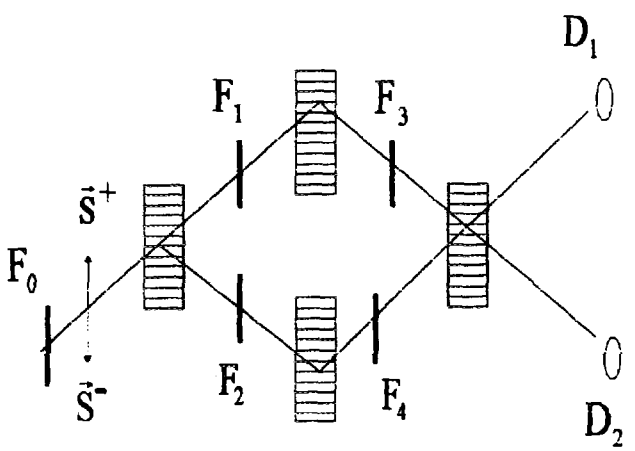

Fig. 4. 'Scheme of interferometer based on the perfect crystal. F_0, F_1, F_2, F_3, F_4 - flippers, D_1, D_2 - detectors

This scheme allows us also to study P-violating $\vec{S}(\vec{P}_i + \vec{P}_f)$- correlation and strong $\vec{S}[\vec{P}_i \times \vec{P}_f]$- correlation at the corresponding direction of neutron polarization. Unfortunately, the experimental scheme is restricted in the choice of studied materials.

III.A. At last let us take a look at the possibility to search T-violation at the reflection of ultracold neutrons (UCN) from the material surface.

Fig.5a) show UCN trap placed in magnetic field with strong divergence. UCN polarization keep track of magnetic field at the UCN storage in the trap. The average value for $\vec{S}\vec{q}$- correlation is not equal to zero due to strong divergence of magnetic field whereas the average values for $\vec{S}(\vec{P}_i + \vec{P}_f)$ - correlation and for $\vec{S}[\vec{P}_i \times \vec{P}_f]$ - correlation is equal to zero because of repeated collisions with the trap walls. Thus the search for T-violating effect is the measurement of UCN storage time in the trap at the different sign of magnetic field (τ_+, τ_-). There are no problem with false effect due to weak and strong correlations ($\vec{S}(\vec{P}_i+\vec{P}_f)$ and $\vec{S}[\vec{P}_i \times \vec{P}_f]$), but transfer momentum $(\vec{q})$ is very small, what suppress the expected effects.

The experimental scheme is shown in Fig.5b. Superconducting solenoid provide the polarization of UCN came in trap. The divergence of magnetic field at the end of solenoid provides simultaneously the necessary configuration of magnetic field. The dependence of UCN storage time from the sign of current in the solenoid (τ_+, τ_-) is measured to observed T-violation.

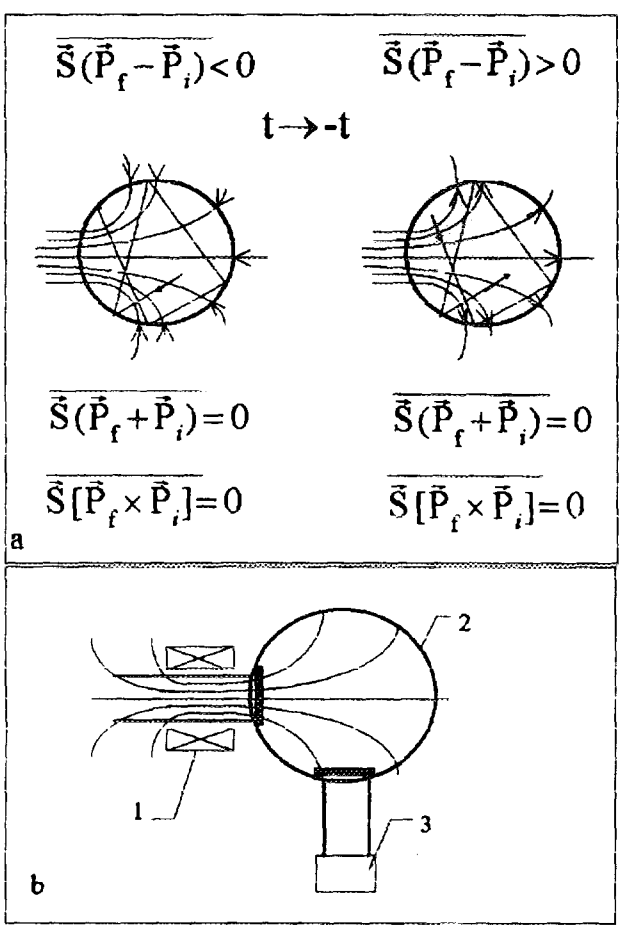

Fig. 5. T-violation at the UCN reflection; a) UCN trap in magnetic field with strong divergence; b) experimental scheme: 1 - super conducting solenoid; 2 - UCN-trap; 3 - UCN detector

The estimation of possible effect due to nuclear absorption shows that the value $(\tau_+ - \tau_-)/(\tau_+ + \tau_-)$ could be about $10^{-5}\lambda$, where λ - parameter of T-violation. The possible experimental accuracy for τ is restricted by 10^{-5}, therefore the range $10^{-3} \div 10^{-4}$ for λ, which is interesting for T-vilation problem, is not yet achieved now. However the estimation was done for nuclear absorbtion, another part of UCN losses in the trap is happened due to upscattering cross sections at the interaction of UCN with solid state. T-violation at the neutron interaction with solid state is the question which require the special consideration and is a valid one for direct experimental investigation. High density of states for the system neutron and solid state allowed to look forward for enhancement of the P and T- violating effects like nuclear enhancement mechanism observed experimentally.

III.B. The experiment to search P-violation at the neutron reflection from the material surface can be realized by the experimental scheme shown in Fig.6. Multislit

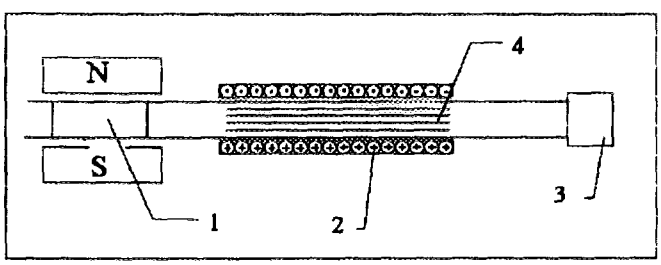

Fig. 6. Experimental scheme to search P-violation at the neutron reflection from the material surface. 1 - polarizer, 2 - solenoid, 3 - detector, 4 - multislit neutron guide coated by the studied material

neutron guide system with coating from studied material is connected to polarize with transverse magnetic field. The solenoid with longitudinal magnetic field provides the best condition for $\vec{S}(\vec{P}_i + \vec{P}_f)$ - correlation. The changing of detector counting rate is measured at the changing of current direction in the solenoid.

Concluding one would like to remark that the problem of P and T- violation in neutron optics is not practically developed, the aim of the publication is to attract the attention of experts to the interesting physics problem and to more in-depth study of the questions which were touched on in the article.

1) Y.Masuda, T.Adachi, A.Masaike et al. Nucl. Phys.,A **504**. 269. 1989.
2) C.D.Bowman, J.D.Bowman, V.W.Yuan et al. Phys. Rev. C **39**. 1721. 1989.
3) A.P.Serebrov. JETP. Lett. **53**. 14. 1993.

Development of polarized ^{3}He filter for polarized neutron experiment

K. Sakai[a)], H. Sato[a)], A. Yoshimi[a)], K. Asahi[a)], Y. Masuda[b)], S. Muto[b)]
S. Ishimoto[b)] and K. Morimoto[b)]

[a)] Dept. of Applied Physics, Tokyo Inst. of Tech., Meguro-ku, Tokyo, 152, Japan
[b)] National Laboratory for High Energy Physics (KEK), Oho,Tsukuba, 305, Japan

Abstract

A high-pressure polarized ^{3}He gas cell, pumped with two diode lasers, has been developed at KEK for use as a polarizer and a spin analyzer for low energy neutrons. The polarization attained of ^{3}He was determined through the measurement of the transmission of the unpolarized neutrons through the ^{3}He cell. So far we obtained $P_{\rm He} = 18\%$ at 10 atm and $P_{\rm He} = 12\%$ at 20 atm.

1 Introduction

Neutron-nucleus scattering at low energies is a promising tool for the study of violation of fundamental symmetries. For example, the measurement of $\boldsymbol{s}\cdot\boldsymbol{k}$ and $\boldsymbol{s}\cdot(\boldsymbol{k}\times\boldsymbol{I})$ correlations allows us to study the violation of parity (P) and time reversal invariance (TRI). Here the symbols $\boldsymbol{s}$, $\boldsymbol{k}$ and $\boldsymbol{I}$ denote the spin, momentum of a neutron, and the spin of a target nucleus. Although such effects of symmetry violations are small in the nucleon-nucleon level [1], recent experimental and theoretical studies [2-7] have shown that the P-violating effect is enormously enhanced in neutron-nucleus resonances. The same enhancement is expected to occur in effects of the TRI violation [8, 9, 10].

In order to observe the symmetry-violation effects in neutron-nucleus scattering, polarization and analysis of the spin of neutrons are the key experimental techniques. A gas of polarized ^{3}He provides a great advantage in such techniques [11] because of its large cross section ($\sigma = 820$ b at $E = 1.0$ eV) and its strong spin selectivity due to presence of the ^{3}He+n ($J^\pi = 0^+$) resonance state at $E = -518$ keV. By passing through a gas of ^{3}He with polarization $P_{\rm He}$, neutrons get polarized. The polarization $P_{\rm n}$ of neutrons thus attained and the neutron transmittance $T_{\rm n}$ of the ^{3}He system are described as

$$P_{\rm n} = \tanh(N\sigma P_{\rm He} l), \quad (1)$$

$$T_{\rm n} = e^{-N\sigma l}\cosh(N\sigma P_{\rm He} l), \quad (2)$$

where N and l denote the number density of atoms and the thickness of ^{3}He gas. The figure of merit for polarizing or analyzing the neutron spins in spin-correlation measurements should

be given by $Y_n = T_n P_n^2$. Figure 1 shows calculated values of Y_n for l = 8 cm, as a function of the incident neutron energy E for three different values of ^{3}He gas pressure. In the case of $P_{He} \sim 60\%$, Y_n takes values as large as 0.17 at peak, which is well compared with the performance of the currently operating neutron polarizer at KEK, the polarized proton filter ($Y_n \sim 0.18$) [12]. Thus the scheme of polarizing neutrons by means of the polarized ^{3}He cell is capable of producing larger Y_n by selecting the pressure of ^{3}He gas.

For use as a spin analyzer, we previously reported on the development of a polarized ^{3}He cell at 3 atm pressure in which polarization of $P_{He} \sim 40\%$ was obtained by optically pumping with Ti-Sapphire (Sa) lasers [13]. According to the behavior of Y_n shown in Fig. 1, however, the previously employed pressure of 3 atm is not the optimum values if one considers a measurement of the symmetry violating spin correlation in the eV energy range where the p-wave neutron-nucleus resonances are located. For the polarization of a high pressure ^{3}He gas, the pumping with a diode laser is much more efficient by a Ti-Sa laser, as shown in the next section. This paper reports the present status of the development of polarized ^{3}He cell with diode lasers at KEK.

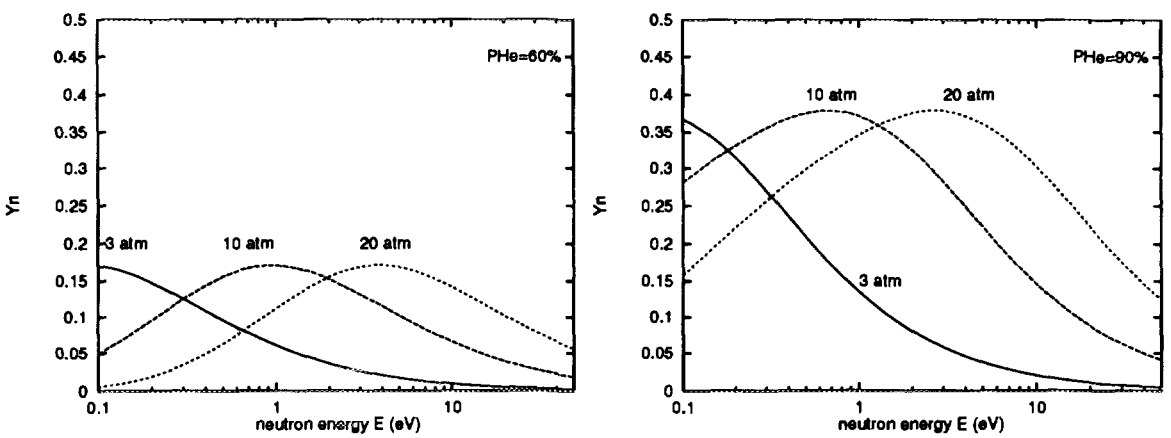

Fig. 1: Calculated values of figure of merit Y_n as a function of incident neutron energy E from 0.1 eV to 50 eV, where ^{3}He polarisation P_{He} and the length of ^{3}He cell l are fixed (P_{He} = 60%, 90% and l = 8 cm). Three kinds of lines represent the difference of ^{3}He gas pressure (3, 10 and 20 atm).

2 Principle of ^{3}He polarization with diode lasers

^{3}He nuclear spins are polarized by spin exchange with optically polarized Rb atoms [14, 15, 16]. Rb atomic spins, in turn, are polarized by resonance absorption of circularly polarized laser light of 795 nm wave length. By irradiating Rb vapor with a circularly polarized light ϕ_+ whose quanta have the magnetic projection +1, only the excitation of atoms in the $5S_{1/2}$, m=$-1/2$ state to the $5P_{1/2}$, m=$+1/2$ state can take place. Unpolarized light from the $5P_{1/2}$ state is quenched with buffer gas. In the presence of buffer-gas collisions, the $5P_{1/2}$ states are mixed and the branching ratios of the decays to the two $5S_{1/2}$ magnetic sublevels become 1/2 each. The absorption of two circularly polarized photons thus implies the transfer of a single unit of

angular momentum, and as a result, Rb atoms are polarized. The polarization in Rb atoms is transferred to ^{3}He nuclei through the spin exchange interaction. The polarization $P_{\rm He}$ of ^{3}He thus attained and the average Rb polarization, $P_{\rm Rb}$, by the optical pumping method can be described as

$$P_{\rm He} = P_{\rm Rb}\frac{\gamma_{\rm se}}{\gamma_{\rm se}+\Gamma_{\rm W}} \tag{3}$$

$$P_{\rm Rb} = \int \frac{\gamma^+_{\rm opt}}{\gamma^+_{\rm opt}+\Gamma_{\rm sd}}dx. \tag{4}$$

Here $\gamma_{\rm se}$ denotes the spin exchange rate between Rb atoms and ^{3}He nuclei, $\Gamma_{\rm W}$ the relaxation rate of ^{3}He polarization, $\Gamma_{\rm sd}$ the spin destruction rate of Rb atoms and $\gamma^+_{\rm opt}$ is the optical pumping rate of Rb atoms by circularly polarized light ϕ_+. $\gamma^+_{\rm opt}$ is given as $\gamma^+_{\rm opt} = I^+_\nu\sigma_0$, where I^+_ν is the flux of ϕ_+, while σ_0 which has a form of Lorentzian curve as a function of the light frequency ν ($= c/\lambda$; c and λ are the velocity and wave length of light) represents the resonance absorption cross section of the linear polarized light ϕ_0. According to Eqs. (3) and (4), the conditions $\Gamma_{\rm W}/\gamma_{\rm se} \ll 1$ and $\Gamma_{\rm sd}/\gamma^+_{\rm opt} \ll 1$ are required for getting a large value of $P_{\rm He}$.

In the case of polarizing the high pressure ^{3}He cell, we should consider two effects caused by the increase of ^{3}He pressure. One is a broadening of the Rb absorption line as shown in Fig. 2 [15].

This effect results in a decrease of $\gamma^+_{\rm opt}$. The other is the increase of $\Gamma_{\rm sd}$ due to three body (Rb-^{3}He-^{3}He) collisions. As a result, $P_{\rm Rb}$ decreases rapidly with increasing $\Gamma_{\rm sd}/\gamma^+_{\rm opt}$. For example, the full width at half maximum (FWHM) of σ_0 in Fig. 2 increases from $\Delta\lambda \sim$ 0.04 nm at 3 atm to $\Delta\lambda \sim$ 1 nm at 20 atm. Thus in the case of polarizing the high pressure cell, a large power and $\Delta\lambda$ are desirable. In such a situation, a diode laser is suited to polarization of a high pressure cell because $\Delta\lambda$ and power $I_{\rm w}$ is large ($\Delta\lambda \sim 3$ nm and $I_{\rm w} \sim 20$ W/set in one case) in comparison with those of Ti-Sa laser ($\Delta\lambda \sim 0.04$ nm and $I_{\rm w} \sim 4$ W/set). At present we use diode lasers instead of Ti-Sa lasers for polarizing a high pressure ^{3}He cell.

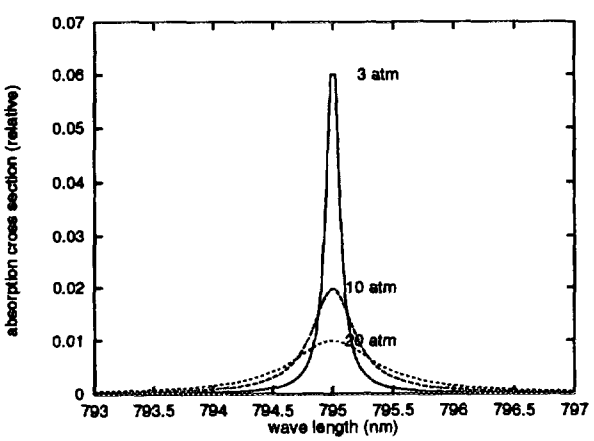

Fig. 2: Pressure broadening effect of the resonance absorption cross section σ_0 of the linear polarised light. Three kinds of lines represent the difference of ^{3}He gas pressure (3, 10 and 20 atm).

3 Experimental procedure and the result

The experimental setup for ^{3}He polarization is shown in Fig. 3 [13]. A gas of ^{3}He is contained in a cylindrical glass cell 2.5 cm in diameter, 8 cm long. The cell also contains in a N_2 gas of 100 torr and a small amount of Rb. The cell was produced in the following procedure. Two pieces of glass cells and a branch of glass tube to which they were jointed were washed. They

were put in an oven and baked for 5 days at a temperature of $\sim$ 480 K by pumping the inner volume of the branch cell system to $\sim 10^{-7}$ torr. Then after filling them with Rb, N_2 and ^{3}He gases, the cells were cut off from the branch by using a gas burner. In order to control ^{3}He quantity, the cell temperature and the ^{3}He pressure were kept within the respective ranges of 8–20 K and 150–300 torr throughout gas filling procedure.

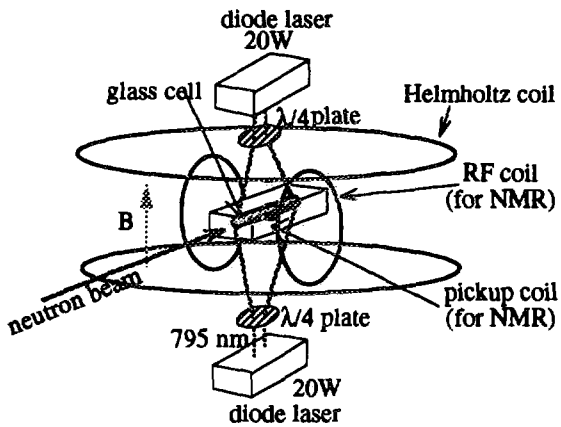

Fig. 3: The experimental setup for the ^{3}He polarisation.

A cell thus obtained was mounted in a oven made of vespel which was placed at the center of a Helmholtz coil in Fig. 3. In order to keep the Rb atomic number density at 10^{14}cm^{-3} for the optimum spin exchange rate, hot air flow was introduced to the oven. Linearly polarized lights from diode lasers were transformed to circularly polarized lights by passing through $\lambda/4$ plates, which then illuminated the cell. Around the cell, a pair of radio-frequency (RF) coils and a pickup coil were mounted for measuring NMR signal with the adiabatic fast Passage (AFP) method.

The polarization of ^{3}He was experimentally determined by measuring the unpolarized neutron transmission through the cell. For the measurement we used a pulsed neutron beam from the spallation source at KEK. The neutron energy E was determined by the time-of-flight (TOF) method. The neutron transmission through the cell was measured by counting the transmitted neutrons with a ^{10}B loaded liquid scintillator placed downstream of the cell. The intensity of the incident neutrons was monitored with BaF scintillators, which detected γ-rays from In(n,γ) reaction induced in a In foil placed upstream of the cell. According to Eq. (2), the ratio R between the neutron transmissions with ^{3}He polarized and unpolarized is given as

$$R = \cosh(N\sigma P_{\mathrm{He}} l). \tag{5}$$

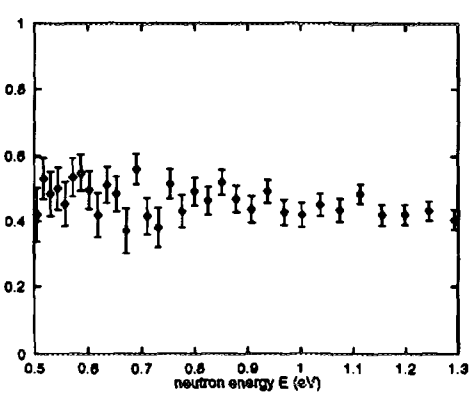

Fig. 4: Typical values of $f = N\sigma P_{\mathrm{He}} l$ as a function of neutron energy E

Thus, by reversing the relation (5), the quantity $f = N\sigma P_{\mathrm{He}} l$ can be determined from the measurement of R. The experimental f thus obtained is plotted in Fig. 4 as a function of the neutron energy E. Furthermore, the quantity $N\sigma l$ can be independently determined by comparing the neutron transmissions measured with the unpolarized ^{3}He and with the cell empty. The experimental f was decided by the $N\sigma l$ values to obtain the experimental P_{He}.

The results are listed in Table 1 together with the P_{He} calculated from Eqs. (3) and (4). Table 1 also includes the relaxation time of ^{3}He, τ ($=1/\Gamma_W$) obtained from measured NMR signals. There are large discrepancy between the experimental and calculated P_{He} values, but the reason is presently not known.

Cell N.O.	τ (h)	^{3}He pressure (atm)	P_{He}(obs) %	P_{He}(cal) %
N.O. 1	11.6	9.6 ± 0.3	17.7 ± 2.1	48
N.O. 2	9.0	19.2 ± 0.7	12.0 ± 1.6	40
N.O. 3	11.4	19.3 ± 0.9	12.3 ± 1.4	45

Table. 1: The result of the neutron transmission experiment. τ denotes the relaxation time of ^{3}He polarisation, P_{He}(obs) the observed value of ^{3}He polarization, P_{He}(cal) the calculated value of ^{3}He polarization.

Summarizing, a polarized ^{3}He cell with diode-laser pumping was developed at KEK for use as a neutron polarizer and spin analyzer for eV-energy neutrons. Diode lasers were shown to be quite suitable for the polarization of a high pressure ^{3}He gas. From the measurement of the transmission of unpolarized neutrons, the ^{3}He polarization of $P_{He} = 18\%$ at 10 atm and $P_{He} = 12\%$ at 20 atm were obtained. Diode lasers have several superior points concerning the cost performance, machine maintenance and miniaturization. By activing a larger P_{He} and higher ^{3}He gas pressure, a compact and movable analyzer/polarizer for low energy neutrons can be realized, which by no doubt should make an important contribution in the study of the fundamental symmetries.

We express our thanks to the staff members of the KEK Booster Facility for their supports. We are grateful to M. Iinuma, Y. Matsuda, K. Okumura and T. Haseyama for their valuable discussion and suggestions. We also thank J. Kura, M. Doi, M. Harada, P.P.J. Delheij and Y. Mori in the development of the polarized ^{3}He filter.

References

[1] R. Balzer et al., Phys. Rev. C30, 1409(1984).

[2] O.P. Sushkov et al., Sov. Phys. Usp. 25, 1 (1982).

[3] V.E. Bunakov et al., Z. Phys. A 303, 285 (1981).

[4] D.F. Zaretskii et al., Sov. J. Nucl. Phys. 37, 3 (1983).

[5] V.P. Alfimenkov et al., Nucl. Phys. A 398, 93 (1983).

[6] Y. Masuda et al., Nucl. Phys. A 478, 737 (1988).

[7] C.D. Bowman et al., Phys. Rev. C 39, 1721 (1989).

[8] V.E. Bunakov et al., Z. Phys. A308, 363 (1982).

[9] L. Kabir, Phys. Rev. D 25, 25 (1982).

[10] L. Stodolsky, Phys. Lett. B 172, 5 (1986).

[11] K.P. Coulter et al., Nucl. Instr. Meth. A 270, 90 (1988).

[12] Y. Masuda et al., Nucl. Instr. Meth. A 264, 169 (1988).

[13] H. Sato et al., Hyp. Int. 84, 205 (1994).

[14] M. E. Wagshul et al., Phys. Rev. A 40, 4447 (1989).

[15] B. Larson et al., Phys. Rev. A 44, 5, 3108 (1991).

[16] W. Happer et al., Phys. Rev. A 29, 3902 (1984).

Plans for an Ultra Cold Neutron Source at Los Alamos

Susan J. SEESTROM, Thomas J. BOWLES, Roger HILL, and Geoffrey L. GREENE,
Los Alamos National Laboratory, Los Alamos, NM 87545, USA

Ultra Cold Neutrons (UCN) can be produced at spallation sources using a variety of techniques. To date the technique used has been to Bragg scatter and Doppler shift cold neutrons into UCN from a moving crystal. This is particularly applicable to short-pulse spallation sources. We are presently constructing a UCN source at LANSCE using method.. In addition, large gains in UCN density should be possible using cryogenic UCN sources. Research is under way at Gatchina to demonstrate technical feasibility of be a frozen deuterium source. If successful, a source of this type could be implemented at future spallation source, such as the long pulse source being planned at Los Alamos, with a UCN density that may be two orders of magnitude higher than that presently available at reactors.

1. Introduction

The coherent scattering of low energy neutrons can be described by an index of refraction. The index of refraction n is a function of the coherent scattering length b of the medium and the neutron energy E:

$$n^2 = 1 - \frac{2\pi\hbar^2\rho b}{mE} .$$

At a given energy neutrons will be totally externally reflected for glancing angles of incidence satisfying Snells law for an angle of zero in the medium. Because the index of refraction is energy dependent, there exists for most materials an energy below which neutrons are totally externally reflected for all angles of incidence. This typically occurs for neutron velocities below 5-7 m/sec (500 Å), and these neutrons are called ultra cold. This leads to the possibility that UCN can be totally confined within a bottle for periods in excess of 100 seconds, making a compact source of stored neutrons for use in measurements of fundamental physics.

An area in which UCN have had and will continue to have a great impact is the study of neutron beta decay. Neutron beta decay is the simplest example of a nuclear beta decay, and one whose interpretation is not plagued by uncertainties in nuclear structure. The comparison of neutron lifetime, neutron beta-decay asymmetry, and decay rates for nuclear super-allowed beta decays can be used to test the Minimal Standard Model (MSM) prediction of V-A structure of the weak interaction. Neutron data of sufficient accuracy can be used to determine the weak vector and axial vector coupling constants G_V and G_A independent of the information from nuclear decays. The ability to make neutron lifetime measurements using both cold neutron beams and stored UCN was an important advantage in understanding the systematic effects in these measurements. We believe UCN will be similarly important in measurements of the various decay correlations in neutron beta decay.

2. UCN Rotor Sources

The highest UCN density to date has been achieved at the ILL reactor by converting cold neutrons into UCN by multiple reflection from the rapidly moving blades of a turbine. This technique involves Doppler shifting 40–50-m/s neutrons down into the UCN regime (< 8 m/s) and can make effective use of the high cold neutron flux from cold moderators at reactors to provide continuous beams of UCN. This device has produced measured UCN densities of 87 UCN/cm^3, a world record. [1] The ILL source first gravitationally decelerates the cold neutrons in an 18-m vertical guide tube between the liquid deuterium moderator and the turbine converter. This novel approach substantially reduces the losses in the transport of the cold neutrons as thick windows in the guide tube can be avoided and transport losses are less due to the smaller number of average reflections necessary for a neutron to reach the turbine. Thus, the ILL source provides the benchmark that other sources must be compared to.

The considerations for UCN production at a spallation source are quite different from a reactor. In a spallation source, a proton beam strikes a high-Z target in which approximately 1 neutron per 30 MeV of beam power (compared to about 180 MeV for a reactor) is produced. [2] These fast neutrons are then thermalized and cooled in a variety of moderators. For UCN production, the spallation neutrons must be first moderated in a liquid hydrogen moderator. We will discuss UCN production at two different types of spallation sources: short pulse (SPSS) and long pulse (LPSS) spallation sources. The SPSS is characterized by facilities like LANSCE, ISIS, and IPNS where the proton pulse is typically a few microseconds or less. In this case, the pulse width of cold neutrons is determined by the moderator. At a LPSS, the pulse width may range from a millisecond to continuous wave (cw). In this case, the pulse width of the cold neutrons is dominated by the pulse width of the proton beam. A LPSS is characterized by either SINQ (cw) or the proposal at LANSCE to construct a 1-MW spallation source using the beam directly from the LANSCE accelerator.

At a SPSS, the high-energy spallation neutrons are not fully moderated and at present, the time-averaged flux is at least an order of magnitude less than that at the ILL reactor. However, one can take advantage of the pulsed nature of the source to produce and store UCN at the peak intensities available, which are comparable to or can exceed that at a reactor. A technique for doing this was demonstrated many

years ago at the ZING-P' source at Argonne National Laboratory [3] and at a test setup at LANSCE. This technique involves Doppler-shifted Bragg scattering of neutrons to convert 400-m/s neutrons down into the UCN regime. A rotor carrying a scattering crystal (for example, Mica) moves away from the neutron pulse from the liquid hydrogen moderator at one half of the velocity of the neutrons that will be converted into the UCN regime. The rotor velocity required is determined by the Bragg scattering condition associated with the lattice spacing of the crystal. For mica one reflects 199 m/s neutrons in the center of mass frame; the incident neutrons are reflected back from the crystal with the same velocity at which they impinge on the crystal. In the laboratory frame, the 398 m/s neutrons are stopped. Thus, a puff of UCN is produced which then begins to expand. Some fraction of the UCN cloud will drift into a guide tube placed close to the position at which the rotor intersects the neutron beam. A shutter at the entrance to the guide tube opens while the puff is expanding and closes after a few ms. Thus, it is possible to bottle the UCN at the peak flux rather than the average flux. The penalty paid is that the filling time will be longer at a SPSS than at a reactor. However, for a rather wide range of experiments, this is not a serious concern.

At Los Alamos, we are installing such a rotor converter on the existing LANSCE cold moderator. The moderator is a gadolinium-decoupled liquid para-hydrogen LH_2 moderator 12 cm × 12 cm × 5 cm deep, irradiated by fast neutrons from two tungsten targets arranged in a flux-trap geometry. The moderator is viewed by a ^{58}Ni-lined guide tube with a cross-section of 6 cm × 6 cm. A Mica crystal, moving away from the neutron pulse at a velocity of 199 m/s, will be installed on the end of a rotor that rotates in synchronism with the beam pulse rate (20 Hz) at a position about 8 m from the moderator

A schematic view of the apparatus planned at LANSCE is shown in Fig. 1. We expect to produce UCN at a density of at least 10 UCN/cm^3 using the existing liquid hydrogen moderator at LANSCE. It is expected that in the near future LANSCE will begin operations on a nine-month production schedule every year. This will allow a fundamental physics program to begin. A new fully coupled moderator (i.e., without any poisons) will be installed in 1997. This will increase the width of the neutron pulses and will result in an increase in the density of UCN by a factor of about three. As the power of SPSS is expected to increase from the current 100-kW level to initially 1 MW and later to 5–10 MW, one can expect substantial advances in the UCN densities to be achieved.

3. Cryogenic UCN Sources

A rotor converter is a fairly simple instrument to implement and is well suited to a SPSS and would be compatible with a LPSS as long as the neutron pulse lengths did not exceed several hundred microseconds. Even with longer neutron pulse lengths, a rotor would still operate, but with lower efficiency. Ultimately it seems that in order to obtain substantial gains in densities one will need to go to some form of cryogenic UCN moderators. Investigations have been carried out to study production of UCN in superthermal (e.g. producing a UCN density *higher* than the *thermal* UCN density of the source) sources in which neutrons are down scattered by phonon emission in liquid ^{4}He. [4] The upscattering rate should be very low as the phonon density in such a moderator is very low. Proof-of-principle tests of this idea have been carried out at reactors and it appears that high densities of UCN can be obtained in the liquid He moderator. [5] However, it has proven difficult to implement this as a realistic source because there have been technical problems in trying to efficiently extract the UCN from the source. Efficient extraction from the liquid source requires a windowless extraction system that is compatible with the reactor requirements.

While the LHe superthermal source certainly merits further efforts, especially for experiments that can be performed in the LHe production volume, a potentially attractive scheme for producing UCN is a technique now under development by the research group of A. Serebrov at the Gatchina reactor. [6] This employs a frozen D_2 moderator at 4–6 K placed close to the active zone of the reactor. The density of UCN in this source is significantly increased over that in a liquid D_2 cold source by the Boltzmann factor at the lower temperature. Very preliminary results from the Gatchina group have shown a gain in UCN densities achieved of a factor of 10 compared to a liquid deuterium source. Such a source implemented at a LPSS has the advantage that the heat loads on the moderator are much less than at a reactor, thus providing one more freedom to optimize the moderator design and minimize its distance from the spallation target, thus increasing the flux.

A 1-MW Linac-only spallation source based on the LANSCE accelerator has been proposed as a means to provide complementary capabilities to those available at the short-pulse MLNSC spallation source. The new spallation target would be constructed in Experimental Area A at LANSCE, an area that will no longer be used for nuclear physics research after 1996. The LANSCE linac is envisaged to operate at 60 Hz providing 1.25 mA (with some potential to go to 2.5 mA) current of 800-MeV protons with a duration of 1.0 ms per pulse. The accelerator would operate at 60 Hz to the LPSS with a 1-ms beam pulse width, thus yielding a 6% duty factor. The beam would impinge on a tungsten flux trap split target viewed by up to six moderators that could be either water or liquid hydrogen. These moderators would produce beams of thermal and cold neutrons for use in materials science and defense programs. We are planning for a UCN source that could be installed at the LPSS.

The time-averaged beam power of this source is as much as sixty times less than the thermal power of research reactors. However, the energy required to produce a neutron at a spallation source is roughly 30 MeV as compared to 180 MeV at a reactor. In addition, it is possible to make a brighter neutron source using a spallation target than at a reactor. These factors yield a gain of ten for thermal neutrons and a gain of fifteen for cold neutrons relative to a reactor. In addition, it is possible (for some classes of experiments) to make use of the time structure of the beam to advantage.

For UCN, estimates indicate that densities of 10^3-10^4 UCN/cm^3 could be achieved. Such a source would provide

the densities required to carry out a fundamental physics research program that could probe for physics beyond the standard model with substantially improved sensitivity. The existence of such an intense UCN source may also prove of interest to materials science. Assuming funding is provided in the near term, a cryogenic UCN source could be implemented at a LANSCE LPSS within the next five years.

The authors would like to thank R. Golub, S. Lamoreaux, Y. Masuda, F. Mezei, A. Michaudon, and M. Pendlebury, for useful discussions.

References

1) A. Steyerl and S. S. Malik, Nucl. Instrum. Methods. **A284** (1989) 200.
2) J. S. Fraser et al., Physics in Canada **21** (1965) 17.
3) T. O. Brun et al., Phys. Lett. **A75** (1980) 223.
4) A. I. Kilvington et al., Phys. Lett. **A125** (1987) 416.
5) H. Yoshiki et al., Phys. Rev. Lett. **68** (1992) 1323.
6) A. Serebrov et al., submitted to Nucl. Instrum. Methods.

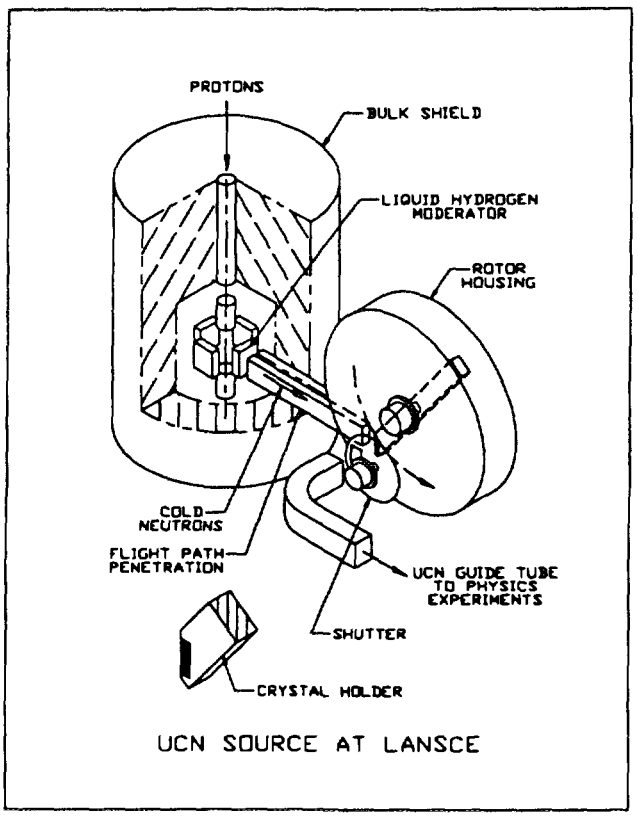

Figure 1: Schematic of planned UCN apparatus at LANSCE

On the Superthermal UCN Production*

Hajimé Yoshiki

Department of Engineering, Ibaraki University, Hitachi, 316, Japan
KEK, National Laboratory for High Energy Physics,Tsukuba, 305, Japan

In 1992, the production of ultracold neutrons (UCN) by means of superthermal method predicted by Golub and Pendlebury [1] was verified quantitatively by changing incident cold neutron wavelengths to observe the maximum of UCN production [2,6] at a certain wavelength. At this wavelength the dispersion curve of the superfluid liquid helium and the energy momentum curve of a free neutron crosses and the energy and momentum of incident neutron can be converted entirely to those of a produced phonon (Fig.1), leaving the neutron with an infinitesimal energy, a UCN. The value obtained was 8.78±0.06Å, in contrast to the value hitherto often quoted number of 8.9Å for 1.1K liquid, and it fits exactly to our particular liquid temperature of 0.45K[3]. What we have learned here is that the calculation by Cohen and Feynman is correct and we can now calculate the rate of UCN production per unit time. The resultant **UCN intensity** is overwhelming, compared to the Turbine[4], or Boltzmann methods. It must be emphasized that 1) this method allows cold neutrons to come from whole 4π–directions to produce UCNs, unlike the Turbine, where rather fine beam collimation of cold neutron is necessary; 2) the produced UCNs are automatically trapped in the superfluid helium vessel, whereas the parent cold neutrons can penetrate freely through the wall, resulting in the build-up of UCN density in time in the vessel. In other methods the UCN transfer to an experimental volume, like a Ramsey Chamber, is necessary and the balancing between inflow and outflow of UCNs to and from it occurs quickly. Golub predicted that required temperatures would be below 0.8K, where the production of UCN creating phonons (down-scattering) would not be surpassed by phonons reabsorbed by UCN (up-scattering). This statement is experimentally demonstrated as shown in Fig.2 [2]. The attenuation coefficient at 0.45K is mainly attributed to a vertical duct open downward on the storage vessel (so called gravity acceleration tube) which was adopted to detect UCN with good efficiency.

---

*Based on the talk given at "the Baryon Instability Workshop"(Oak Ridge, March 28-30,1996)

In 1987, we calculated the heat that would be produced in the liquid helium, if it was exposed to a cold neutron field of 3×10^{12} /cm^2/s [5]. If such situation is realized it would produce 5000 UCN/cm^3/s (defined UCN energy upper limit=2×10^{-7}eV) , a strongest UCN source up till now. However the final estimate of the heat to be removed from the liquid amounts to 3000 mW under a certain number of assumptions. They include that irradiated part of the vessel is a steel cylinder of 50 cm in length, 10 cm in diameter and 0.1 mm in wall thickness. Table 1 gives the answer to the problem by combining a new set of circulation pumps for He^3 and a new heat exchanger which has four times as many number of fins as before. The proposed set of circulation pumps for He^3, which were purchased in 1994, is five times larger in displacement than before. From the existing data of Fig. 3 we can extrapolate that this combination is enough to stand 3 x10^{12}cold neutrons/cm^2/s [5]which is to **produce 2 x 10^7 UCN/s** in the aforementioned part of the liquid. Such irradiation will be accomplished most conveniently and most realistically by use of a spallation source, and *not* by a reactor.

The **two main objectives** for getting a strong UCN source are a more precise determination of the neutron lifetime and the search for the electric dipole moment of neutron, a manifestation of the time irreversibility. As for neutron lifetime, there is a proposal with superthermal source and magnetic confinement [7], and we are planning a similar device [8] incorporated in Cooling Tower II (see below). We will look into the latter more specifically in this talk. The search for the electric dipole moment of free neutron has been carried out by two groups[9,10,11], whose latest upper limit for this quantity is ~1.2×10^{-25}e.cm. In order to go a step further it would be necessary 1) to have UCN more in number and 2) to control systematic errors more in precision, such as magnetic field in its stability and uniformity, or problem of dark current when a strong electric field is applied. Since we are to produce UCN by the low-temperature engineering, the logical solution for 2) would be to take advantage of this orientation. In Fig.4 we show the e.d.m. measurement machine integrated with refrigeration parts, which now is dubbed **Mark3001**. Cooling Tower I does the He^3 refrigeration, Cooling Tower II supplies liquid heilium to superconducting shield and solenoid, and furnishes a space for gravity acceleration and UCN detection. The part where the e.d.m. is measured is conventional in layout[11] except that the shields have to be coaxial by technical reasons and the chamber is filled with 0.5K purified liquid helium in place of vacuum. The Ramsey Block, a cylindrical object 3 m long and 0.8 m in diameter is a vacuum chamber. It contains three layers of high-permeability magnetic shield at room temperature. Coaxially toward the center, a

superconducting magnetic shield and a **superconducting solenoid** exist, which are enclosed in a double layered cylinder containing liquid helium to keep them at 4.2K. Those are all made out of aluminum except for the superconducting material. We are aiming at a magnetic field whose instability in space and time will be in the order of 10 ngauss. Fig.5-8, show how those elements are made and look like. Explanations are given in figure captions.

Preliminary measurement was done for the three layer **high-permeability** ($\mu=10^5$) shield at room temperature, which turned out 0.1 mgauss at the center of the shield in ambient magnetic field, satisfying the designed attenuation[12]. As for superconducting shield, lead foil of 0.1 mm thick, 80 mm wide has been used for the shield material. This was wound on the aforementioned aluminum bobbin, which was fabricated with an accuracy of one hundredth of a millimeter near Ramsey Chamber, in 8 mm pitch so that ten turns would make a 1 mm thick shield. A model experiment was done to see the validity of our approach. A cup made out of the same lead foil and wound in the same way was made and submerged in liquid helium in a cryostat. Given an external field by means of a solenoid wound on the outer wall of cryostat, the axial magnetic field at the center of the cup was measured by SQUID to see if the attenuation as a function of the depth varies as theory. For a semi-infinite superconducting cylinder, the theory says that the attenuation is proportional to $\exp(-kz/R)$ where z is the depth from the end of the cylinder, R, its radius, and $k=3.83$ for the axial field. Our data produced $k=3.71\pm 0.13$ (Fig. 9)[12]. This shows that our approach is justifiable and the superconducting shield will be working as designed. By combining the high-permeability magnetic shield and the superconducting shield, we expect that our aim of 10 ngauss stability is going to be accomplished. The system is being assembled and is ready for test this summer.

In Table 2, we present the achievement in past and the prospect in future of the electric dipole measurement of neutron. The intensity of UCN depends on the intensity of parent cold neutrons and it can change orders of magnitude whether one use a cold neutron *beam*, or a *field* of cold neutrons (neutron bath created by spallation source). This is because of the difference in solid angle as discussed before. The number (5000 cm^{-3}) is conservative even taking into account the diffusion of UCN into the whole vessel out of the region they are created (50 cm long, 10 cm wide, see above and ref.7), resulting in dilution in density. We therefore belive that we will not face the paucity of UCN but rather the problem of the systematic errors, we have been discussing in measuring the edm.

The issues on **neutron spallation sources** with particle accelerators have been discussed by many neutron laboratories (JHP,LANL, ORNL, Savannah River, Jülich, Wien etc). The main advantage of spallation source is that it is pulsed and has a high peak intensity, suited for neutron spectroscopy very well. We

should not however overlook another big advantage in spallation source. It is the dedicatablity of a source (or sources) to a paricular experiment (or experiments). By the **dedicatability** we mean that each experimenter is able to easily adjust his beam specifications at his own. This is impossible in case of a reactor. If a cold neutron source or a superthermal source are to be installed near the core of a reactor, it would need a very precise evaluation of flux distributions in planning. Once the reactor is on, it is virtually impossible to move these equipments and the relations among different experiments are fixed. On the other hand, a proton beam can be tailored to orders by experimenters. It can be controlled in current, space and time. The primary beam can be even fanned out. By owning one's own spallation target, the experimenter can design his own neutron source(s) or beam(s), taking no attention to other groups. The serious contradictions among different types of experiments, whether a high time resolution or a high intensity, will be solved by designing a target station in each case. For instance the Superthermal UCN production need no time resolution but a little proton current (~10μA) *adjustable* in intensity or able to be *shut off* if it is not wished. The experimenters will benefit much from the mobility and the dedicatability of the spallation source in this way[5,13] and this is one of the essential advantages in working with spallation sources.

The works mentioned in this talk have been supported by Monbusho under Grant-in-Aid for Scientific Research on Priority Areas (UCN,No.04244106).

REFERENCES

[1] R.Golub and J.M.Pendlebury, Phys. Ltrs.**62A**(1977)337

[2] H.Yoshiki,K.Sakai,M.Ogura,T.Kawai,Y.Masuda,T.Nakajima,T.Takayama, S.Tanaka and A.Yamaguchi, Phys. Rev. Ltrs. **68** (1992) 1323

[3] H.Yoshiki, to be published.

[4] the latest information can be found in the paper by Kitagaki *et al* submitted to Int. Symp. on Advance in Neutron Optics and Related Facilities (1996), KUR, Osaka, Japan.

[5] H.Yoshiki, S.Ishimoto and M.Utsuro, Z.Phys.B - Condensed Matter **67** (1987) 161

[6] H.Yoshiki, K.Sakai, T.Kawai and S.Goto'o, Cryogenics.**34**(1994)277

[7] J.M.Doyle and S.K.Lamoreaux, Europhys. Lett. **26** (1994) 253
[8] N.Inoue, to be published
[9] K.F.Smith, N.Crampin, J.M.Pendlebury, D.J.Richardson, D.Shiers, K.Green, A.I.Kilvington, J.Moir, H.B. Prosper, D.Thompson, N.F.Ramsey, B.R.Heckel, S.K.Lamoreaux, P.Ageron, W.Mampe and A.Steyerl, Phys. Lett.**234**(1990)191
[10] I.S.Altarev, Yu.V.Borisov, N.V.Borovikova, S.N.Ivanov, E.A. Kolomensky, M.S.Lasakov, V.M.Lobashev, V.A.Nazarenko, A.N.Pirozhkov, A.P.Serebrov, Yu.V. Sobolev, E.V. Shulgina and A.I.Yegorov, Phys. Letters **B276**(1992)242
[11] J.M.Pendlebury, K.F.Smith, R.Golub,J.Byrne, T.J.L.McComb, T.J.Sumner, S.M.Burnett, A.R.Taylor, B. Heckel, N.F.Ramsey, K.Green, J.Morse, A.I. Kilvington, C.A.Baker, S.A.Clark, W.Mampe, P.Ageron and P.C.Miranda, Physics Letters **136B** (1984) 327
[12] E.Gravador, H.Yoshiki and F.Huang, to be published
[13] H.Yoshiki, Proceedings of ICANS-IV, *KEK* (1981) 758;
R.Golub, K.Böning and H.Weber, Realisierungstudie zur Spallations-Neutronenquelle (Teil III), Jülich & Karlsruhe (1981)5;
M.Utsuro and H.Yoshiki, Proceedings of the Meeting on BSF Future Prospects-II, *KEK* (1983)223;
H.Yoshiki, KENS Report-V, *KEK* (Editors; Y.Ishikawa, N.Niimura, M.Misawa) (1984)215;
R.Golub, NBS Special Publication 711(Editor, G.Greene) (1986) 143;
H.Yoshiki, KEK Report 88-3 (1988) 163;
T.Kawai et al, KEK Report 89-13(1983) 91(specially Fig.10);
K.Hosoyama, KEK Report 89-13(1989) 107

FIGURE & TABLE CAPTIONS

Fig.1 Superthermal UCN counts in the experiment as described in ref.2 *vs* cold neutron wavelength.

Fig.2 Distribution of arrival time of UCN at the counter, determining the storage lifetime of the UCN in the vessel at different temperatures.

Fig.3 Cooling performance of two types of heat exchanger. "New" stands for the He^3 pot with 29 fins.

Fig.4 EDM measurement machine. A pipe extends to the left of the figure to be bathed in a cold neutron field of $10^{12}/cm^2/s$ or to receive a cold neutron beam of any strength. Cooling Tower I cools all the purified superfluid liquid helium down to 0.5K by He^3 coolant. Cooling Tower II supplies liquid helium to superconductiong shield and solenoid in Ramsey Block. It also provides space for UCN detection.

Fig.5 Cylinders in Ramsey Block are being assembled. The 10,000 m^3/hr He^3 circulation pump is seen in the background.

Fig.6 Three layers of high-permeability magnetic shield at room temperature are being housed into the outer jacket of Ramsey Block.

Fig.7 Completed superconducting magnetic shield.

Fig.8 Almost completed superconducting solenoid.

Fig.9 Attenuation of magnetic field with depth by superconducting magnetic shield.

Table 1 Combination of a larger set of He^3 circulation pumps and an enlarged heat exchanger, which meets the required heat removal.

Table 2 Numbers associated with EDM measurement in tha past and the future.

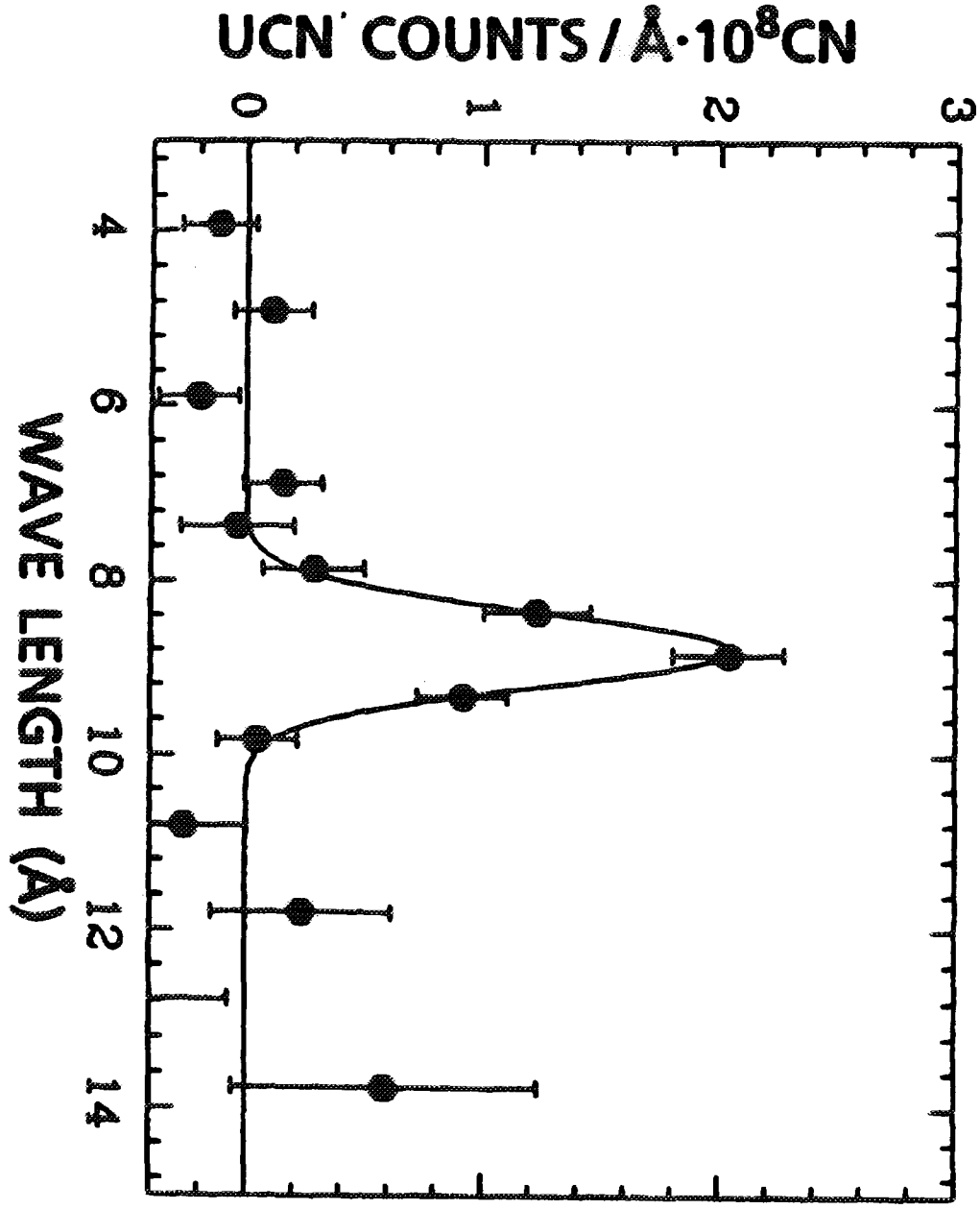

Fig. 1

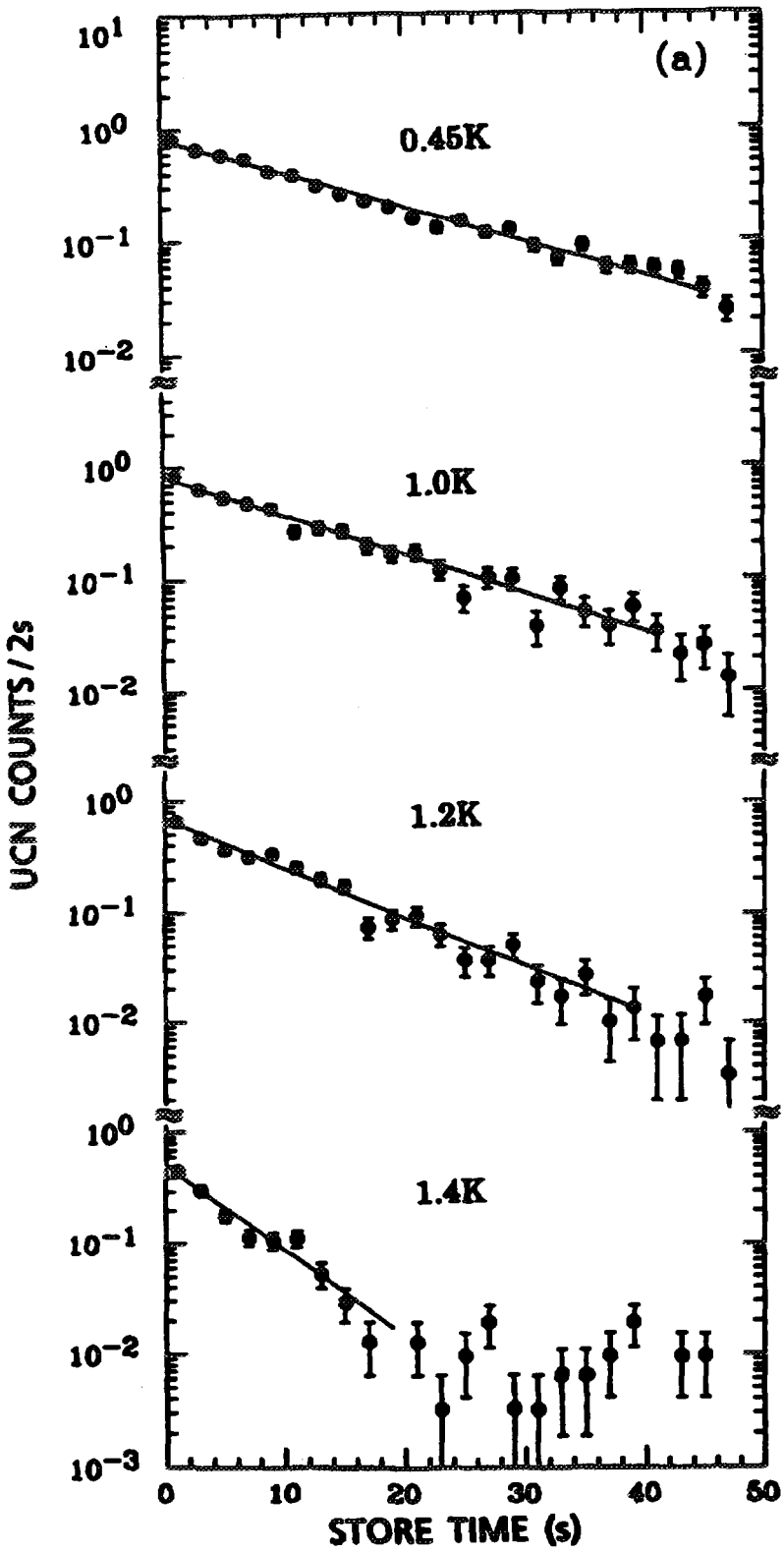
(a)
0.45K
1.0K
1.2K
1.4K
UCN COUNTS / 2s
STORE TIME (s)
10^{1}
10^{0}
10^{-1}
10^{-2}
10^{-3}
0
10
20
30
40
50

Fig. 2

Heat load in the UCN bottle (mW)
0
50
100
150
0.0
0.5
1.0
1.5
Temperature in the UCN bottle (K)
New type
Old type

Fig. 3

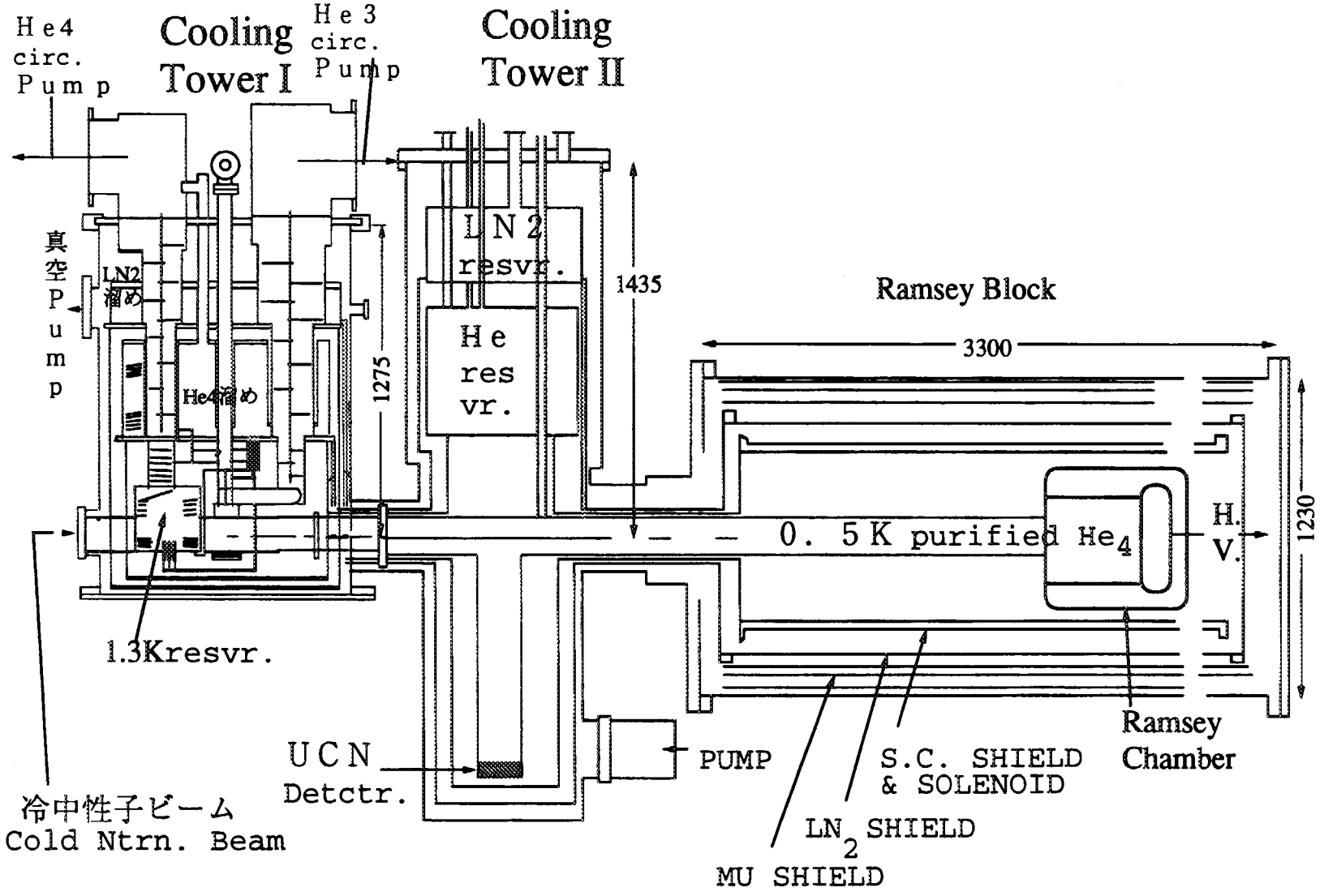
He4 circ. Pump
Cooling Tower I
He3 circ. Pump
Cooling Tower II
真空 Pump
LN2 溜め
He4溜め
1275
LN2 resvr.
He res vr.
1435
Ramsey Block
3300
0. 5K purified He4
H. V.
1230
1.3Kresvr.
UCN Detctr.
PUMP
S.C. SHIELD & SOLENOID
Ramsey Chamber
冷中性子ビーム
Cold Ntrn. Beam
LN2 SHIELD
MU SHIELD

Fig. 4

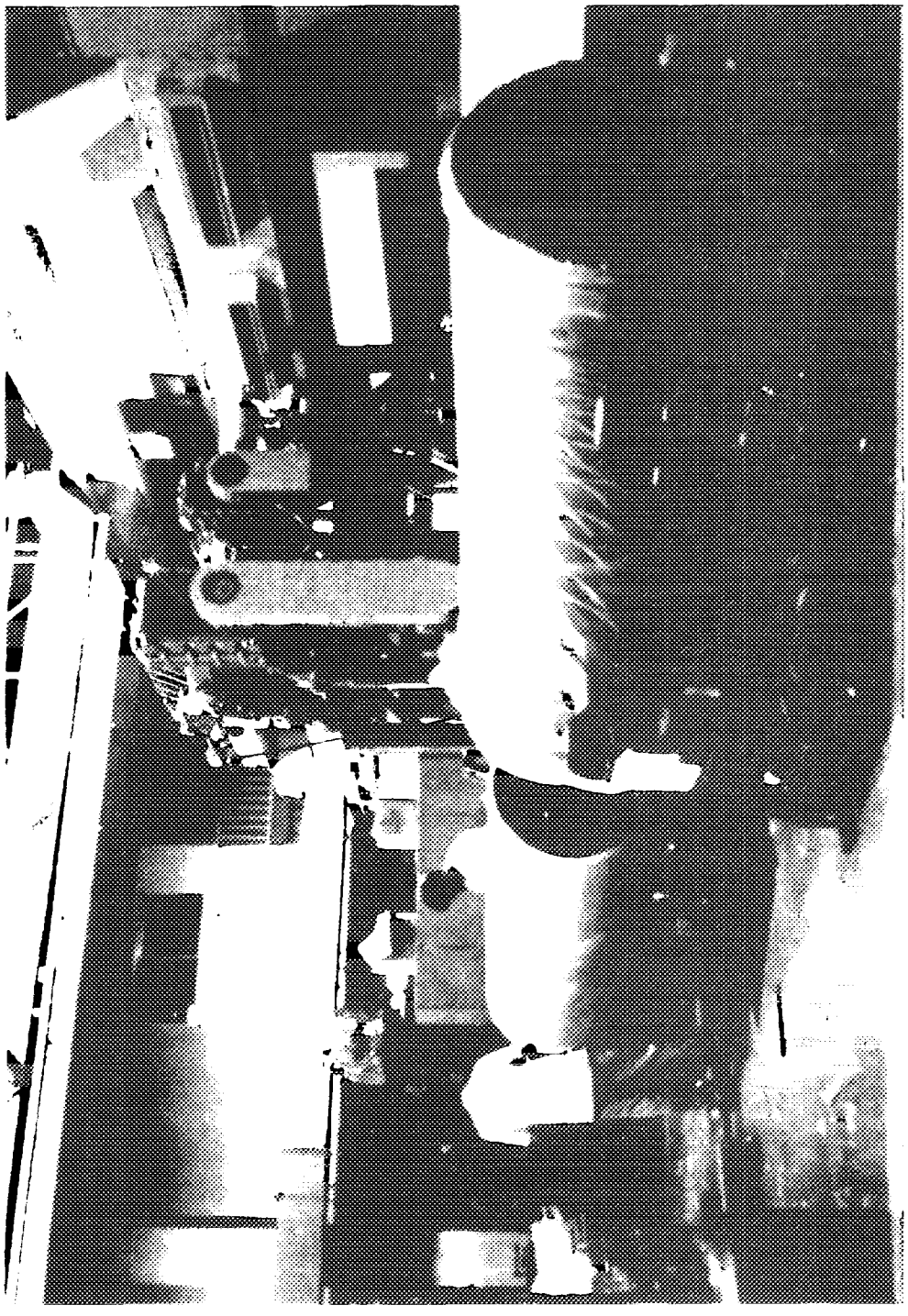

Fig. 5

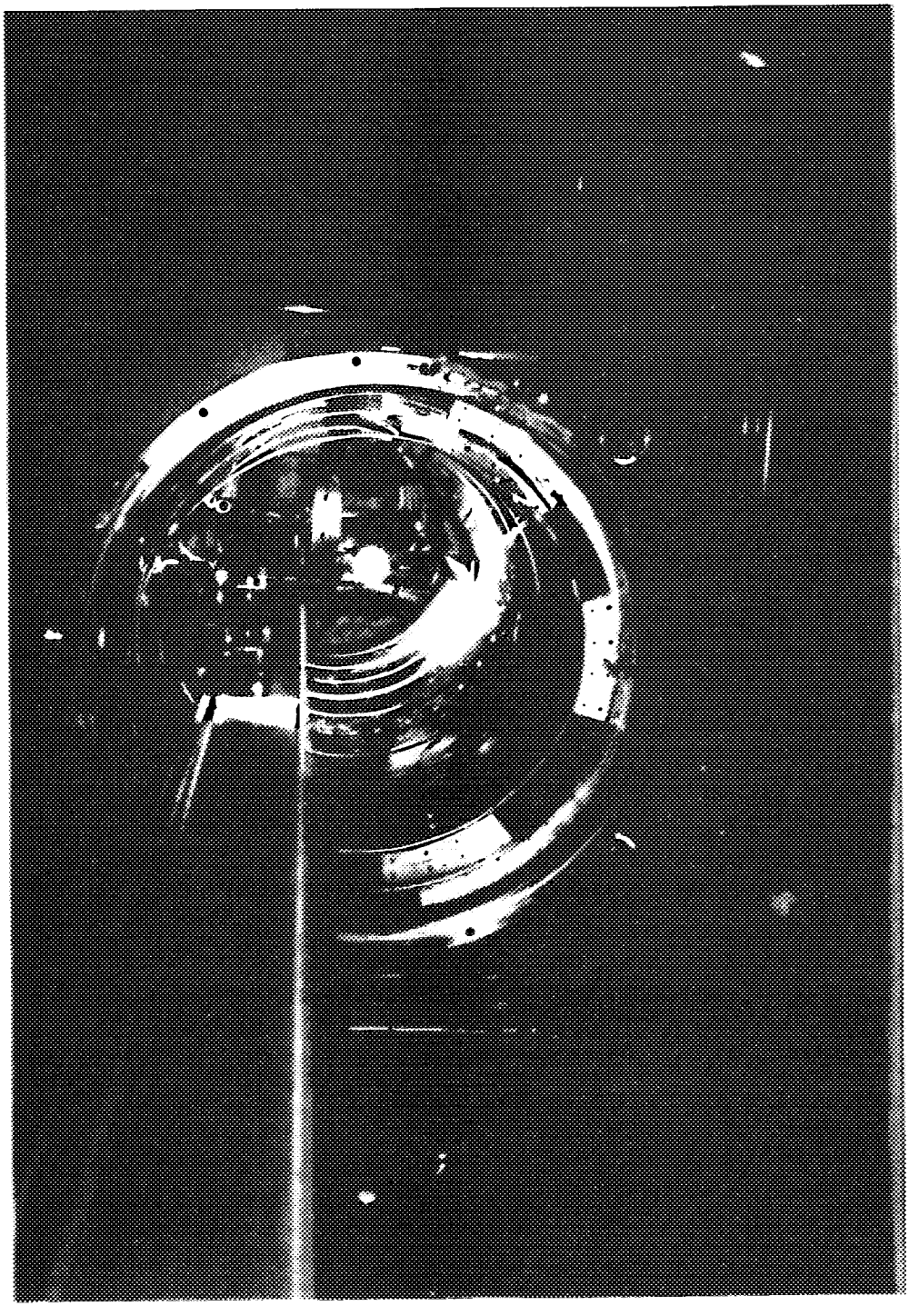

Fig. 6

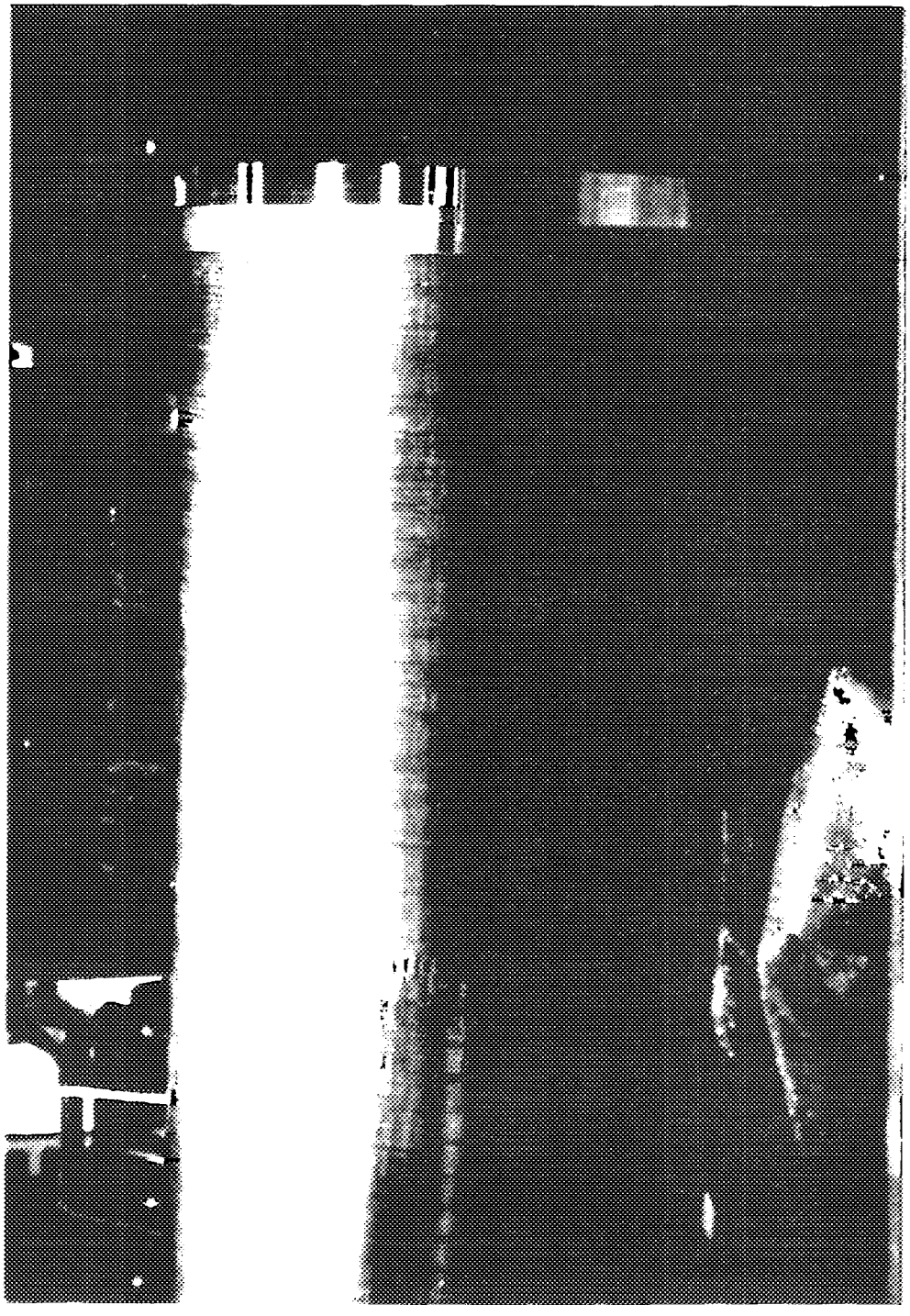

Fig. 7

Fig. 8

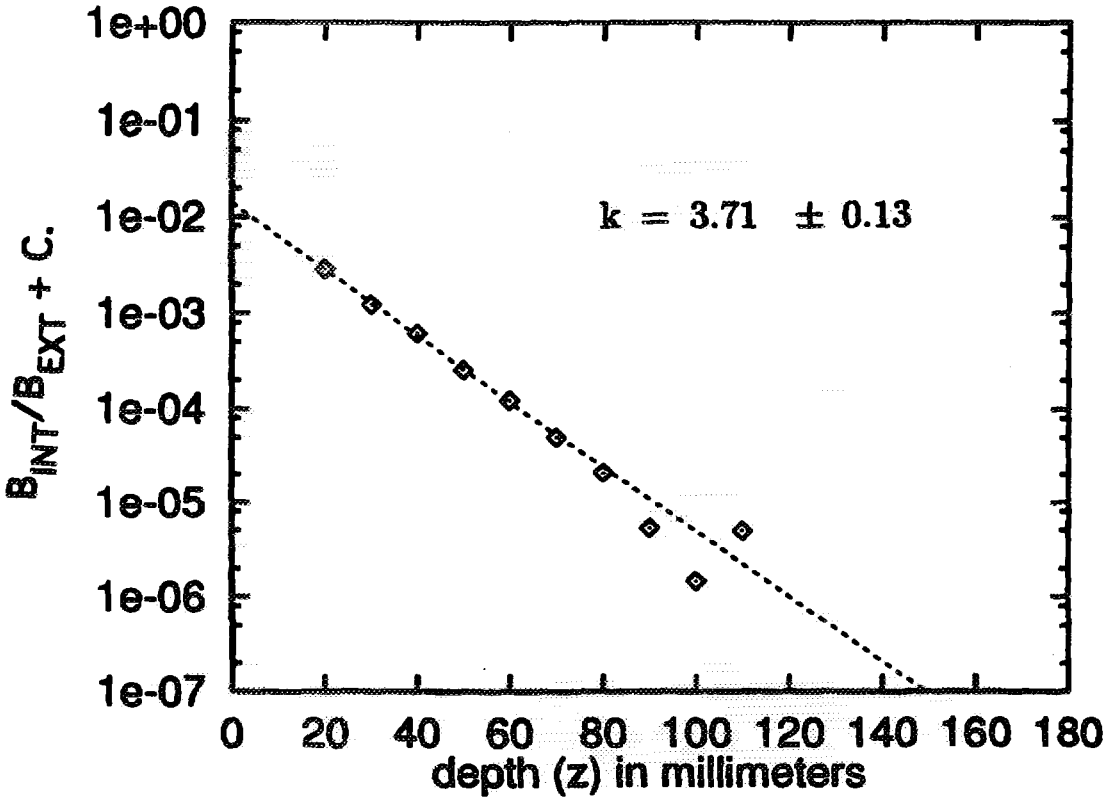
1e+00
1e-01
1e-02
1e-03
1e-04
1e-05
1e-06
1e-07
B_{INT}/B_{EXT} + C.
k = 3.71 ± 0.13
0 20 40 60 80 100 120 140 160 180
depth (z) in millimeters

Fig. 9

	Mark3000 (P.R.L.68(1992)1323)	Mark3001
He^3 Circulation Pump	2,000 m^3/hr (550 *l*/s)	10,000 m^3/hr (2300 *l*/s)
Heat Exchanger		
# of Fins	29	116
Total Fin Area	5450 cm^2	21800 cm^2
Cooling Power at 0.5K	150 mW(measured)	3000 mW enough to stand 3 x 10^{12} cold neutrons /cm^2/s = 5 x 10^3 UCN/cm^3/sec (Z.Phys.B-CM67(1987)161)

Table 1

	type	chamb. volume	UCN CM^{-3}	stored UCN	values	system. error	statis- tical e.	upper limits
DONE								
ILL (PREVIOUS,89)	R.T. BEAM	5*l*	40	$2 \cdot 10^5$	-3.3 ± 3.9	± 1.9		$<1.2\ 10^{-25}$
					10^{-26}e.cm			
GATCHINA(91)	R.T.	20*l*	10	$2 \cdot 10^5$	+2.6	± 1.6	± 4.2	$<1.2\ 10^{-25}$
KEK/JAERI(91)	HeII BEAM	15*l*	5	$8 \cdot 10^4$	NO ATTEMPT MADE FOR EDM			
FORECAST								
ILL (PRESENT)	R.T. BEAM	20*l*	50	$1 \cdot 10^6$	X	2.0	1.0	$< 5\ 10^{-26}$
ILL/KEK(3001)	HeII BEAM	20*l*	350	$7 \cdot 10^6$	X	1.0	0.2	$< 2\ 10^{-26}$
spallation s./KEK	HeII BATH	20*l*	5000	$1 \cdot 10^8$	X	X'	<0.1	$< X''\ 10^{-27}$

BATH=cold neutron bath

Table 2

Experimental Study of a Solid-deuterium Source of Ultracold Neutrons

A.P.Serebrov[1], V.A.Mityukhlyaev[1], A.A.Zakharov[1], A.G.Kharitonov[1], V.V.Nesvizhevskii[1], M.S.Lasakov[1], R.R.Tal'daev[1], A.V.Aldushchenkov[1], V.E.Varlamov[1], A.V.Vasil'ev[1], G.Greene[2], T.Bowles[3]

[1] *St.Petersburg Institute of Nuclear Physics, Russian Academy of Sciences, 188350 Gatchina, Russia*
[2] *National Institute of Standards and Technology, Washington*
[3] *Los-Alamos National Laboratory, Los-Alamos, New Mexico 87545*

(Received)

The results of experimental studies of the yield of ultracold neutrons (UCN) from solid deuterium, which were performed on a model source in the WWR-M reactor at the St.Petersburg Institute of Nuclear Physics, are reported. The temperature gain factor in the UCN yield at 13-14K from solid deuterium relative to the UCN yield at room temperature from a gaseous state is equal to 1230 and 550 at solid-deuterium temperature of 18.7K (triple point).

KEYWORDS: ultracold neutrons, neutron sources

The possibility of increasing the density of ultracold neutrons (UCN) by using as a source solid deuterium at low temperatures was analyzed in[1)]. In the present letter we report the results of an experimental study of UCN yield from solid deuterium, performed on a model UCN source in the WWR-M reactor at the St. Petersburg Institute of Nuclear Physics.

Fig.1 show the arrangement of the source in the reactor.

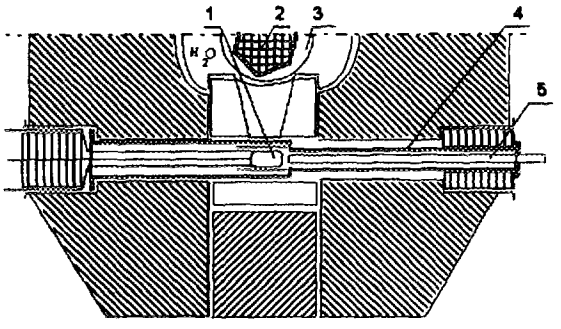

Fig. 1. Arrangment of the solid-deuterium source in the reactor. 1 — chamber with solid deuterium; 2 — reactor core; 3 — beryllium reflector; 4 — vacuum container; 5 — UCN guide

The 6-liter zirconium chamber of the source (cylinder D = 150 mm, l = 350 mm with elliptic bottoms) has a double wall (2 × 0.5 mm) where helium flows into the gap from a 150-W cryogenic refrigerator at a temperature of 4.5K. As the chamber is cooled, the deuterium from a 6-m^3 receiver flows into the chamber, condenses, and solidifies.

To obtain deuterium temperatures below 10-12K, a special construction of the source chamber is required. The problem is that as the temperature decreases, the thermal contact between the cooled wall of the chamber and deuterium breaks down. Cooling is possible as long as the saturated-vapor pressure does not fall below several Torr. For example, the saturated-vapor pressure is equal to only 0.75 Torr at a temperature of 12K and 5×10^{-2} Torr at 10K. A possible technical solution is to place an additional cooled spiral tube on the inner wall of the chamber. On cooling, the tube will be squeezed by the deuterium, which should solve the problem of thermal contact. Before making the design of the chamber more complicated, however, we decided at the first stage of the investigation to use a simple design, and then to use the same design but with deuterium containing a small quantity of helium in order to ensure heat transfer, and finally to use a more sophisticated design of the source if necessary. In the present letter we report the result of the first stage of the study at temperatures above 13K.

One of the most complex problems in this investigation is to determine the temperature profile of the solid-deuterium source. However, the temperature of the source could be easily determined with low accuracy - according to the residual deuterium pressure in the receiver, since the source, which is connected to the receiver by a pipeline, is a vapor- pressure thermometer in which the saturated vapor presssure is determined by the source temperature. Unfortunately, because of the large volume of the receiver, the relaxation time of the process which establishes an equilibrium pressure is long, which results in a pronounced hysteresis of the experimental dependence of the UCN yield on the pressure in the receiver. The UCN gain factor as a function of the pressure in the receiver during the cooling and heating

of the source is shown in Fig.2.

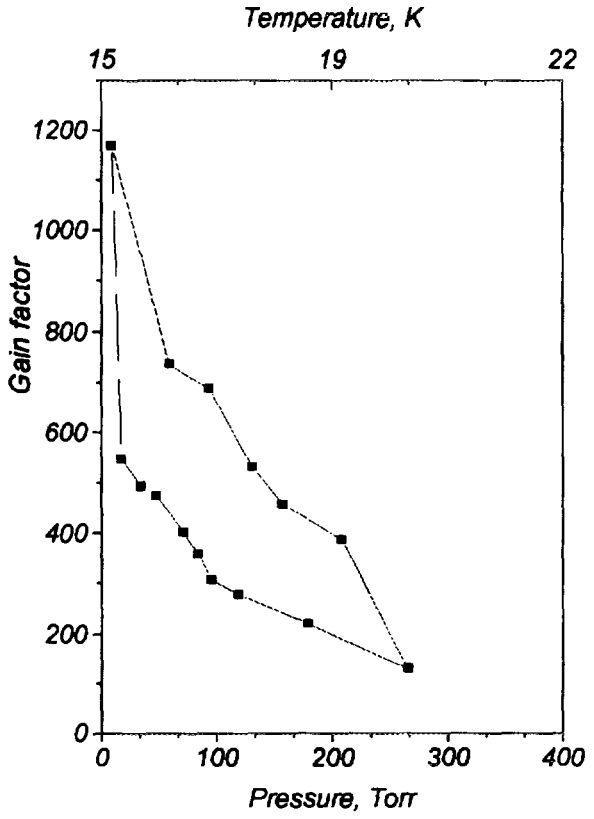

Fig. 2. Measurement of the UCN yeld upon cooling down of the source (upper curve) and the heating of the source (lower curve)

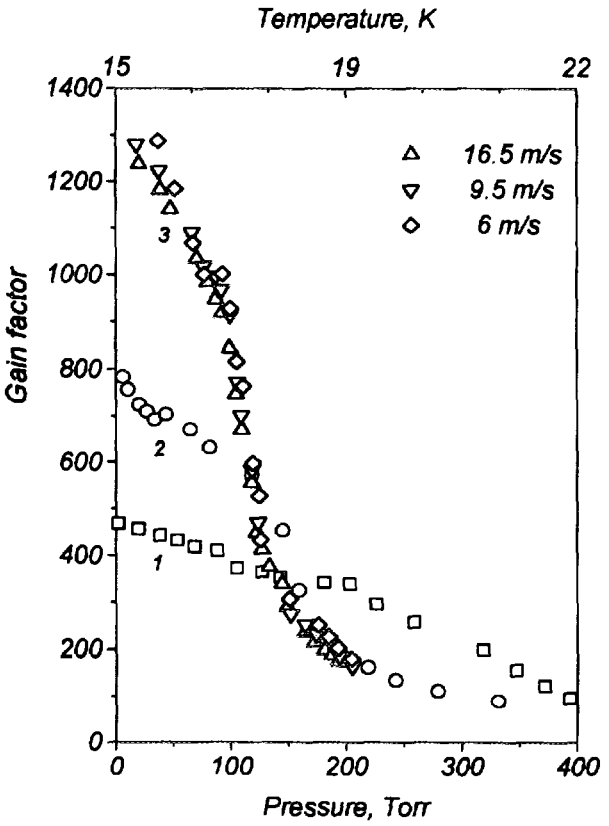

Fig. 3. Measurement of the UCN yield with the first chillings of the source: curves *1*, *2*, *3* (the measurements at the curve *3* have been carried out with UCN (6 m/s) and with VCN (9.5 m/s; 16.5 m/s))

Another, but not so trivial, uncertainty in the UCN yield that was observed in the experiment is apparently associated with a change in the ortho-para composition of deuterium under the influence of low temperatures and the radiation from the reactor. Curve *1* in Fig.3 was obtained in the first experiment on cooling of the source.

This experiment was performed at a rapid rate and low reactor power (2 MW). The temperature gain factor in this experiment was equal to only 450. Subsequent cooling of the source (curve *2* in Fig.3) was performed at a slow rate and with a reactor power of 14 MW; the temperature gain factor was equal to 790. After the source was warm, virtually all of the deuterium in the receiver was in the ortho phase ($95 \pm 5\%$) and remained in this phase without any visible changes in the composition. In subsequent cooling of the source, the temperature gain factor reached 1230 and stayed at this level. The curve *3* in Fig.3 corresponds to the fourth cooling. The dependence of the UCN yield on the ortho-para composition of deuterium is the most probable explanation for this phenomenon.

One obvious problem in obtaining a high UCN yield from a solid-deuterium source is that the source must be transparent to UCN. Cracking of solid deuterium as a result of the large temperature stresses could cause the UCN to be scattered by nonuniformities (cracks). When the effective path between nonuniformities is less than the path determined by the inelastic scattering and capture cross sections for UCN, the gain factor no longer increases as the temperature decreases. To investigate this question, we measured the temperature factor of the gain simultaneously for UCN with an average velocity of 6 m/s and for very cold neutrons in two velocity ranges, so that the average velocities were equal to 9.5 m/s and 16.5 m/s. It was done by using neutron guide system, which consist of branches with the different radius of curvature. The neutron guide curvature determine the average velocity of extracted neutrons (6 m/s, 9.5 m/s, 16.5 m/s). Since the refraction index depends strongly on the neutron velocity, the effective turbidity of the solid deuterium due to cracking should be manifested primarily for UCN (the refractive indices for 6 m/s, 9.5 m/s, and 16.5 m/s are, respectively, 0.68, 0.886, and 0.964). Curve *3* in Fig.3 is represented by measurements for all neutron

velocities indicated above. No appreciable difference in the temperature dependence of the neutron yield for different velocities is observed. This shows that the turbidity of the medium is not yet manifested. The free path at a deuterium temperature of 13K is, according to the calculations, 4 cm, 8 cm, and 16 cm for velocities of 6 m/s, 9.5 m/s, and 16.5 m/s, respectively. Since there is no dependence in the gain factor, it can be concluded that the depth of transparency of solid deuterium in any case is not lower than the indicated values. A more detailed study of this question requires lowering the temperature of the source to 5-6K.

In addition to measuring the UCN yield during cooling heating of the source with a refrigerator (Fig.2), we measured the dependence of the UCN yield with the source heated by radiation with the refrigerator switched off. These experiments made it possible to determine more accurately the gain factor at the triple-point temperature for solid and liquid deuterium, and also the power of the radiation load. Figure 4 shows the UCN yield and the pressure in the receiver during heating at a constant thermal load (radiative heating). During the first 28-30 minutes ($t_0 - t_2$) the pressure in the receiver increases linearly and is determined mainly by the heat of sublimation. Linear increase continues until an equilibrium sublimation pressure of 128 Torr at the triple point is established. During the next 25-30 minutes ($t_2 - t_3$) the solid deuterium melts and the liquid evaporates and is heated at the same time. At this time, the flow of gas into the receiver slows down, since some power is expended on melting. The melting process is completed by the time t_3, after which the flow of gas into the receiver again becomes constant and is determined by the heat of evaporation of deuterium. The heating power, which is equal to 36 W when the reactor is running and 6 W when the reactor is shut down, is determined from the rate of influx of the gas.

A plateum is present in the time dependence of the UCN yield between the times t_1 and t_2. This plateum corresponds to the triple-point temperature.

Initially, at time t_0, the temperature gain factor is equal to 1230 at a temperature of 13-14K. At the time t_1 the deuterium is heated to 18.7K and because of sublimation, this temperature remains constant up to the time t_2, when the pressure in the receiver reaches the equilibrium sublimation pressure. The temperature gain factor for solid deuterium near the triple point is equal to 500-550. At the time t_3, when the deuterium is completely liquid and its temperature is 19.5-20K, the gain factor is equal to 120. Further decrease of the gain factor is attributable to heating of the liquid.

Appreciable increase in the yield during the crystallization (by a factor of 4-4.5) is due to the improved thermalization of the neutron flux in the solid deuterium as compared to liquid deuterium, because of the increase in the total interaction cross section due to Bragg scattering. Though the Bragg scattering is elastic one, it increase the time of wandering in the source and influence

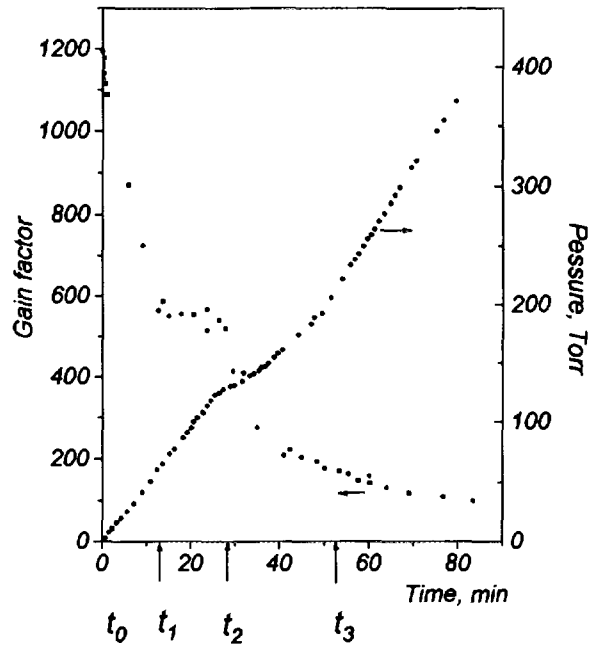

Fig. 4. Time diagrams of UCN gain factor and deuterium pressure in the tank at the heating of the source by radiation from reactor

on the thermalization. This effect was observed directly in the measurements of the total spectrum of neutrons from the source. Figure 5 shows the time-of-flight spectrum before condensation of deuterium (curve *1*), after condensation (deuterium in the liquid phase (curve *2*), and after crystallization (deuterium in the solid phase, curve *3*).

The effective temperature of the spectrum of the neutrons incident on the source is equal to 600K. Thermalization in the deuterium substantially softens the spectrum, and a difference in the thermalization effect for the liquid and solid phase is observed in the region 4-6 Å. For the solid phase we observed in the neutron spectrum characteristic irregularities associated with Bragg reflections. It is interesting to note that the structure of the reflections was found to be different for the first and second coolings, which could be attributed to the dependence on the ortho-para composition and on the cooling rate. The neutron spectrum from a solid-deuterium source (curve *3* in Fig.5) can be represented as a sum of two spectra: 56% of the intensity with an effective temperature of 180K and 44% of the intensity with effective temperature of 30K. The calculation of the UCN yield with the indicated shape of the spectrum was found to be very close to the calculation with an effective temperature of 100K. Neutrons with wavelength greater than 3Å can become UCN through a one-phonon process. An increase in the fraction of long-wavelength neutrons therefore increase the UCN yield upon crystallization of the deuterium. As one can see, the solid-deuterium source is

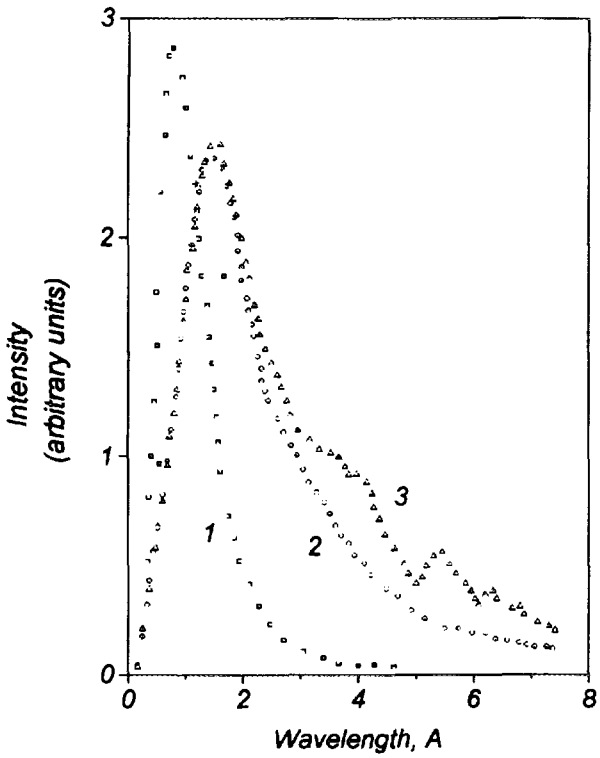

Fig. 5. Time-of-flight spectra of the source for different phase states of deuterium

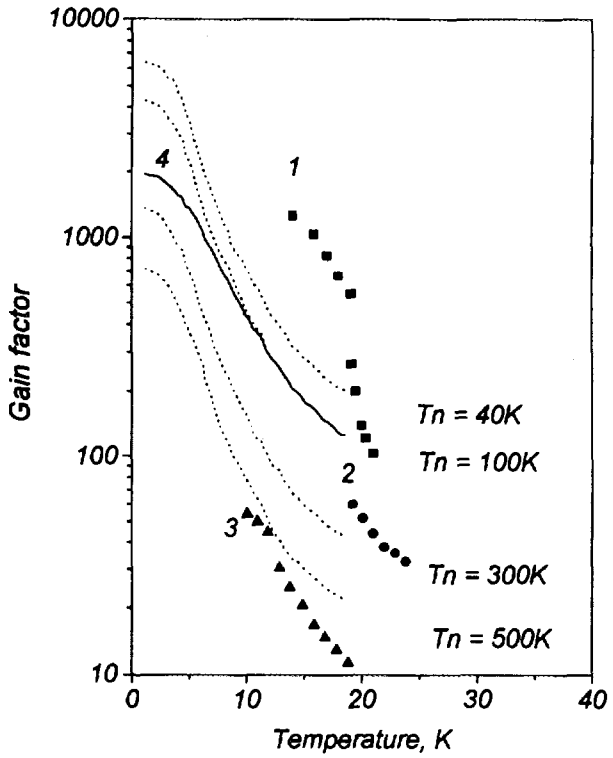

Fig. 6. Analysis of the UCN gain factor for deuterium sources with different volumes

more efficient for production of cold and very cold neutrons.

Another reason for UCN gain factor increasing at the crystalization can be related that upscattering cross section for solid state is smaller then for liquid. It can increase the depth of UCN yield. Both effects - improvement thermalization and supression upscattering cross section - gave together factor 4-4.5 in the increasing of UCN intensity at the crystalization of deuterium.

The final analysis of the experimental results is illustrated in Fig. 6, where the experimental temperature dependence (curve *1*) and the results of previous investigation for a 1-liter liquid-deuterium source[2] (curve *2*) and for a 0.15-liter solid-deuterium[3] (curve *3*), are shown.

The UCN yield is increased by decreasing the temperature of the source and by decreasing the effective temperature of the neutron flux as a result of increasing the volume of the source. The computation results of[1] are for absolutely pure deuterium and for effective neutron flux temperatures of 40, 100, 300 and 500K. The solid curve *4* was computed for an effective temperature of 100K and absorbtion cross sections in deuterium taking into account the hydrogen impurity (0.2 vol.%) and nitrogen impurity (4.6×10^{-3} vol.%). It should be mentioned that calculated gain factors are normalized at the room temperature ($T_{D_2} = 300$K) of the source and the room temperature of the neutron flux ($T_n = 300$K). Experimental normalization (curve *3*) was done at the room temperature of the source, but at the temperature of reactor neutron flux 600K. Therefore discrepancy between curve *3* and curve *4* at the source temperature $(13 \div 19)$K is not dramatic, it arised because of perfect thermalization of neutron flux is not happened inside the reactor moderator.

The next stage of the investigations presupposes that the temperature of the source is lowered to 6-7K for the purpose of studying the possibility of increasing the UCN yield. It should be noted that the thermal conductivity of solid orthodeuterium is an order of magnitude higher at 6-7K. This should improve the properties of the source with respect to the thermal load.

The experimental results can be used to develop designs for a solid-deuterium source of cold and ultracold neutrons in high-flux reactors with a heavy-water reflector, since the heavy water provides effective shielding from fast neutrons and γ-rays and gives a low level of heat transfer while preserving a high flux of thermal neutrons (the PIK reactor under construction in Gatchina, Russia and the ILL reactor in Grenoble, France, new project of heavy water reactor at Garching, Germany). The other possibility is to use a solid-deuterium source based on neutron spallation sources, where the ratio of the heat transfer and the neutron flux is appreciably better than for reactors. For example, a solid-deuterium UCN source based on a 1-MW spallation source is being designed at Los Alamos (USA). This type of source could be proposed for spallation neutron source at the

Japan Hadron Project (KEK), also for European Spallation Source (ESS).

There is a big interest to develope project of the special source of cold neutrons (CN) very cold neutrons (VCN) and ultra cold neutrons (UCN) in accordance with scheme shown on the Fig.7, where the spallation neutron target is surrounded by the volume with solid deuterium in the bath with liquid helium to provide maximal thermalization of neutron flux.

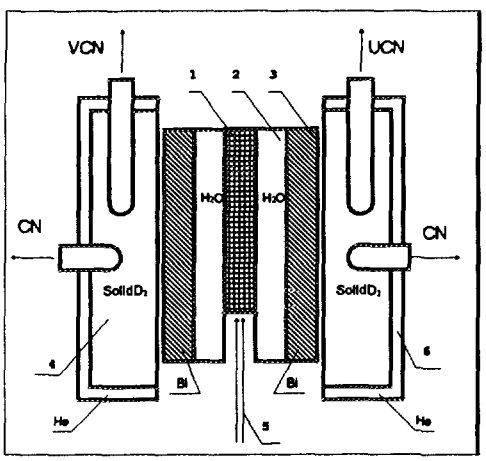

Fig. 7. 1 - spallation target, 2 - H_2O moderator, 3 - Bi -shielding, 4 - solid D_2 moderator, 5 - proton beam, 6 - He 4K bath

At last, the solid deuterium neutron source can be successfully used at reactors with moderate power. For example, the placement of solid deuterium neutron source in the thermal column of the reactor KUR (Japan) or the reactor WWR-M (Russia) could significantly increase experimental facilities.

It should be mentioned that solid deuterium source can give almost the same gain factor for very cold neutrons (30-50 m/s) therefore it can be used in the scheme of UCN extraction by means of turbine.

The authors are grateful to A.V.Strelkov at the Joint Institute for Nuclear Research; N.G.Kolyvanova, V.V.Runov and M.O.Khonina at the St.-Petersburg Institute of Nuclear Physics, the staff at the Division of the Reactor Physics and Technology; R.G.Pikulik, Chief Reactor Engeneer, and the staff of the Cryogenic Division of the Institute and the workshop for active participation in taking the measurements and the preparatory work.

This work was supported by the National Institute of Standards and Technology (USA), the Los Alamos National Laboratory (USA), the Russian Fund for Fundamental Research (Grant 93-02-14382), the International Science Foundation ISF (Grant R59300), and the European Science Foundation (Project 93-298).

1) Serebrov A.P., Mityukhlyaev V.A., Zakharov A.A. et al. JETP Lett., **59**. 757. 1994.
2) Altarev I.S., Borovikova N.V., Bulkin A.P. et al. JETP Lett. **44**. 344. 1986.
3) Altarev I.S., Borisov Yu.V., Brandin A.B. et al. Phys.Lett. A **80**. 413. 1980.

Confinement of Ultra-Cold Neutron in a Multiple Cusp Magnetic Field

Nobumichi AKIYAMA Nobuyuki INOUE, Hitoshi NIHEI, and Ken-ichi KINOSITA

Department of Quantum Engineering and Systems Science, Faculty of Engineering, Uneversity of Tokyo 7-3-1, Hongo, Bunkyo-ku, Tokyo 113, Japan

A new confinement system of ultra-cold neutrons is proposed. The neutron bottle is made of a rectangular vacuum chamber with the size of 40 cm × 40 cm × 30 cm covered with arrays of bar type permanent magnets. The operation of bottle requires neither cooling system nor high electric power supply, and thereby the bottle is appropriate to use in the room which is located in controlled area. The maximum kinetic energy of neutrons confined is 20 neV. Experimental scheme to test the performance of the bottle is described.

KEYWORDS: ultra-cold neutrons, UCN, magnetic bottle, multiple cusp, permanent magnet

§1. Introduction

Ultracold neutrons (UCN) with the energy typically about 0.2 μeV are of extensive use in basic physics experiments such as neutron-antineutron oscillation study[1], precise measurement of the neutron life time[2], studies of condensed matter properties[3], and of fundamental particle interactions[4], and so forth. In general, the UCN's are produced through cooling down[5] or mechanical slowing down[6] processes of very cold neutrons which are obtained by cooling thermal neutrons emitted from the nuclear reactor.

In this report we consider the magnetic bottle for UCN's and analyze their motion in the bottle. Neutrons have magnetic dipole moment and the direction of the magnetic moment with respect to the external magnetic field is conserved as long as the precession frequency of neutron in the magnetic field is much higher than the characteristic frequency of the magnetic field[7]. This requisite is called adiabatic condition.

In section 2 and 3, we report a new magnetic bottle and the result of calculation of the UCN orbit in the bottle, respectively. In the section 4, the experimental system under preparation is described, and the UCN injection method and the detection system of neutron annihilation in the bottle are discussed. The final section is devoted to the conclusive remarks.

§2. Magnetic Configuration

Usually, the magnetic field for UCN trap has been produced by using superconductors, and to activate these conductors, the cooling system is necessary. Generally, in the experimental room around the nuclear research reactor the cooling system is required to close in the room from the safety regulation and the power supply facility is often insufficient to produce magnetic field high enough to confine the UCN.

The magnetic bottle proposed here is composed of many pieces of permanent magnets made of cobalt samarium arranged in such a way as to produce multiple cusp field. The operation of this bottle requires neither electric power supply nor cooling system appropriately for setting up in the experimental room located in a controlled area around the nuclear reactor. The maximum field available at the surface of the permanent magnet is about 0.5 T. We can select the size of permanent magnet from various options provided by the supplier and make the larger magnet by joining many of small magnet pieces. Figure 1 shows the cross section of the magnetic bottle and the arrangement of permanent magnets. The size of the magnetic bottle is 40 cm × 40 cm ×

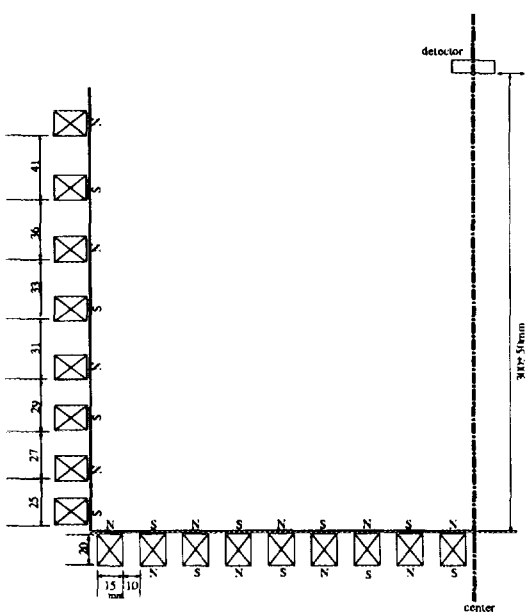

Fig. 1. Cross section of the multiple cusp magnetic bottle.

40 cm and the bars of permanent magnets which surround the vacuum chamber as shown in the figure. The vacuum chamber is evacuated down to the pressure of 10^{-7} torr for the purpose of avoiding the interaction of confined UCN's with the residual gas during their life times. The size

of a magnet bar is 1.5 cm × 2 cm × 40 cm and a bar consists of pieces of small magnets inserted into a aluminum steel tube. All of permanent magnet bars are lined up horizontally. The magnetic field inside the bottle is calculated replacing the permanent magnet with a current loop[8] which produces an magnetic field distribution equivalent to the original permanent magnet. The effect of the finite length of the permanent magnet is taken into account[9]. Figure 2 shows the calculated magnetic isobars projected in the vertical plane crossing across the vacuum chamber diagonally. The horizontal distance is normalized to the diagonal line. The field of the innermost isobar is 0.05

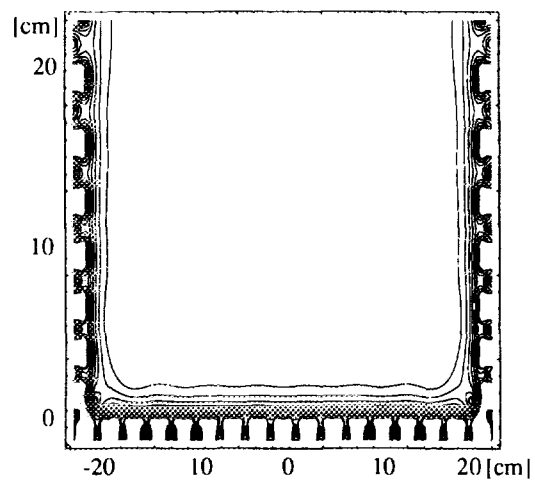

Fig. 2. Magnetic isobars projected in the diagonal vertical plane.

T, and the separation between adjacent isobars is 0.05 T. The last isobar which closes in the vacuum chamber corresponds to the field of 0.35 T. The permanent magnet bars on the vertical wall of the vacuum chamber is arranged so as that the ripple of the magnetic isobar is generated as shown in Fig. 2. The ripple is used for the transfer of the horizontal velocity component of UCN into the vertical component. This transformation mechanism is utilized for filtering untrapped UCN's staying long time in the magnetic bottle.

§3. Orbit of UCN in the magnetic bottle

The neutron possesses a magnetic dipole moment μ_n and a spin $\frac{1}{2}\hbar$. This magnetic moment interacts with an inhomogeneous external magnetic field by the interaction

$$V = -\mu \cdot B \tag{1}$$

Orbit of a UCN in the above-described magnetic bottle has been calculated integrating the equation of motion

$$m\ddot{\boldsymbol{r}} = -\nabla V - m\boldsymbol{g} = \pm|\boldsymbol{\mu}|\nabla|\boldsymbol{B}| - m\boldsymbol{g} \tag{2}$$

where m is the neutron mass, $\boldsymbol{g}$ is the acceleration in the gravity potential and this equation assumes the adiabatic condition. Figure 3 shows equi-potential surfaces of a UCN which is subject to the multiple cusp magnetic field and the gravity force. These potential surfaces are ones projected into

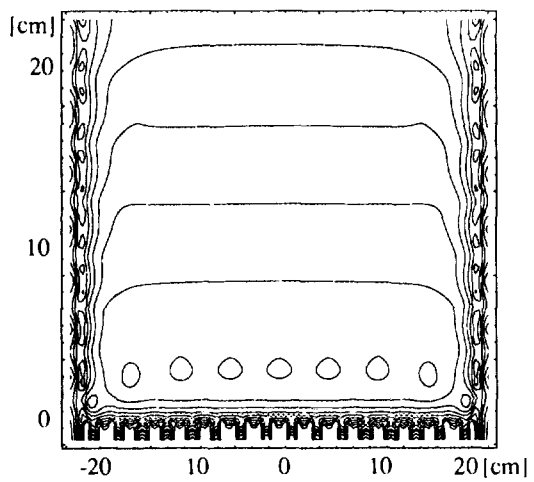

Fig. 3. Equi-potential surfaces which UCN's see.

the vertical diagonal plane similarly to the case of Fig. 2. Existence of closed potential surface assures the feasibility of UCN confinement in the magnetic bottle. The outermost closed potential surface corresponds to 20 neV, and the potential gap between adjacent surfaces is 5 neV. The maximum value of the effective potential for confinement is determined by the outermost closed surface of this figure, because this plane is the weakest. The 3D view of the calculated UCN orbit in the magnetic bottle is shown in Fig. 4 for 50 sec after the start of motion. Initially the UCN is released from nearby the center of the bottle with the velocity components v_x, v_y, and v_z of 0.5 m/s, -0.1 m/s, and 1.0 m/s, respectively. It should be noticed that the UCN orbit is well confined in the magnetic bottle for sufficiently long time. Thus the confinement of UCN's in the multiple cusp field will be successful.

The adiabatic condition is given by

$$\frac{\Omega}{\omega_L} \ll 1, \tag{3}$$

where Ω is the time dependence of the field seen by the neutron as it moves through the inhomo-

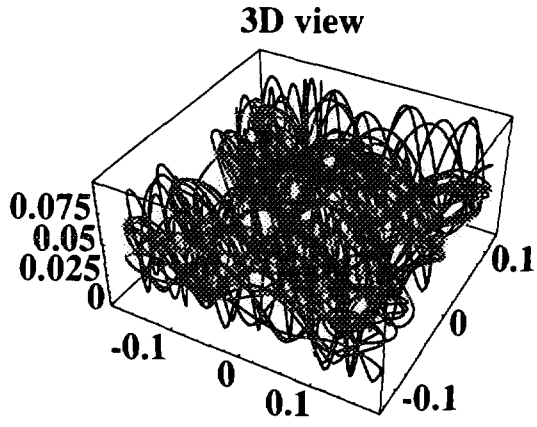

Fig. 4. 3D view of UCN orbit in the multiple cusp magnetic bottle. Times after the start of motion are 50 sec.

geneous field

$$\Omega = \frac{|\dot{\boldsymbol{B}}|}{B}, \tag{4}$$

and ω_L is the precession frequency called Larmor frequency of the neutron moment in the field,

$$\omega_L = \frac{\boldsymbol{\mu} \cdot \boldsymbol{B}}{\hbar} = 1.83 \times 10^8 B_{\mathrm{T}}. \tag{5}$$

Figure 5 shows Ω/ω_L that the neutron in Fig. 3 feels. The mean value of Ω/ω_L in Fig. 5 is 2.09×10^{-4}. Upper limit of the transition probability $w_{\uparrow\downarrow}$ is given[10] by

$$w_{\uparrow\downarrow} < \left(\frac{\Omega}{\omega}\right)^2 \sim 2.21 \times 10^{-9}. \tag{6}$$

We can say that the adiabatic condition is not violated.

§4. Experimental Set-up under Preparation

It is planned to check the performance of the multiple cusp magnetic bottle by the experiment. We inject UCN's provided by the super-mirror turbine[6] UCN source of the Kyoto University Research Reactor (KUR) into the bottle and observe the annihilation of UCN's occurring in the bottle by detecting protons. The velocity distribution of the UCN flux emitted from the super-mirror turbine is peaked at about 6 m/s of the velocity. The UCN is transported from the output of the turbine to the magnetic bottle through the vacuum transmission tube made of neutron mirror, or the magnetic transmission tube. Since the magnetic bottle is located at about 1.8 m higher than the output of

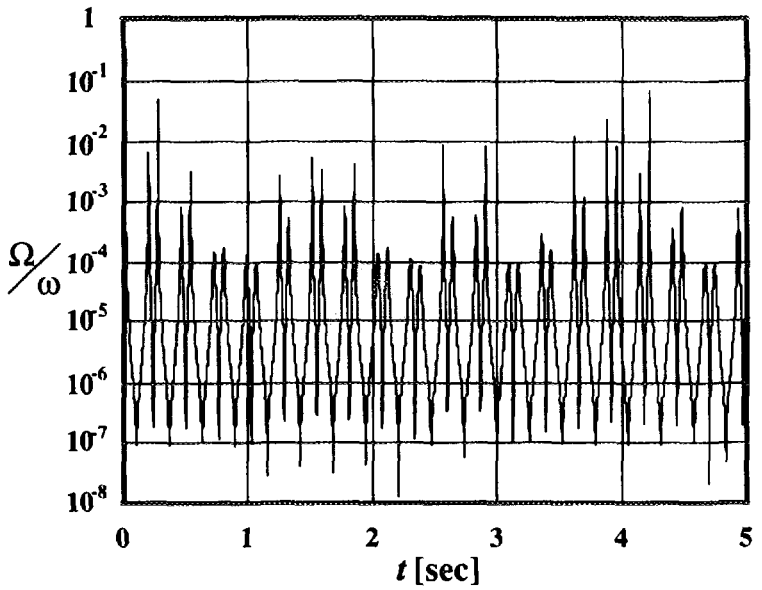

Fig. 5. The adiabatic condition

the super-mirror turbine, vertical velocities of the most of UCN's are nearly zero at the level of the magnetic bottle.

In order to capture UCN's in the magnetic bottle, a small aperture 4 cm in diameter is opened at the bottom wall of the bottle, and the array of permanent magnets in the aperture region are removed. Then UCN's enter into the bottle through this aperture upwards. After filling the sufficient amount of UCN's in the bottle, we close the entrance aperture by restoring the removed permanent magnets. These procedure is performed in the vacuum circumstance. As the time elapses after closure of the entrance hole, the UCN that does not satisfy the trapping condition escapes from the magnetic bottle. UCN's which have large horizontal kinetic energy but is reflected by the side potential wall outside the closed potential surface can stay in the bottle for significant time. But after the horizontal component of their kinetic energy is converted to the vertical one, some of them might escape from the bottle because of the violation of the trapping condition. The magnetic ripple described in the section 2 enhances the conversion of kinetic energy between the horizontal component and the vertical component, and as a consequence assists the escape of untrapped component of UCN's in the magnetic bottle.

In order to detect the annihilation of UCN in the magnetic bottle, a solid state detector with the circular sensitive area of 600 mm^2 and the thickness of the depletion layer of 300 μm is prepared. The detector is installed at 30±5 cm high from the center of the bottom surface of the bottle, and is

biased lower than 30 kV with respect to the inner wall of the vacuum chamber. Protons produced by annihilation of UCN's are accelerated to the detector by the electric field and impinge on the detector surface. Figure 6 shows the electric line of force along which protons are accelerated and collected by the detector. Effect of magnetic field on proton motion is negligible because the multi-

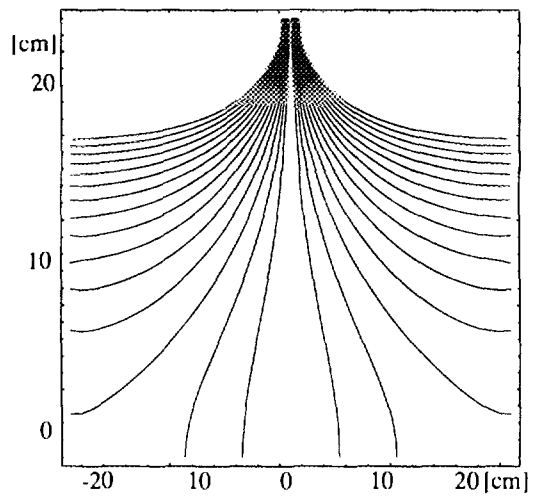

Fig. 6. Electric lines of force. Potential is applied to the detector with respect to the inner wall of the bottle.

cusp field is very small in the UCN confinement region. The shape of detector output signal is processed with computer to discriminate it from the output signal by background gamma rays.

§5. Conclusion

A new magnetic bottle of UCN's based on the multiple cusp configuration is proposed, and the confinement characteristics are analyzed. Since the bottle is composed of array of permanent magnet, neither cooling system nor high power supply is necessary for operation.

Experimental scheme for testing the magnetic bottle using the UCN source of KUR is discussed. Confinement of the UCN will be examined by detecting protons produced by the annihilations of UCN in the bottle. Feasibility of the detection system is shown by the calculation of electric line of force.

1) T. Bitter, F. Eisert, P. El-Muzeini, M. Kessler, E. Klemt, W. Lippert, W. Meinenburg, M. Baldo-Ceolin, D. Gibin, A. Guglielmi, M. Mezzetto, G. Puglierin, and D. Dubbers, Nucl. Instrum. Methods, **A321**(1992)284.

2) P. Ageron, W. Mampe, J.C. Bates, and J.M. Pendleburg, Nucl. Instrum. Methods. **A249**(1986)261.

3) W.G. Williams, Polarized Neutrons, (Clarendon, Oxford, 1988).

4) N. Hoshizaki and A. Masaike, Jpn. J. Appl. Phys., **25**(1986)L244.

5) H. Yoshiki, K. Sasaki, M. Ogura, T. Kawai, Y. Masuda, T. Nakajima, T. Takayama, S. Tanaka, A. Yamaguchi, Phys. Rev. Letters, **68**(1992)1323.

6) M. Utsuro, A. Yamaguchi, T. Miyachi, Y. Kawabata, and K. Okumura, Proc. Int. Conf. on Neutron Scattering, (Sendai, Oct. 11 14, 1994).

7) G.M. Drabkin, E.I. Zabidarov, Ya.A. Kasman, and A.I. Okorokov, Sov. Phys. JETP, **29**(1969)261.

8) H. Nihei, H. Enomoto, and J. Morikawa, Jpn. J. Appl. Phys., **31**(1992)1885.

9) T. Watanabe, J. Plasma and Fusion Res., **63**(1990)482.

10) R. Golub, D. Richardson, and S. K. Lamoreaux Ultracold Neutron (1991)

Construction of a Stable and Homogeneous Magnetic Field at 10 milligauss for Neutron Electric Dipole Moment Measurements: Preparatory Phase

Enrico Gravador, Hajime Yoshiki,Huang Feizeng
Ibaraki University

April 6, 1996

Abstract

A superthermal UCN edm measuring machine is currently under construction at KEK. It utilizes a magnetically shielded superconducting solenoid at liquid helium temperature to generate a stable and homogeneous magnetic field at 10 milligauss. The design of the magnetic shield and solenoid and preliminary evaluation of shielding effectiveness is presented.

1 Introduction

The use of superconducting solenoid in an edm machine has been suggested by Ramsey [1] in 1978. In 1992, H. Yoshiki and others [2] produced UCN in superfluid helium in a prototype cryostat dubbed Mark3000 [3]. Superconducting magnetic shield and solenoid at liquid helium temperature can now be integrated in the superthermal UCN source mentioned above for neutron electric dipole moment measurements. It is aimed that with the use of superconducting shield and solenoid, a drift of 10 nanogauss could be obtained. This will make possible measurements of neutron edm in the order $10^{-25} \sim 10^{-27}$ e.cm .

2 The Design of the Magnetic Shield and Solenoid

The magnetic shield consists of a 3-layer ferromagnetic shield at room temperature and a superconducting shield at liquid helium temperature . The relative positions of the shields and solenoid are shown in Figure 1. The coaxial ferromagnetic cylinders (Figure 2) have the same length (3200 mm), thickness (1.6 mm), and relative permeability (10^5 , TMC-V Tokin). Their inner diameters are ϕ1018 ϕ1098, ϕ1178. They are heated to 1050°C $\sim$ 1150°C for 3 hours and cooled down to 600°C $\sim$ 300°C at 80°C $\sim$ 150°C/hour. The coercive force is 2 amp/meter. The cylinders are spaced equally at 40 mm.

The superconducting shield (2830 mm in length and 725 mm in diameter) is contructed by winding lead foil on an aluminum cylinder (Figure 3) . The foil has a thickness of 0.1 mm and width of 80 mm. It is wound at a pitch of 8 mm. After 10 turns the thickness of the superconducting shield becomes 1 mm. The lead foil windings are fastened by Kapton tapes.

The superconducting solenoid (2630 mm in length and 684 mm in diameter) is constructed using NbTi/Cu composite wire (ϕ0.48 mm after insulation) wound on an aluminum cylinder, double-layer, with 4129 turns/meter (Figure 4). The persistent current necessary to generate 10 milligauss of magnetic field at the center of the solenoid is no more than 2 milliamperes.

The superconducting shield and solenoid are contained in a liquid helium inner vessel of a cryostat (see Figure 1). The outer vessel is maintained at 77°K.

3 Shielding Effectiveness of Ferromagnetic Shield

Shielding effectiveness can be expressed in terms of shielding factor which is the ratio of the attenuated field (field inside the shield) and the external field. We measured the ambient magnetic field and the attenuated field inside the ferromagnetic shield using Bartington^{TM} fluxgate meter. Let z-axis be parallel to the axis of the shield and let x-axis be a radial axis. Figures 5 - 9 describe the shielding of external magnetic field. The scattered points refer to the ambient field while the different lines correspond to different radii. At

the center of the shield we get a shielding factor of 10^{-4}. Figures 6 and 8 are magnified views near the center of the shield.

4 A Model Superconducting Shield

The shielding effectiveness of the combination of ferromagnetic and superconducting shields will be evaluated soon. As a preliminary investigation we constructed a model shield made from the same lead foil being used in the actual shield. We investigated its shielding effectiveness and its performance in time (i.e., drift) .

At this stage, using analytical means to get a physical grasp of magnetic shielding in the model shield is sufficient. Let us consider magnetic shielding by a semi-infinite superconducting hollow cylinder for an applied field parallel to the axis of the cylinder (Figure 10). The shielding is governed by the equation

$$B_{axial} = A\ e^{(-kz/R)} \tag{1}$$

where R is the shield radius and z is measured from the open end along the axis of the shield. k is theoretically 3.83 .

To measure the shielding factor for the model shield, parameter k and constant A must be determined. Figure 11 describes the experimental setup. The lead foil is wound on a Teflon tube (200 mm in length and 92 mm in diameter). The bottom is closed by a cap made from the same lead foil and is fastened by Kapton tape. The creases in the cap at its edges could provide apertures where external field can penetrate the shield. (We had to close the bottom to reduce noise level inside the shield).

A coil is wound on the body of the cryostat which provides applied magnetic fields. In calculating the shielding factor we use the method where magnetic intensity is determined at a given point in space when shield is not present and when shield is present. The absolute value of the applied field can be determined . Determination of the attenuated field, however, employs a differential measurement.

In measuring the magnetic field inside the shield, we use a dc Superconducting Quantum Interference Device (SQUID) which is sensitive to changes in magnetic field in the order of microgauss (Figure 12). Figure 13 illustrates

SQUID response to excitation current in the coil. The zero point in the differential measurement is set when the current in the coil is equal to zero. The different lines correspond to different depths. From these lines we can read out the magnetic field inside the model shield at different depths for a given current. We can now determine the shielding factor. Figure 14 is a plot of the shielding factor against depth. The datapoints correspond to a current of 10 milliamperes. By fitting the datapoints from z=20 mm to z=80 mm we determine k to be 3.758 ± 0.139 . It differs from theoretical value of 3.83 by 1.87% and is within the error (1σ) . The points which diverge starting from the center (z=90 mm) indicate magnetic flux penetration thru the bottom edge. These points no longer obey Eq(1). Near the center, the shielding factor is 10^{-5}.

We also investigated the performance of the model shield. We monitored the ambient field for 22 hours. Figure 15 shows transition to thermal equibrium in the first 10 hours, after which a stable output was obtained. This continued with a drift of about 1 microgauss. A large spike indicate disturbance from outside. This part of work is still under test.

5 Conclusion

The design of magnetic shields and superconducting solenoid, parts of a superthermal UCN edm machine, is given. Preliminary evaluation of the shielding effectiveness of the shields are also given.

References

[1] Ramsey, N., Physics Reports. **43**,(1978) 409.

[2] Yoshiki, H., et.al., Physical Review Letters. **68**, (1992) 1323.

[3] Yoshiki, H., et.al., Cryogenics. **34**,(1994) 277.

[4] Cabrera, B., *"The Use of Superconducting Shields for Generating Ultra-Low Magnetic Field Regions and Several Related Experiments"* Ph.D. Thesis, Stanford University, 1975 .

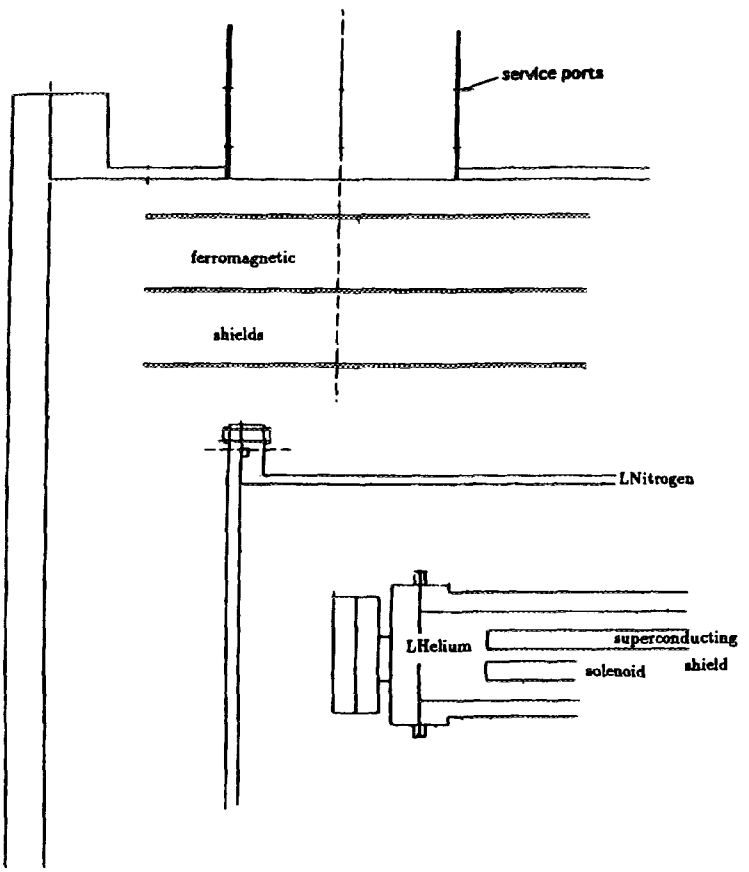

Figure 1: Schematic cross-section showing relative positions of the shields, solenoid, inner (LHelium) and outer (LNitrogen) vessels of the cryostat.

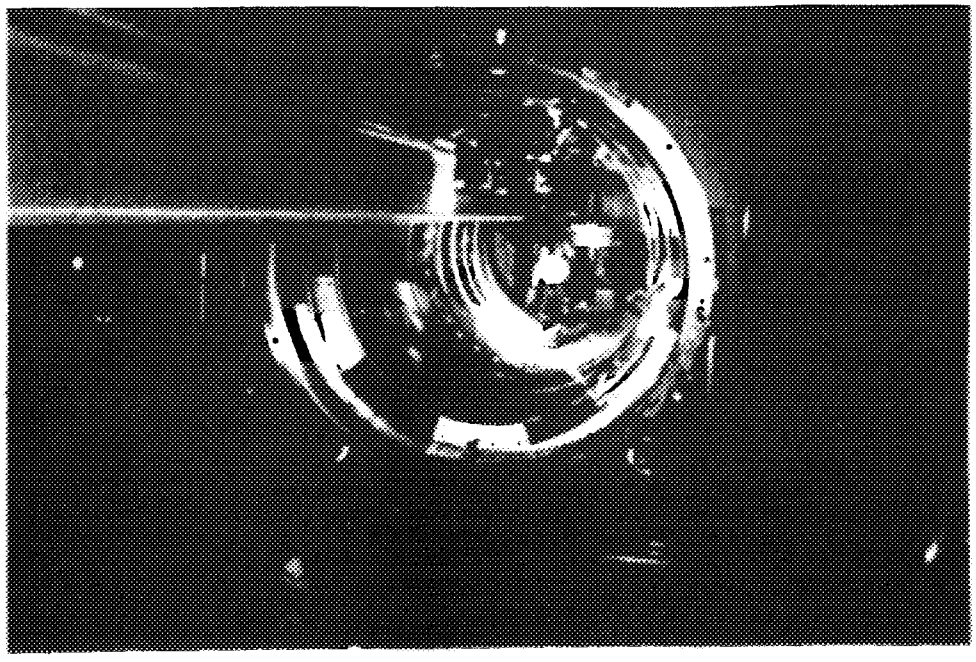

Figure 2: The 3-layer ferromagnetic shield.

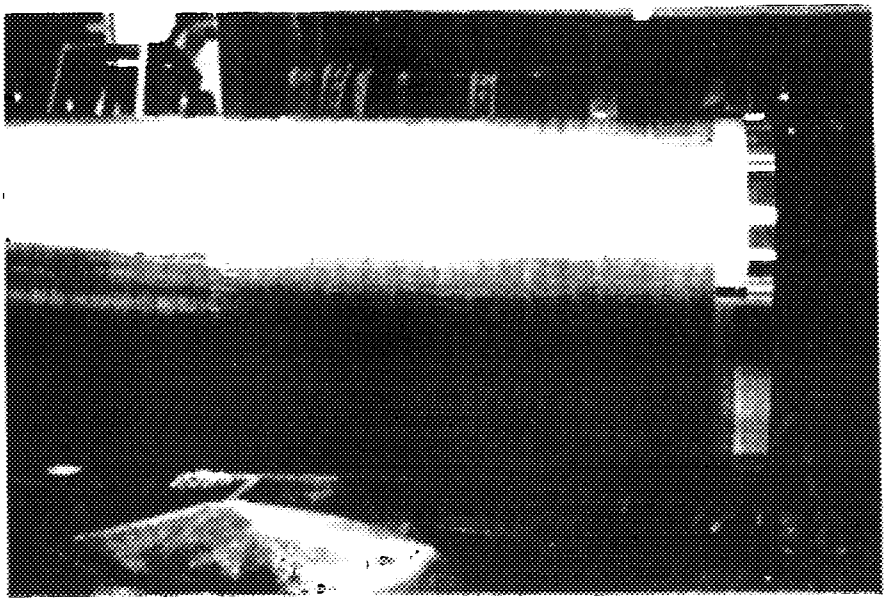

Figure 3: The Superconducting Lead Shield.

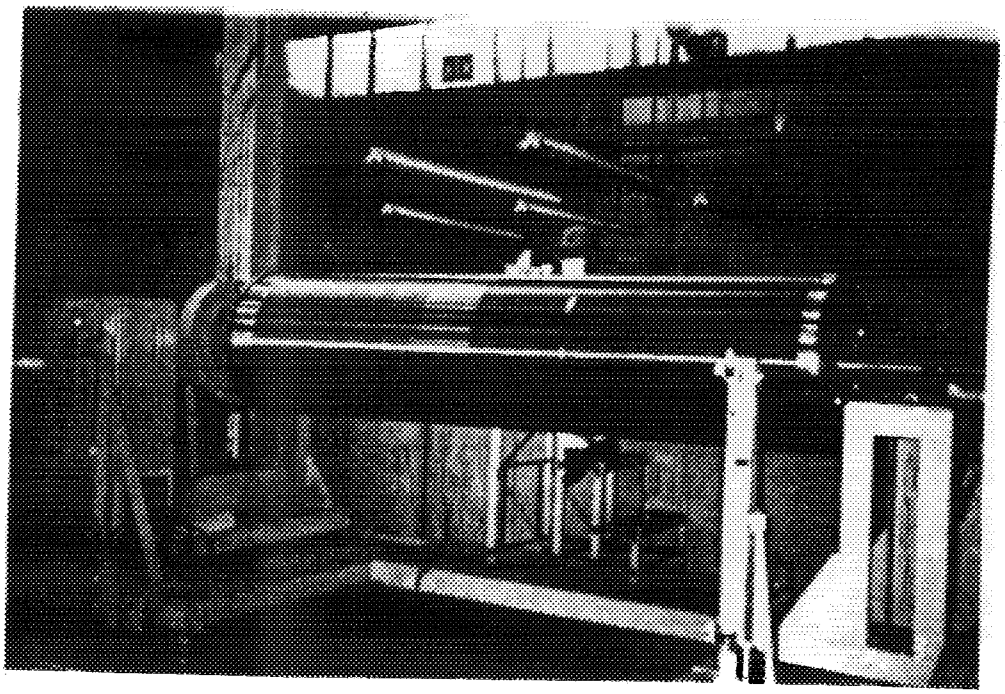

Figure 4: The solenoid.

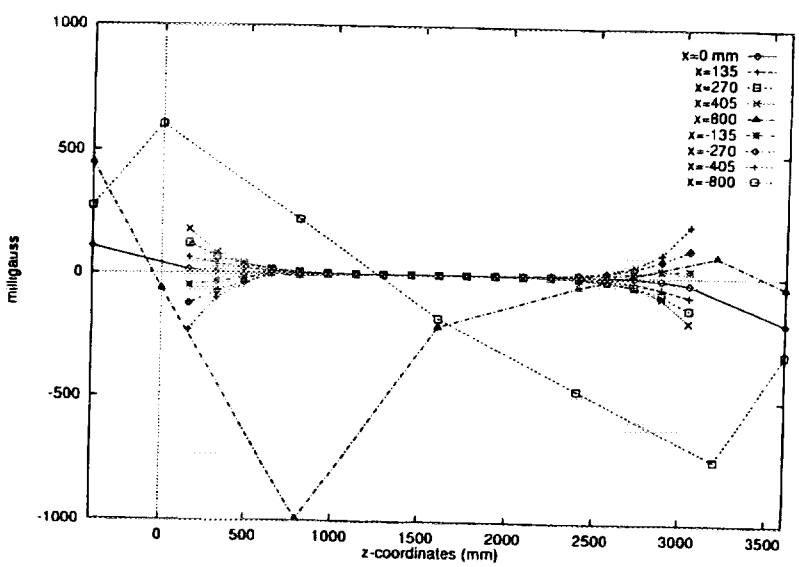

Figure 5: Attenuation of ambient magnetic field by the 3-layer ferromagnetic shield along a radial direction x.

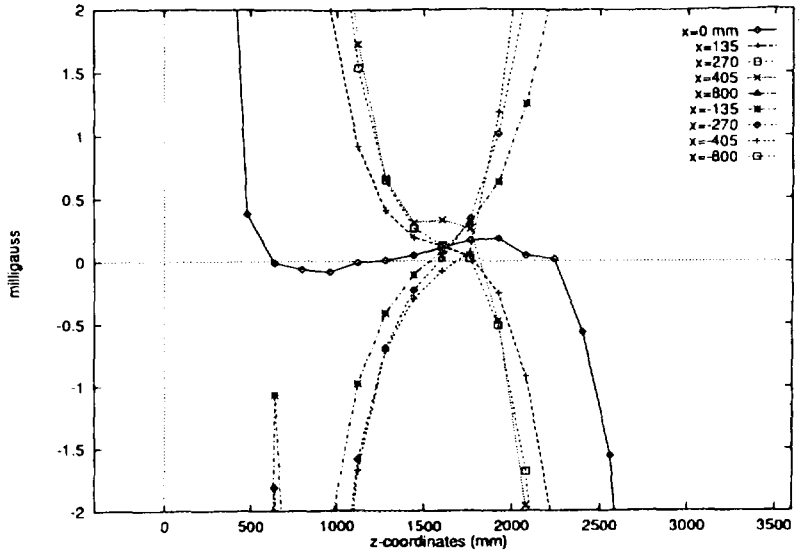

Figure 6: This is a magnified view of Figure 5 near the center.

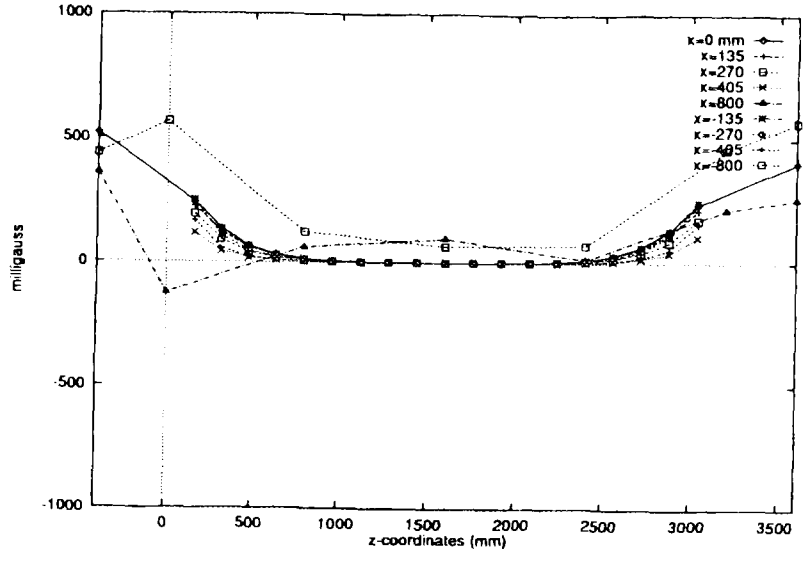

Figure 7: Attenuation of ambient magnetic field by the 3-layer ferromagnetic shield along axial direction z.

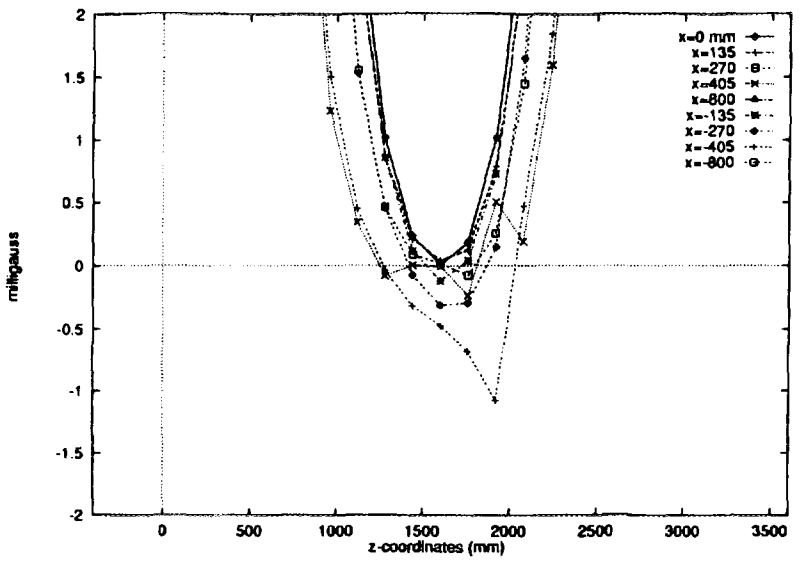

Figure 8: This is a magnified view of Figure 7 near the center.

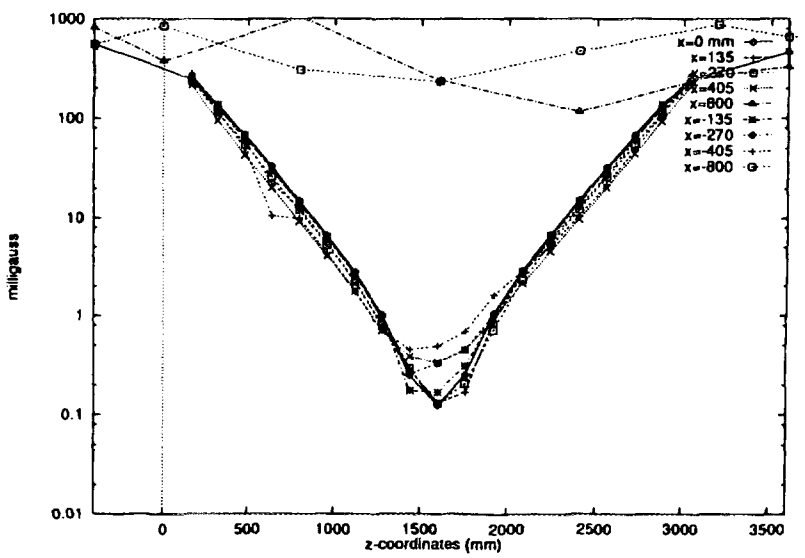

Figure 9: This is the absolute value of the magnetic field inside the ferromagnetic shield.

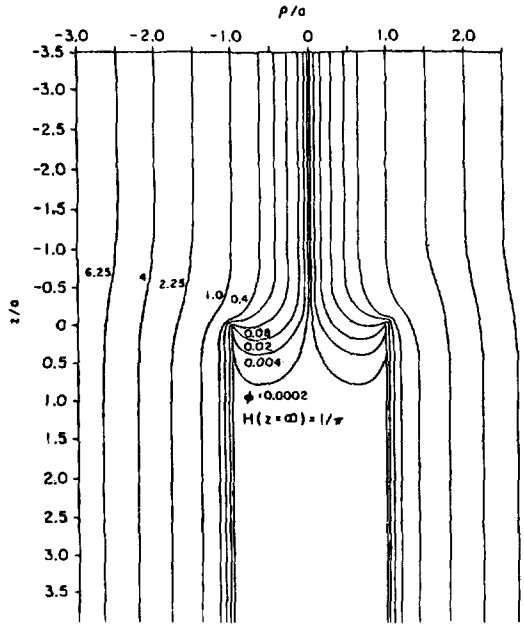

Figure 10: Tubes of constant flux centered about $\rho = 0$ for an infinitely thin semi-infinite cylinder in an axial field (Cabrera [4], p.19) .

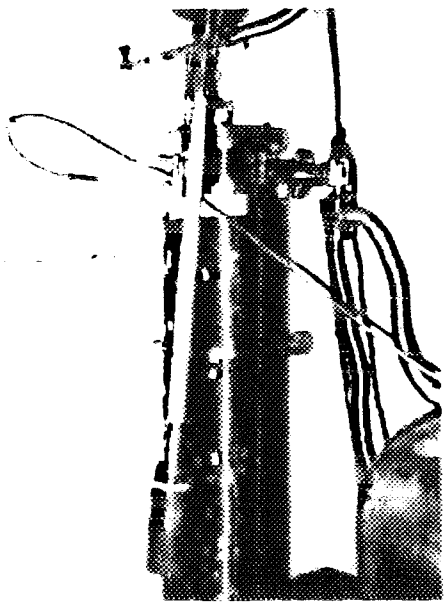

Figure 11: The experimental set-up for meausrement of parameter k.

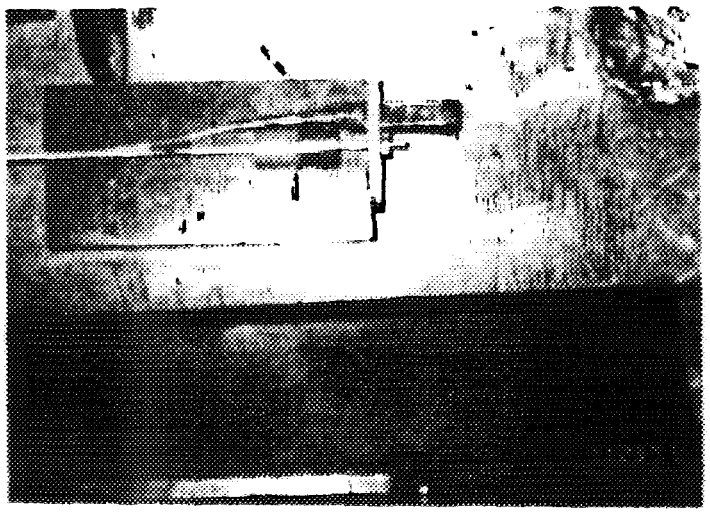

Figure 12: Setup of SQUID sensor inside a Nb casing and a 3-turn pick-up coil mounted on a G10 cylinder.

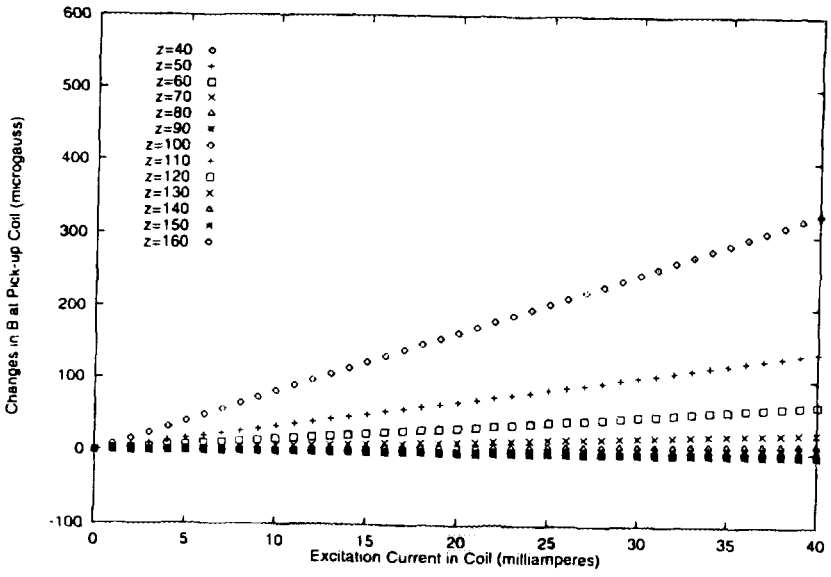

Figure 13: SQUID response to coil exitation current.

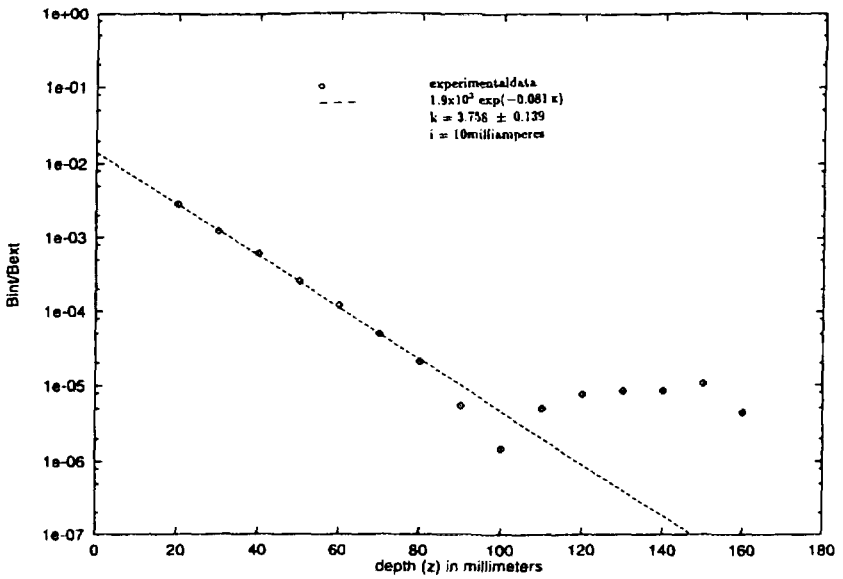

Figure 14: Shielding effectiveness of the model shield.

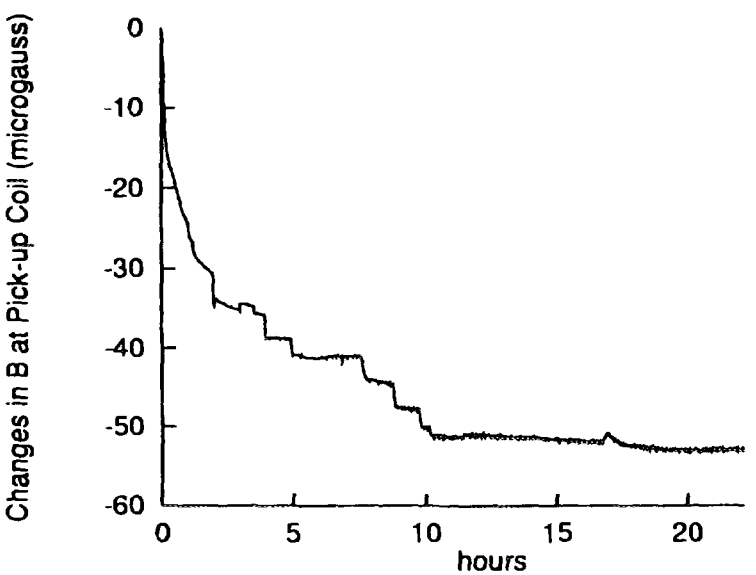

Figure 15: Performance of the model shield with time.

International Workshop on Science in Neutron-Arena of JHP
KEK, Tsukuba, Japan
March 26-27, 1996

Fundamental Physics Research and Neutron Interferometry

Ioffe, Alexander

Berlin Neutron Scattering Center, Hahn - Meitner - Institut,
Glienicker Str. 100, 14109 Berlin, Germany
and
St. Petersburg Nuclear Physics Institute Acad. Sci. of Russia,
Gatchina, 188350 Russia

ABSTRACT

The possibility of the use of an extremely sensitive neutron interferometry technique for the study of electromagnetic structure of the neutron and the parity non-conservative effects in neutron spin rotation is discussed.

1. The mean square electrical radius of the neutron and its polarizability

One of fundamentals problems of nuclear physics is the electrical structure of the neutron. The characteristics of such a structure is an electrical charge distribution inside it - the mean square electrical radius of the neutron and its polarizability, i.e. the induced electrical dipole moment that appears in the external field.

The problem of determination of the neutron-electron scattering length a_{ne} and following from it the question about the sign of the mean square intrinsic charge radius of the neutron $\langle r_{in}^2 \rangle_n$ is a subject of active studies and discussions last years [1-5]. This value is a characteristic of the electrical charge distribution inside the neutron:

$$\langle r_{in}^2 \rangle_n = \int \rho(r) \cdot r^2 \cdot d^3r \Big/ \int \rho(r) \cdot d^3r$$

It can be determined by the neutron-electron interaction amplitude a_{ne} and the Foldy parameter a_F:

$$\langle r_{in}^2 \rangle_n = \frac{3h^2}{Me}(a_{ne} - a_F)$$

Thus, for an experimental determination of $\langle r_{in}^2 \rangle_n$ one has to measure a_{ne} and compare its value with the Foldy parameter.

Values of the amplitude of the neutron-electron interaction amplitude a_{ne} obtained in experiments on neutron transmission

$$a_{ne} = -(1.309 \pm 0.024)\ 10^{-3}\ \text{fm} \qquad [4]$$

$$a_{ne} = -(1.577 \pm 0.034)\ 10^{-3}\ \text{fm} \qquad [5]$$

result in fatal uncertainty in the determination even of the sign of the mean square electric charge radius of the neutron.

At present it is practically common acceptable, that this difference is connected with methods of the data treatment, because both groups have used practically the same set of experimental data [1, 3]. It should be noted, that experiments on neutron diffraction on a monocrystal of ^{186}W [6] have resulted in $a_{ne} = -(1.60 \pm 0.05) \cdot 10^{-3}$ fm, so that the difference of values of a_{ne} is significant.

One way to study the electromagnetic structure of the neutron is to investigate its interaction with atoms of heavy elements. The value of the neutron - electron interaction amplitude can be principally obtained from the energy dependence of the total neutron cross section $\sigma_{tot}(E)$ ($E = 1 \div 20$ eV), measured in neutron transmission experiments and $\sigma_{tot}(0)$.

In spite of the relative weakness of effects of neutron - electron interaction in comparison with the strong nuclear interaction, they can be detected because of the interference between neutron waves, scattered at a nucleus and at atom electrons, that allows an experimental determination of the mean square electrical radius of the neutron and its polarizability.

We are going to carry out experiments, which will increase an accuracy of the determination of the neutron-electron scattering amplitude a_{ne} and the polarizability α_n of the neutron. The values of a_{ne} and α_n can be obtained from energy dependence of the coherent scattering cross section $\sigma_{coh}(E)$ in rather wide energy range $E = 0$ - 200 keV. This cross section can be defined as a potential part of the total neutron cross section $\sigma_{tot}(E)$, which can be experimentaly measured. However, to do this $\sigma_{tot}(E)$ should be corrected for incoherent scattering, absorbtion and resonance contributions for all isotopes, which contain in the sample.

At thermal energies the total cross section is also strongly influenced by interference solid state effects (connected with the agregate state of the sample), which can be evaluated only with a limited precision [4]. These corrections are small and defined with a reasonable accuracy in electron-volt region, but are very large and uncertain for the very low energies ($E \sim 0$). Therefore, is proposed to obtain $\sigma_{coh}(0)$ from the neutron scattering length b_{coh} measured by thermal neutrons ($E \sim 10^{-3}$ eV).

Because of the Z-dependence of a_{ne}, these measurements have to be carried out on atoms of heavy elements. The lead isotope ^{208}Pb is particularly interesting, because its nucleus has only two resonance levels [3], that significantly contribute to the total neutron cross section.

For these reasons we are going to carry out the precision measurements within the accuracy of about 10^{-4} of $\sigma_{tot}(E)$ by the method of resonance detectors [7] and of b_{coh} by the neutron interferometry method [8] with a high enriched ^{208}Pb sample. All these experiments will be carried out with the same sample: such approach will allow us to eliminate uncertainaties, resulting from possible contaminations in the sample.

2. Neutron Interferometry Method of Study of Parity Violation in Cold Neutron Transmission

The phenomenon in weak interaction provides a possibility to investigate the nature of the weak force in the presence of the much stronger electromagnetic and strong interactions and is the subject of permanent interest during decades. Weak currents result in small parity-nonconservation (PNC) effects under the propagation of neutrons through the ordinary matter [9-11].

The scattering amplitude in this case can be written as the sum of parity conservative and non-conservative terms:

$$f(\vartheta) = f_{PC}(\vartheta) + f_{PNC}(\vartheta) \tag{1}$$

For polarized neutron beam transmission through a non-polarized target the weak term in neutron - nucleus interaction results in an average interaction, that depends on the neutron spin $\vec{\sigma}$ and the momentum of the beam $\vec{p}$

$$f_{PNC}(0) = C\langle\vec{\sigma}\cdot\vec{p}\rangle \tag{2}$$

where the complex coefficient C is expected to be proportional to G, the weak interaction coupling constant. The real part of the coefficient C, which is constant at low energy, results in a helicity dependence of ϕ_{PNC}. It was shown [12], that for a neutron beam with polarization vector $\vec{P}$, the rotation angle of this vector around $\vec{p}$ is

$$\phi_{PNC} = -4\pi \cdot N \cdot l \cdot \mathrm{Re}(C)$$

where the positive sign of ϕ_{PNC} corresponds to a right hand rotation of $\vec{\sigma}$ around $\vec{p}$.

The experimental approach used in a number of experiments, where such effects were observed [13, 14], is neutron polarimetry, that is the measurement of the angular rotation of the neutron beam polarization vector ϕ_{PNC} . A major problem in these experiments was the separation of a small PNC effect from the neutron precession in the residual magnetic field. In order to extract a net PNC signal from this background, a spin flip coil was inserted in the centre of a low field region. Measurements were carried out with the sample alternately placed before or behind the spin flip coil: the sign of ϕ_{PNC} was changed for these two sample's positions, whereas the angle of the neutron precession in the residual magnetic field did not change sign; it allowed the compensation of the large systematical effect.

However, the small angle neutron scattering in the sample makes trajectories of neutrons different for the two target positions (before and behind the spin flip coil). The angles of the neutron spin precession in stray magnetic fields before and behind of this coil are in general different. Thus, because of the change of sample positions induces an uncompensated systematical error, which limits the accuracy of experiments.

Here a new method of the study of PNC effects on neutron spin rotation is proposed. It is based on methods of neutron interferometry and principally does not require the change of the sample position in order to identify a small PNC effect above the neutron precession in magnetic field, so that it is free from the systematical error discussed above.

The neutron-nucleus weak interaction results in the helicity dependence of the coherent forward scattering amplitude $f(0)$. It can also be described by the neutron refraction index n

$$n = \left[1 + \frac{\lambda^2 N}{\pi} f(0)\right]^{1/2}$$

where λ is the neutron wavelength and N - the atomic density. If $f^+(0)$ and $f^-(0)$ are the amplitudes for helicity +1 and -1, respectively, then one can write using Eq. (1):

$$n^+ = 1 + \frac{\lambda^2 N}{2\pi}\left[f_{PC}^+(0) + f_{PNC}^+(0)\right] = n_{PC}^+ + n_{PNC}^+$$

$$n^- = 1 + \frac{\lambda^2 N}{2\pi}\left[f_{PC}^-(0) + f_{PNC}^-(0)\right] = n_{PC}^- + n_{PNC}^-$$

so that the neutron refraction index consists of a parity conservative part n_{PC} and a comparatively small parity nonconservative part n_{PNC}.

Let us consider a neutron interferometry experiment, where a sample is placed in one of the interferometer arms

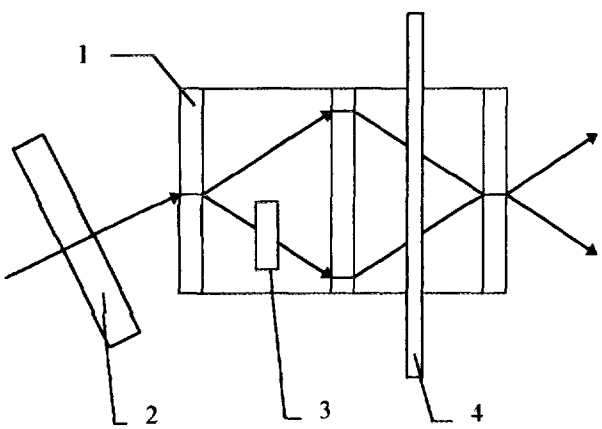

Fig. 1. Layout of the experiment. 1 - neutron interferometer, 2 - flipper, 3 - sample, 4 - shifter

and the spin state of the polarized incident beam is controlled by a flipper, installed in front of the interferometer (Fig. 1). Total phase shifts, acquired by the transmission through the sample of neutron waves with opposite spin states $|\uparrow\rangle$ and $|\downarrow\rangle$, parallel and antiparallel to the neutron momentum

$$\Phi^+ = p \cdot t \cdot n^+ \tag{3a}$$

$$\Phi^- = p \cdot t \cdot n^- \tag{3b}$$

so that the phase difference between beams I and II (see Fig. 1), which is actually measured by the interferometer can be written as

$$\varphi^+ = p \cdot t \cdot (n^+ - 1) = p \cdot t \cdot n_{PC}^+ + p \cdot t \cdot n_{PC}^+ = \varphi_{PC}^+ + \varphi_{PNC}^+ \tag{4a}$$

$$\varphi^- = p \cdot t \cdot (n^- - 1) = p \cdot t \cdot n_{PC}^- + p \cdot t \cdot n_{PC}^- = \varphi_{PC}^- + \varphi_{PNC}^- \tag{4b}$$

Here, parity nonconcervative parts of the phase shift are

$$\varphi_{PNC}^{\pm} = p \cdot n_{PNC}^{\pm} \cdot t \tag{5}$$

where t is the sample thickness.

Two different ways for the determination of φ_{PNC} in a neutron interferometry experiment are the use of the transversally or longitudinally polarized incident neutron beams.

In the first case, the experiment is just neutron interferometry analogue of PNC experiments described above and principally is the measurement of the rotation angle of the spin of transversally polarized incident neutron beam, that is the rotation of the polarization vector. The phase shift φ_{PNC} can be defined by the angle of the PNC spin rotation, as $\varphi_{PNC} = \phi_{PNC} / 2$.

In the second case, the neutron spin is parallel or antiparallel to the momentum, so it does not lead to any rotation of the polarization vector. However, opposite helicities +1 and -1 will result in parity nonconcervative phase shift (Eq. (4)).

In both cases the parity conservation part φ_{PC} (Eqs. (4a) and (4b)) consists of nuclear and magnetic phase shifts

$$\varphi_{PC} = \varphi_{nucl} + \Delta\varphi_m$$

Here

$$\varphi_{nucl} = (1 - n_{nucl}) \cdot p \cdot t = N \cdot \lambda \cdot b_c \cdot t$$

(b_c. is the coherent scattering length of the sample under the study) and $\Delta\varphi_m$ is the difference of the neutron spin precession angles in the residual magnetic field, which can have a rather small value of about 0.5 mG (defined by a proper magnetic shielding), but which principally can be different for each of interferometers' arms.

Reversing the spin states of the incident beam changes only the signs of the PNC effect and the magnetic phase shift, so that one can write (φ_0 is an initial phase shift)

$$\varphi_{|\uparrow\rangle} = \varphi_0 + \varphi_{nucl} + \Delta\varphi_m + \varphi_{PNC} \qquad (6a)$$

$$\varphi_{|\downarrow\rangle} = \varphi_0 + \varphi_{nucl} - \Delta\varphi_m - \varphi_{PNC} \qquad (6b)$$

Thus, in this case one avoids the use of the spin flip coil in the low field region to change sign of the PNC effect and problems connected with it. The effect caused by residual magnetic field slightly violates the symmetry of the experiment, but can be corrected for measurements without sample (Eq. (6)), wherefrom one can easily evaluate such asymmetry.

The crux of the matter is that the change of trajectories of neutrons because of the scattering in the sample will result in very much reduced systematical error. Indeed, the scattering violates extremely rigid interference conditions, so that scattered neutrons will not contribute to the interference pattern, only to the background and slightly reduce the interference pattern visibility. Only neutrons scattered within a small angular acceptance $\Delta\theta \approx 1$ sec of arc will still contribute to the interference pattern, but the artefact they can cause is proportional to $(\Delta\theta)^2$ and is negligible.

Thus, only one of the considered effects mimics the PNC spin rotation. However, in the proposed method the measuring process is confined in the size of the interferometer, so that the length of the magnetic field-free space is about 6 cm, in contrast to the conventional polarimetry technique, where it amounts up to 30 cm. This fact reduces significantly the problem of residual magnetic field in the neutron interferometry method.

Moreover, in our case the change of the spin state of the neutron beam is realized by a flipper which is placed *not inside* , but *outside* of the apparatus. Thus, recording two interference patterns (Eqs. (6a, b)), which correspond to the spin-up and spin-down states of the incident beam one can determine $\Delta\varphi_{PNC}$. Certainly, an accuracy of determination of $\Delta\varphi_{PNC}$ is defined by an accuracy of phase measurements in neutron interferometry experiment and the latter depends on the visibility of interference pattern and count rate. Simulations shows that for 30 days experiment by the neutron interferometer installed at the reactor of

HMI (P = 10 MW) [18], the neutron optical activity at the level of $5 \cdot 10^{-5}$ can be determined. Certainly, the use of more intensive neutron sources will allow the improvement of this value. For the high-flux reactor of ILL this level can be put down up to 10^{-5} for the same time of data collection, that is comparable with the sensitivities reached in experiments [13-15, 17].

Acknowledgements.

The first part of this article is research, carrying out in the close collaboration with M. Vrana (NPI, Rez) and V. Zabiyakin (St. PNPI). The author is also thankful to F. Mezei (HMI, Berlin), P.Krupchitsky (ITEP, Moscow) and S. Lamoreaux (University of Washington, USA) for fruitful discussions.

References:

1. Leeb H. and Teichtmeister C., Phys. Rew. C **48**, 1719 (1993).
2. Alexandrov Yu., Z. Phys. A **344**, 219 (1992).
3. Nikolenko V., Popov A, Z. Phys. A **341**, 365 (1992).
4. Koester L., W.Waschkowski, Mayer J., Z. Phys. A **329**, 229 (1988).
5. Alexandrov Yu., Vrana M., Garsia J. Manrike, Machekhina T., Sedlakova L., Sov. J. Nucl. Phys. **44**, 900 (1986).
6. Alexandrov Yu., Machekhina T., Sedlakova L., Fykin L., Sov. J. Nucl. Phys. **20**, 623 (1975).
7. W.Waschkowski, Koester L., Z. Naturforsch., Teil A **31**, 115 (1976).
8. Ioffe A., Lukas P., Mikula P., Vrana M., Zabiyakin V. Z. Phys. A - Hadrons and Nuclei 348 (1994) 243.
9. F.C. Michel, Phys.Rev. **133B**, (1964).329.
10. L.Stodolsky, Phys.Lett. **50B**, (1974) 352.
11. M. Forte, Inst. Phys Conf. Ser. **42** (1977) 86.
12. M. Forte, Nuovo Cim. A4 (1973) 276.
13. M. Forte, B. R. Heckel, N. F. Ramsey, Phys. Rev. Lett. **45** (1980) 39.
14. S. Saha, Ph.D. Thesis, University of Washington, 1989.
15. B. R. Heckel, Phys. Lett. **B119** (1982) 298.
16. D. Zaretsky, V. Sirotkin, Sov. J. Nucl. Phys. **42** (1985) 561; **45** (1987) 808; **57** (1994) 39.
17. P. Krupchitsky, V. Bolotsky, O. Ermakov, I. Karpikhin, S. Lamoraeux, R. Golub, Berlin Neutron Scatterig Centre Experimental Reports - 1994, p. 364; S. Lamoraeux, R. Golub, Berlin Neutron Scatterig Centre Experimental Reports - 1994, p. 365.
18. T. Baranova, G. Drabkin, A. Ioffe, S. Kirsanov, F. Mezei, M. Vrana, V. Zabiyakin, Physica B, **213&214** (1995) 839.

Non magnetic neutron spin quantum precession using multilayer spin splitter and a phase−spin echo interferometer

T. Ebisawa, S. Tasaki, T. Kawai, T. Akiyoshi (Research Reactor Institute, Kyoto Univ.)
N. Achiwa, M. Hino (Physics Department, Kyushu Univ.)
Y. Otake (Ibaraki National College of Technology)
H. Funahashi (Physics Department, Kyoto Univ.)

1 Introduction

We have developed cold neutron optics and interferometry using multilayer mirrors for a long time[1, 2]. Advantages of multilayer mirrors are its applicability to long wavelength neutron and a great variety of the mirror performance[3]. I like to focus our presentation on recent development cold neutron spin interferometry using multilayer spin splitters.

It was pointed out that the neutron spin echo spectroscopy is regarded as a spin interferometer[4], because the neutron spin precession can be expressed as coherent superposition of two spin eigenstates perpendicular to the precession plane. As interesting applications based on the coherent superposition principle of spin echo spectroscopy, coherent scattering cross section measurements using different refractive indices in non magnetic matters of the two spin states was proposed by V. G. Baryshevskii et al. [5] and realized experimentally by M. Hino et al. [6]. Studies on tunneling phase shift in magnetic thin layer have been made experimentally by M. Hino et al. [7, 8] and N. Achiwa et al. [9].

The idea of the present spin interferometry is based on non magnetic neutron spin quantum precession using multilayer spin splitters[10]. In the report, we describe the structure and principle of the multilayer spin splitter and discuss the successful performance test results of the spin splitters[11]. As an application of the spin splitters, a new phase−spin echo interferometer was proposed[10]. We demonstrate experimentally the performance of the phase−spin echo interferometers[11].

2 Multilayer spin splitter and non magnetic neutron spin quantum precession

We consider a polarized neutron in the X−Y plane in a vertical magnetic field. We take the X−Y plane in the horizontal plane and the Z−axis in the vertical direction. The polarized neutron makes Larmor precession in the X−Y plane. Quantum mechanics gives the equation (1) for the polarized neutron.

$$\begin{aligned} |S_{xy}(\theta)\rangle &= (1/2)\{|\uparrow_z\rangle + \exp(i\theta)|\downarrow_z\rangle\} \\ &= (1/\sqrt{2})\exp(i\theta/2)\{\cos(\theta/2)|\uparrow_x\rangle - i\sin(\theta/2)|\downarrow_x\rangle\} \end{aligned} \quad (1)$$

Where θ is the precession angle.

This equation means that the polarized neutron is equivalent to the coherent superposition of the two spin eigenstates parallel to the Z−axis. The phase difference θ between the two spin states is related to the precession angle θ of the polarized

neutron. Therefore, if we can produce the two spin eigenstates with a phase difference by a multilayer spin splitter, we could have another precession device as well as conventional Larmor precession in a magnetic field[10].

Experiment on the coherent spin superposition was proposed firstly by E. P. Wiger as Gedanken experiment [12] and later by A. Zeilinger with silicon interferometer [13, 14]. The coherent spin superposition was realized experimentally by J. Summhammer et al. using silicon interferometer[15, 16]. It should be noted that in the silicon interferometer a neutron makes no precession as the whole, because the forward beam is complementary to the deviated beam and the both precession of the two subbeams is canceled each other [14, 16].

We consider a multilayer spin splitter which consists of a magnetic multilayer mirror on top, followed by a Ge gap layer and a non magnetic multilayer mirror, as shown in Fig. 1[10, 11]. When a polarized neutron in the X−Y plane is incident on the multilayer, $+1/2$ spin component of the neutron is reflected by the magnetic mirror on the top side and $-1/2$ spin component is reflected by the non magnetic mirror on the back side. The phase difference between the two spin states is produced by the gap layer and given by,

$$\phi = 4\pi \, \mathrm{D}\sin\theta / \lambda . \tag{2}$$

The above description means that the multilayer spin splitter could be an another spin precession device and the non magnetic gap layer of the multilayer spin splitter gives rise to neutron spin quantum precession, which depends on the gap layer thickness, the neutron incident angle and the neutron wavelength.

3 Performance tests on multilayer spin splitters.

Performance tests of the multilayer spin splitter were made with a new spin interferometer[17]. The spin interferometer is analogous optically to a spin echo system with vertical precession field. The interferometer has a polarizer, two $\pi/2$−flippers, a π −flipper, two vertical precession field, a vertical guide field and an analyser, as shown in Fig. 2.

Polarized neutron parallel to the Z−axis is turned to the Y−axis by the first $\pi/2$−flipper. Then, neutron spin make precession in the X−Y plane in a vertical magnetic field produced by a guide coil and two precession coils. We measure the neutron spin precession angle using the second $\pi/2$−flipper and the analyser.

The spin interferometer has notable features different from conventional spin echo systems, as followings.

(a) Magnetic mirrors used in the interferometer function in very low magnetic field less than 10 gausses[18].
(b) Very low magnetic field is applied to the system and the spin precession in the system has very low rotation number. It allows us easy observations of the optics and interferometry in the interferometer.
(c) Neutron spin states are controllable by multilayer mirrors.
(d) A multilayer interferometer can be mounted in the system.

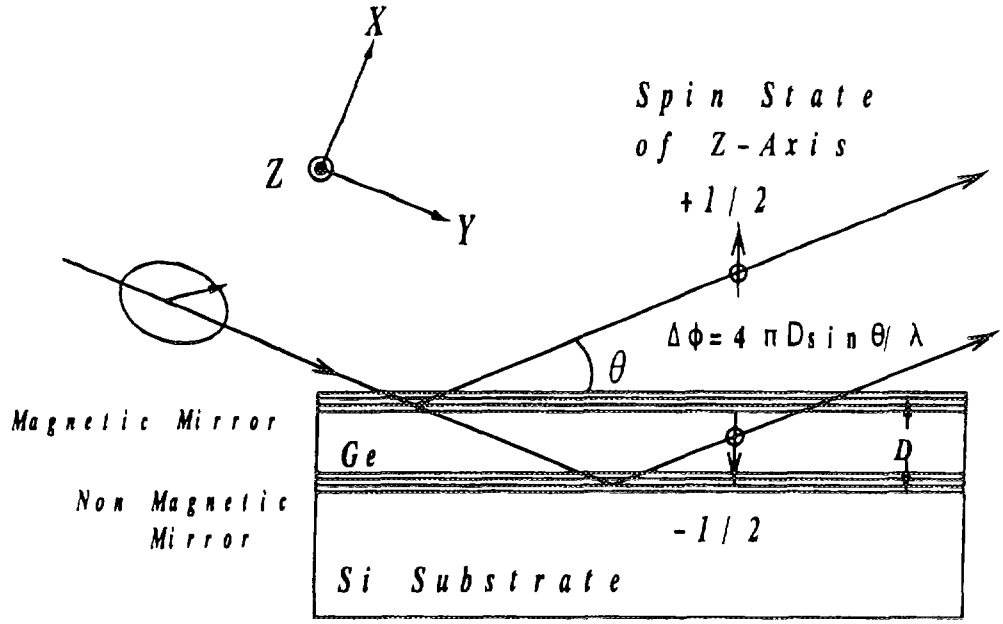

Fig. 1 Structure and principle of a multilayer spin splitter. The multilayer consists of a magnetic multilayer on top, followed by a gap layer and a non magnetic multilayer, which are deposited on a well-polished silicon substrate. The spin splitter produces coherent superposition of the two spin eigenstates with phase difference.

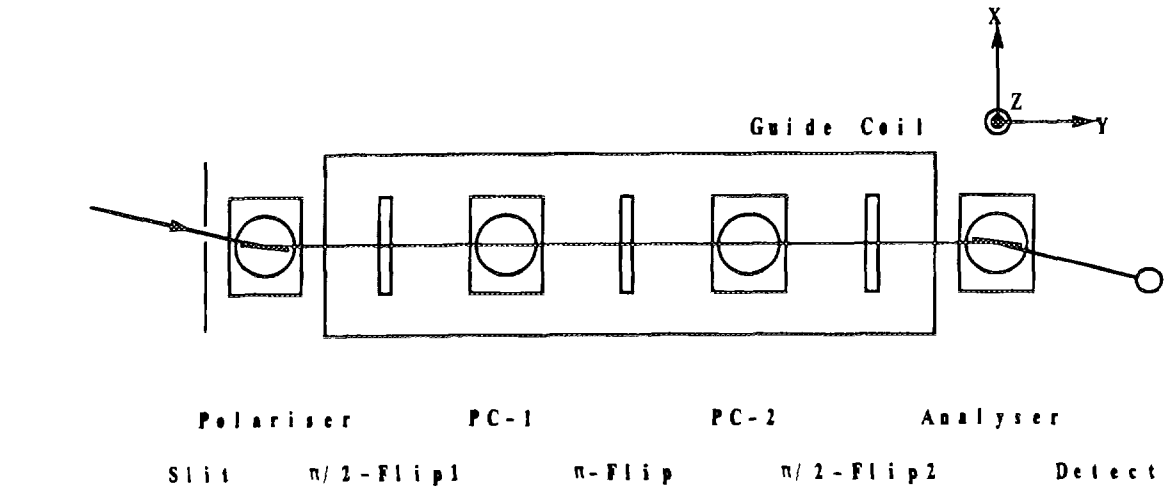

Fig. 2 Structure of a new spin interferometer. The interferometer is designed for cold neutron optics and spin interferometry using multilayer mirrors, which is analoguos optically to a spin echo quipment with vertical precession field. The two goniometer in the precession fields allow us to mount a multilayer interferometer and the magnetic field applied to the interferometer is much lower than that of a conventional spin echo system.

The first spin interferometer was set at Kyoto university research reactor in the last autumn. An another spin interferometer was installed in this February (1996) at JRR-3 reactor. The beam port for the interferometer at JRR-3 reactor is for cold neutron optics and interferometry[19]. Incident neutrons are monochromatized by four sequential Bragg reflections using four multilayer monochromators. The neutron wavelength is 12.6 A and the wavelength resolution is 3.5 %.

In order to make performance test of a multilayer spin splitter, we set it in the second precession coil. Firstly spin echo profiles were measured as function of current of the first precession coil PC-1, in order to find the current value of the best contrast.

Two multilayer spin splitters with effective gap thickness D of 3900 A and 7200 A. are prepared for performance tests. The multilayer spin splitters are deposited on well polished silicon substrates which are placed in magnetic field of about 100 gausses. The magnetic multilayer on top consists of 7 bilayers of 45-permalloy and germanium layers of 100 A thickness in the optical length, which function as a magnetic mirror in low magnetic field of 5 gausses. The non magnetic multilayer on the back side is a conventional Ni/Ti multilayer, which has the same optical design as the magnetic multilayer. The actual thicknesses of deposited layer are 152 A, 132 A, 108 A and 98 A for Pa layer, Ni layer, Ge layer and Ti layer, respectively, taking their refractive indices into account. The gap layer thicknesses of germanium are 2200 A and 5500 A for D of 3900 A and 7200 A, respectively. Their thickness is given by gap thickness added by half the total thickness of the two multilayers of the both sides.

Figure 3 shows measured spin echo profile for multilayer spin splitter with D=7200 A. The abscissa indicates the PC-1 current and the ordinate the neutron counts. The current of PC-2 is 4.5 amp. Spin echo condition for the magnetic Larmor precession is satisfied at PC-1 current=4.5 amp, where we can not observe any contrast of the spin echo profile. We, however, find out the contrast restored in lower current region of PC-1. The later experiments are made in the current region of PC-1 which gives a maximum contrast of the spin echo profiles. The measured profile shows that the system has the mechanism restoring contrast of the profile, which is related to the echo phenomena between phase difference and Larmor precession [20].

When we change the neutron incident angle θ of the multilayer spin splitter by $\Delta\theta$, the phase difference changes also. The change $\Delta\phi$ is given by the equation

$$\Delta\phi = 4\pi D\cos\theta\,(\Delta\theta/\lambda)$$
$$\Delta\phi = 4\pi D(\Delta\theta/\lambda) \qquad (3)$$

$\Delta\phi$ is equal to the change of neutron spin precession angle, which brings the shift of the measured spin echo profile. Goal of performance test is that we demonstrate experimentally whether or not the shift of the spin echo profile measured for angle displacement $\Delta\theta$ corresponds to the change of the phase difference $\Delta\phi$ by the angle displacement.

Typical measured spin echo profiles for the spin splitter of D=3900 A are shown in Fig. 4 together with fitted curves for sequential angle displacements of 0.03 deg step. The abscissa is the current of PC-1 precession coils. The solid line indicates the

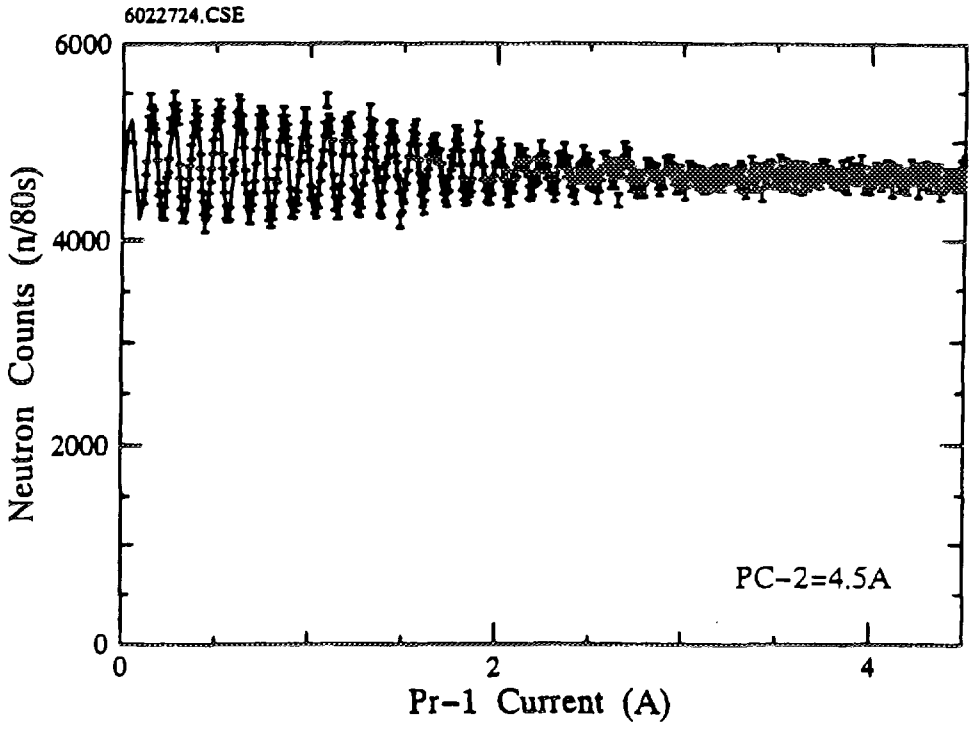

Fig. 3 Measured spin echo profile for a multilayer spin splitter with effective gap thickness of 7200 A. The data is taken as function of the current of the first precession coil PC-1 for the constant current of 4.5 amperes of the second precession coil PC-2. Some restoration of the profile contrast is observed in lower current side than that satisfying the echo condition for the magnetic Larmor precession.

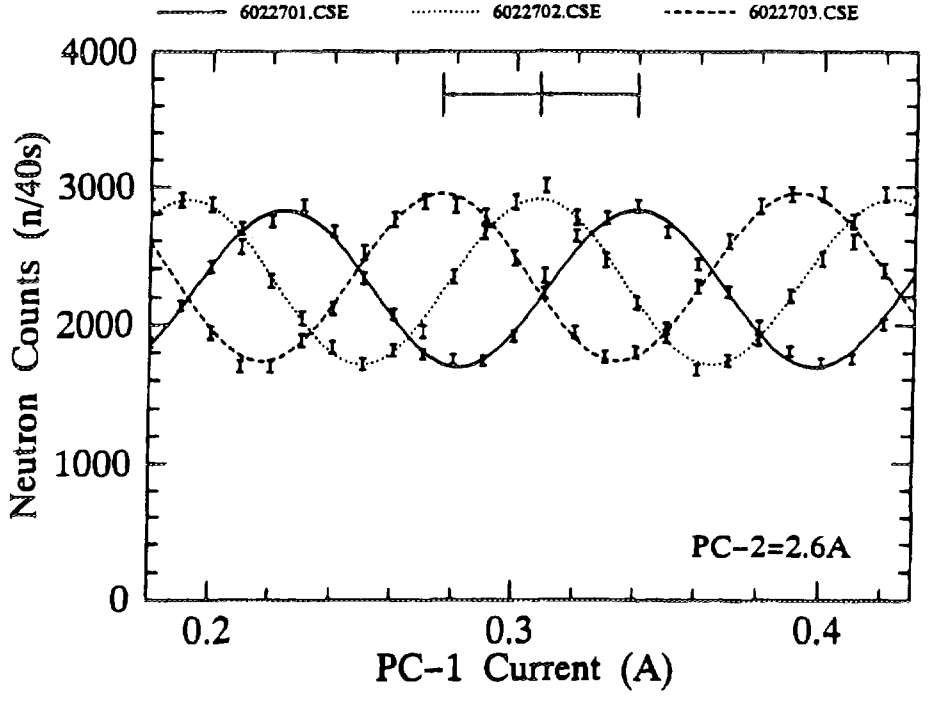

Fig. 4 Typical shifts of the spin echo profiles for D=3900 A measured for sequencial angle displacement of 0.03 deg. step. The data demonstrates that the spin echo profiles shift to low current side with large angle displacement as predicted from Eq. (3).

standard case without angle displacement. The dotted line is for an angle displacement of 0.03 deg, which shifts by 0.036 amp. to lower current side compared with the standard profile. The broken line for more angle displacement of 0.03deg, which shifts by more 0.033 amp. to lower current side compared with the dotted echo profile. The sequential shift of measured spin echo profiles demonstrate a good agreement with the prediction from Eq. 3 for the sequential angle displacements. The period 0.116 amp. of the profiles corresponds to neutron spin precession angle of 2π.

Measured data are summarized for two multilayer spin splitters in Fig 5[11]. The ordinate is measured shift of spin echo profiles and the abscissa is angle displacement. Solid line and broken line are the data for the two multilayer spin splitters with deposited effective gap thickness of 3900 A and 7200 A, respectively. The figure shows that the echo profile shifts is proportional to the angle displacements and the effective gap thickness with a good agreement with the quantum precession predicted from Eq. 3. This demonstrates that the quantum precession by a multilayer spin splitter is equivalent to the Larmor precession in a magnetic field.

4 Performance tests on a new phase-spin echo interferometer

When we arrange two identical spin splitters parallel each other in the two precession field as shown in Fig 6 (a), the system satisfies phase echo[21] and spin echo[22] simultaneously.

The simultaneous occurrence of the two echo phenomena is illustrated in Fig. 6 (b)[10]. A polarized neutron in the X-Yplane split into the two spin states of the Z-axis with a phase difference by the first spin splitter. The π -flipper reverses two subbeams. The reversed subbeams are reflected and superposed by the second spin splitter. The neutron polarization status is restored completely by phase and spin echo phenomena after the second spin splitter. So, we call this system as phase-spin echo interferometer. The measured spin echo profile for the interferometer is shown in Fig. 7 for D=7200 A. Comparison of Fig. 7 and Fig. 4 demonstrates considerable improvement of the contrast of spin echo profiles by the simultaneous occurrence of phase echo and spin echo.

We propose two application of phase-spin echo interferometer. One is the development of a high resolution spin echo system. Because phase difference of 1 mm gap thickness corresponds to the 10^5 rotations of spin precessions. Another is the development of a Jamin type cold neutron interferometer with variable subbeams separation, which is very useful for coherency study of neutron waves. It should be noted that it is not easy to develop a multilayer spin splitter with gap separation of 1 mm in width or variable width.

We would like to thank Prof. A. Masaike for stimulating discussions. This work was suported in part by the Inter-University Program for Common Use JAERI Facility and by the Commom Use Program for KUR Facility, and financially by the Grant in Aid for Scientific Research from the Ministry of Education, Science and Culture in Japan (Project number 04244103).

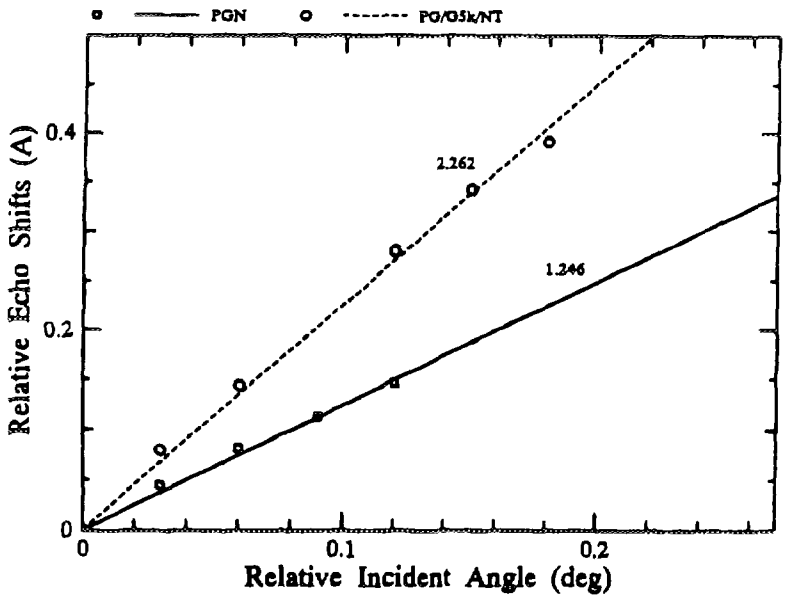

Fig. 5 Summurized data between angle displacement and measured shift of the spin echo profiles. Solid and broken lines are the data for the multilayer spin splitter with effective gap thickness of 3900 A and 7200 A, respectively. These data shows that the graduents are related to the effective gap thicknesses and the quantum precessiones by angle displacement agree with the prediction from Eq. 3.

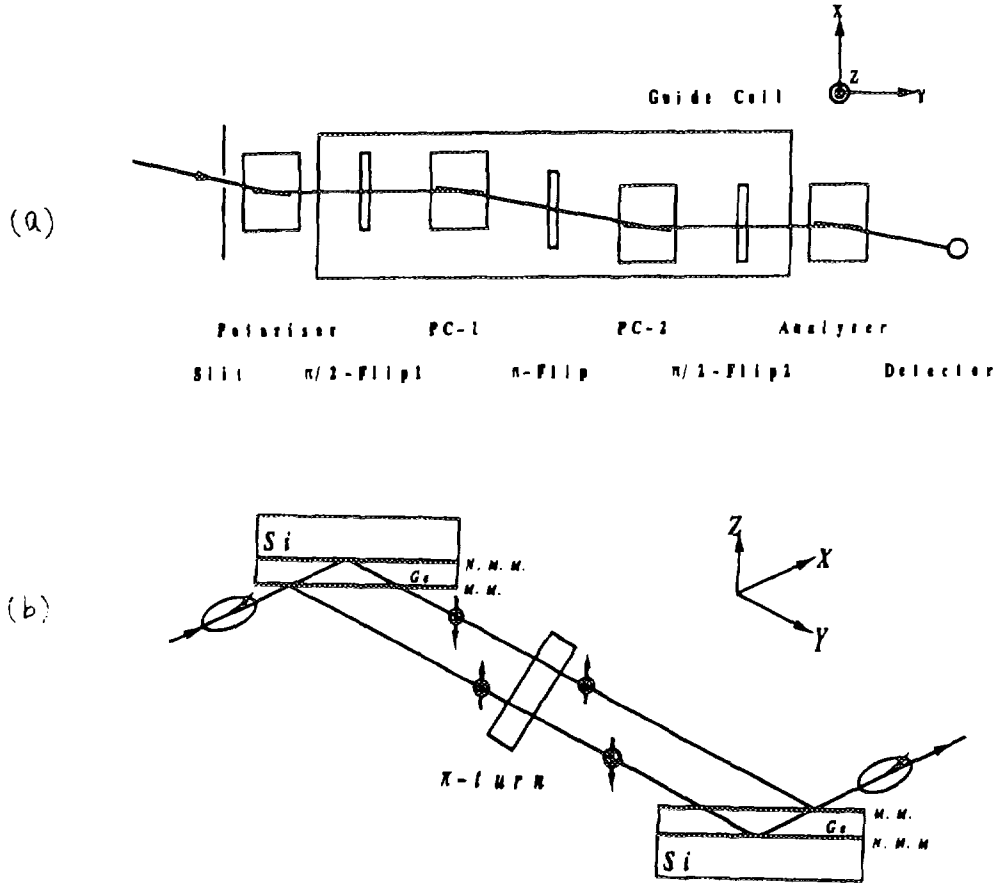

Fig. 6 (a) An arrangement of a phase-spin echo interferometer using two identical multilayer spin splitters. (b) Illustration of the simultaneous occurence of phase echo and spin echo phenomena. The phase echo requires a π -turn flipper as well as a pair of the identical multilayer spin splitters.

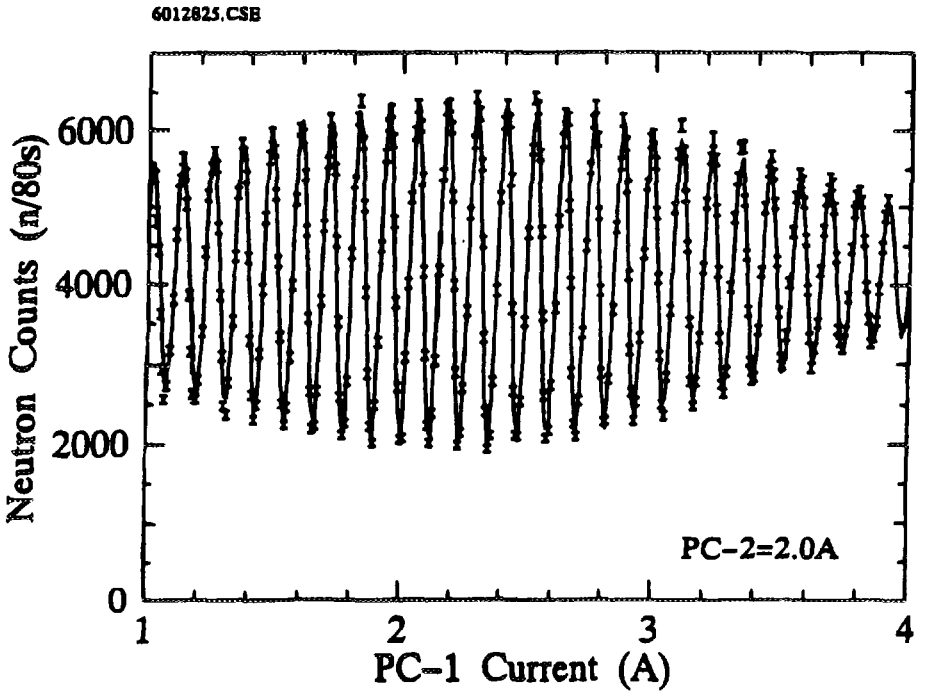

Fig. 7 Measured spin echo profile for a phase–spin echo interferometer with effective gap thickness of 7200 A. Contrast of the spin echo profiles are restored nearly perfectly by the simultaneous occurence of the phase and spin echo phenomana, compared with that in Fig. 4.

References

[1] S. Yamada, T. Ebisawa, N. Achiwa, T. Akiyoshi, S. Okamoto, Ann. Rep. Res. React. Inst. Kyoto University 11, 8(1978).

[2] T. Ebisawa, N. Achiwa, S. Yamada, T. Akiyoshi, S. Okamoto, J. Nucl. Sci. Technol. 16, 647(1979).

[3] T. Ebisawa, S. Tasaki, T. Kawai, T. Akiyoshi, M. Utsuro, Y. Otake, H. Funahashi, N. Achiwa, Nucl. Instr. and Meth. A, 344, 597(1994).

[4] F. Mezei, In "Imaging processes and Coherence in Physics", Edited by M. Schlenker et al., (Lecture Notes Series, Springer Verlag, Heidelberg, 1980) P. 283.

[5] V. g. Baryshevskii, S. V. Cherepitsa, A. L. Frank, Phys. Lett153, 299(1991).

[6] M. Hino, N. Achiwa, S. Tasaki, T. Ebisawa, T. Akiyoshi, Physica B 213&214, 957 (1995).

[7] M. Hino, Doctor thesis(1996), Kyushu Univ.

[8] N. Achiwa, M. Hino, S. Tasaki, T. Ebisawa, T. Akiyoshi, T. Kawai, proceedings of NOK 96.

[9] M. Hino, N. Achiwa, S. Tasaki, T. Ebisawa, T. Akiyoshi, T. Kawai, proceedings of NOK 96.

[10] T. Ebisawa, H. Funahashi, S. Tasaki, Y. Otake, T. Kawai, M. Hino, N. Achiwa, T. Akiyoshi, J. Neutron Research (in press).

[11] T. Ebisawa, S. Tasaki, T. Kawai, N. Achiwa, M. Hino, Y. Otake, H. Funahashi, T. Akiyoshi, proceedings of NOK 96.

[12] E. P. Wigner, Am. J. Phys., 31, 6(1963).

[13] A. Zeilinger, Z. Phys., B25, 97(1976).

[14] A. Zeilinger, Neutron interferometry, edited by U. Bonse and H. Rauch (Clarendon, Oxford, (1979) 241.

[15] J. Summhammer, G. Badurek, H. Rauch, U. Kischko, Phys. Lett. 90A, 110(1982).

[16] J. Summhammer, G. Badurek, H. Rauch, U. Kischko, A. Zeilinger, Phys. Rev. A 27, 2523(1983).

[17] S. Tasaki, T. Ebisawa, T. Kawai, N. Achiwa, M. Hino, Y. Otake, H. Funahashi, T. Akiyoshi, proceedings of NOK 96.

[18] T. Kawai, T. Ebisawa, S. Tasaki, Y. Eguchi, M. Hino, N. Achiwa, J. Neutron Research (in press)

[19] T. Ebisawa, S. Tasaki, Y. Otake, H. Funahashi, S. Soyama, N. Torikai, Y. Matsushita, Physica B, 213&214, 901(1995).

[20] T. Ebisawa, S. Tasaki, T. Kawai, M. Hino, N. Achiwa, Y. Otake, H. Funahashi, T. Akiyoshi, to be published.

[21] H. Funahashi, T. Ebisawa, T. Haseyama, M. Hino, A. Masaike, Y. Otake, T. Tabaru, S. Tasaki, Phys. Rev A, (in press).

[22] F. Mezei, Z. Phys., 255, 146(1972).

Perfect Crystal Interferometer and its Applications

Yuji HASEGAWA

Atominstitu der Österreichischen Universitäten,
Schüttelstraße 115, A-1020 Wien, AUSTRIA

1. Perfect crystal interferometer for x-rays and neutrons

1.1. X-Ray and Neutron Interferometer

Interferometry with wavelengths on the angstrom scale has developed quite steadily. First experimental success was reported in 1965 by Bonse and Hart[1,2]. There, successive Laue case diffractions were used for the beam handling, i.e., splitting, reflecting and recombining, hence it is conventionally called LLL-interferometer. Other types of the interferometer were investigated as well, e.g., BBB(triple-Bragg)[3], LL(double-Laue)[4] and BB(double-Bragg)[5]. Among them, LLL-interferometer is widely used. A skew-symmetric LLL interferometer come to be utilized recently for the advantage of the large space where the samples are inserted[6].

The advent of the x-ray interferometer stimulated new investigations, in the field of fundamental and applied physics. For instance, an extremely high sensitivity of the interferometer made it possible to measure the lattice constant with high precision[7]. The precise measurements on the anomalous dispersion correction were achieved with the use of a synchrotron radiation[8] or multiple-wavelength technique[9]. After that, the x-ray interferometry has been used only for the additional means for the alignment or the referenced observation of the system. The rapid recent development of the synchrotron radiation will bring a new flavor in the x-ray interferometry.

The first neutron interferometry was achieved in 1962 by Maier-Leibnitz et al.[10]. The beam separation in this interferometer, however, was not large enough and it was not suitable for the further experiments. A new type of the neutron interferometer was constructed with a perfect crystal and experimentally performed in 1974 by Rauch et al.[11]. It has stimulated a great deal of new investigations, more or less in the more fundamental and more applied physics. The following investigations with

LLL neutron interferometer were performed; precise measurements on the scattering length[12], the gravitational effects[13], coherence[14-15], Fizeau effects[16], Spin-superposition[17], complementarity[18], and post-selection effects[19].

A number of excellent articles of the interferometer with perfect crystal were already published, e.g., first ten years of the x-ray interferometer[20], first collective book on neutron interferometry[21], neutron interferometer[22], recent proceedings of "Matter Wave Interferometry"[23].

1.2. Double-Slit Experiment

Since the early stage of quantum physics, the double-slit experiment has served as the example of the epistemologically strange features of quantum phenomena. Feynman stated on this situation that the double-slit experiment is a phenomenon "which has in it the heart of quantum mechanics; in reality it contains the *only* mystery" of the theory[24]. In the double-slit experiments, the complementarity of the path (particle) and the interference (wave) is seen very clearly.

At the fifth Solvey Congress, Einstein proposed a modified version of the double-slit experiment, where, he proposed, one could determine the path of each photon by measuring the momentum transfer without destroying the interference pattern[25]. In his reply, Bohr demonstrated that a certain change of momentum necessarily destroys the interference pattern. This is equivalent to the Heisenberg's indeterminacy relation, which is well known with γ-ray spectroscopy[26]. More recently, Wootters and Zurek showed that intermediate cases are possible, where inaccurate determinations still retain the interference pattern with considerable contrast[27].

The complementarity lies in the core of quantum mechanics. To interpret this, Bohr stated "no elementary phenomenon is a phenomenon until it is a registered phenomenon[28]." This stimulated Wheeler and he proposed a new idea of the delayed-choice experiment. In his article, he presented the smoky dragon which symbolizes the fact that we can only get a counter reading without the right how it comes. This shows one epistemological interpretation of quantum mechanics. Some people are not satisfied with this yet and, with a recent development of the

experimental technique, the interpretation (or the reality) of quantum mechanics is still under hot discussions.

2. Time-delayed interferometry with x-ray cavity

2.1. Time-Delayed Interferometry with Nuclear Resonant Scattering of Synchrotron Radiation[29]

Interference of two beams resonantly scattered in an X-ray interferometer has been demonstrated. The interference arises between the beams emitted by different nuclei with some time interval. High visibility interference oscillations show the coherent superpositions, as well as the complete coincidence of these beams in the time domain.

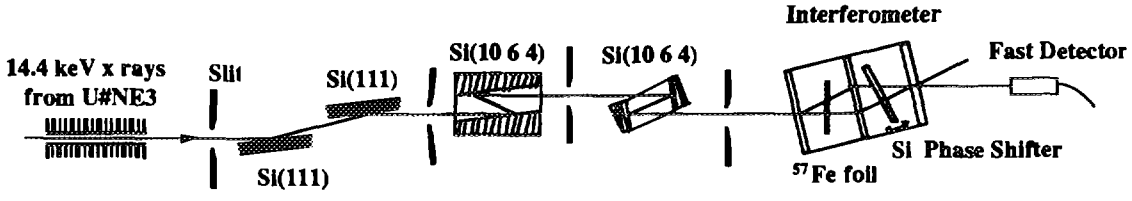

Experimental setup

2.2. Phase transfer in time-delayed interferometry with nuclear resonant scattering[30]

In an interferometry accompanying nuclear resonant scattering with some time-delay, interference was observed on the condition that a phase shifter was set in front of a nuclear scatterer. The observed interference pattern clarified that the phase information is transferred to the re-emitted beam through the intermediate state in nuclear resonance. A storing of phase information in time-delayed scattering is discussed in the system consisting of quantized radiation field combined with nucleus state.

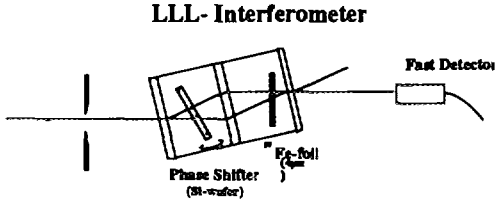

Experimental setup

3. Geometric phase in coupled neutron interference loops[31]

A geometric phase factor is derived for a split-beam experiment as an example of cyclic evolutions. Poincaré sphere descriptions for the split-beam experiment show its geometric property. We observe this geometric phase with a two-loop neutron interferometer, where a reference beam can be added to the beam from one interference loop. The combination of phase shifters and partial absorbers permitted the compensation of the dynamical phase and measurement of the geometric phase. All the experimental results show complete agreement with our theoretical treatment. We discuss a situation where a geometric phase exists even when the dynamical phase becomes zero.

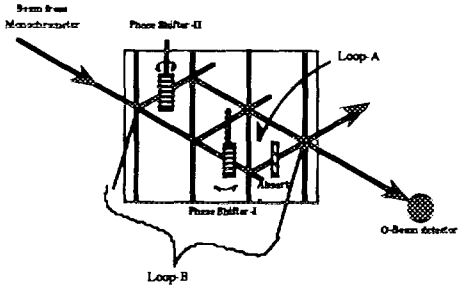

Experimental setup

Acknowledgments

The author would like to thank Prof. S. Kikuta, the university of Tokyo, and all the colleagues at the university of Tokyo and the Photon factory KEK, for the help to accomplish the time-delayed interferometries. He is also grateful to Prof. H. Rauch and Dr. M. Zawisky, Atominstitut der Österreichschen Universitäten, as well as Dr. A. Ioffe, BENSC Hahn-Meitner Institut, with whom the geometric phase measurements were done.

References

[1] U.Bonse, and M.Hart: Appl. Phys. Lett. **6** (1965) 155.

[2] U.Bonse, and M.Hart: Z. Phys. **188** (1965) 154.

[3] U.Bonse, and M.Hart: Z. Phys. **194** (1966) 1.

[4] A.Zeilinger, C.G.Shull, M.A.Horne, and G.L.Squires: in Neutron Interferometry, U.Bonse and H.Rauch eds. (Oxford Univ. Press, London, 1979), p.48.

[5] A.Zeilinger, C.G.Shull, J.Arther, and M.A.Horne: Phys. Rev. **A28** (1983) 487.

[6] W.Bauspiess, U.Bonse, and H.Rauch: Nucl. Instr. Meth. **157** (1987) 495.

[7] P.Becker, K.Dorenwendt, G.Ebeling, R.Lauer, W.Lucas, R.Probst, H.-J.Rademacher, G.Reim, P.Seyfried, and H.Siegert: Phys. Rev. Lett. **46** (1981) 1540.
[8] U.Bonse, and G.Materlik: Acta. Crystallogr. **A31** (1975) 232.
[9] M.Hart, and D.P.Siddons: Proc. R. Soc. London **A376** (1981) 465.
[10] H.Maier-Leibnitz, and T.Springer: Z. Phys. **167** (1962) 386.
[11] H.Rauch, W.Treimer, and U.Bonse: Phys. Lett. **A47** (1974) 369.
[12] W.Bauspiess, U.Bonse, and H.Rauch: Nucl. Instr. Meth. **157** (1978) 495.
[13] R.Colella, A.W.Overhauser, and S.A.Werner: Phys. Rev. Lett. **34** (1975) 1472.
[14] H.Rauch: in *Neutron Interferometry*, U.Bonse and H.Rauch eds. (Oxford Univ. Press, London, 1979), p.161.
[15] H.Kaiser, S.A.Werner, and E.G.George: Phys. Rev. Lett. **50** (1983) 560.
[16] M.Arif, H.Kaiser, S.A.Werner, A.Cimmino, W.A.Hamilton, A.G.Klein, and G.I.Opat: Phys. Rev. **A31** (1985) 1203.
[17] J.Summhammer, G.Badurek, H.Rauch, U.Kischko, and A.Zeilinger: Phys. Rev. **A27** (1983) 2523.
[18] H.Rauch and J.Summhammer: Phys. Lett. **A104** (1984) 44.
[19] S.A.Werner, R.Clothier, H.Kaiser, H.Rauch and H.Wölwitsch: Phys. Rev. Lett. **67** (1991) 683.
[20] M.Hart: Proc. R. Soc. **A346** (1975) 1.
[21] U.Bonse and H.Rauch (Eds.): *Neutron Interferometry*, (Oxford Univ. Press, London, 1979).
[22] A.G.Klein, S.A.Werner: Rep. Progr. Phys. **46** (1983) 259.
[23] G.Badurek, H.Rauch and A.Zeilinger (Eds.): "Matter Wave Interferometry" Physica **B151** (1988).
[24] R.P.Feynman, R.B.Leighton, and M.Sands: *The Feynman Lecture on Physics* (Wesley, Reading, Mass., 1965) Vol.3 p.1.
[25] N.Bohr: In *Arbert Einstein, Philosopher-Scientist*, P.A.Schilipp Ed. The Library of Living Philosophers (Evaston, Illinois, 1949) p.200-.
[26] W.Heisenberg: Z. Phys. **43**(1927)172 (English translation. 1983. In *Quantum Theory and Measurement*. J.A.Wheeler & W.H.Zurek, eds. Princeton Univ. Press.).
[27] W.K.Wootters, and W.H.Zurek: Phys. Rev. **D19** (1979) 473.
[28] W.A.Miller, and J.A.Wheeler: Proc. Int. Symp. Foundation of Quantum Mechanics, Tokyo, 1983, p.140.
[29] Y.Hasegawa, Y.Yoda, K.Izumi, T.Ishikawa, S.Kikuta, X.W.Zhang, H.Sugiyama, M.Ando: Jpn. J. Appl. Phys. **33** (1994) L772.
[30] Y.Hasegawa, Y.Yoda, K.Izumi, T.Ishikawa, S.Kikuta, X.W.Zhang, M.Ando: Phys. Rev. Lett. **75** (1995) 2216.
[31] Y.Hasegawa, M.Zawisky, H.Rauch, and A.Ioffe: Phys. Rev. **A53** (1996) 2486.

List of Participants

Name	Affiliation
V. K. IGNATOVICH	Dubna
Y. HASEGAWA	Wien
A. IOFFE	Hahn-Meitner
S. J. SEESTROM	Los Alamos
R. GAEHLER	Munchen
S. A. WERNER	Missouri
A. P. SEREBROV	Gatchina
E. GRAVADOR	Ibaraki Univ.
V.W. Hughes	Yale University
K. Raum	Fakultat fur
T. ADACHI	KEK
N. AKIYAMA	Univ. of Tokyo
K. ASAHI	Tokyo Inst.Tech.
T. BABA	Tokyo Inst.Tech.
T. EBISAWA	KURRI
K. HAGIWARA	KEK
T. HASEYAMA	Kyoto Univ.
I. HIDEAKI	Tokyo Inst.Tech.
H. HIROTAKA	KEK
M. IINUMA	Kokyo Univ.
H. IKEDA	KEK
J. IMAZATO	KEK
S. ISHIMOTO	KEK
T. ITABASHI	RCNP
S. ITOH	KEK
I. KATAYAMA	INS
T. KII	Tokyo Inst.Tech.
T. KIKUCHI	Tokyo Inst.Tech.
T. KOBAYASHI	Tokyo Inst.Tech.
S. KUBONO	INS
J. MIYAZAWA	Tokyo Inst.Tech.
K. MORIMOTO	KEK
Y. NAGAI	Tokyo Inst.Tech.
H. OGAWA	Tokyo Inst.Tech.
F. OKAZAKI	Tokyo Inst.Tech.
S. ONO	Univ. of Tokyo
T. OTOMO	KEK
K. SAKAI	Tokyo Inst.Tech.
S. SAKAMOTO	UTMSL

Name	Affiliation
M. SAKUDA	KEK
H. SATOH	Tokyo Inst.Tech.
T. SHIBATA	INS
T. SHIMA	Tokyo Inst.Tech.
T. SUZUKI	Univ. of Tokyo
T. SUZUKI	KEK
T. TAKAHASHI	Tokyo Inst.Tech.
K. TAKEMURA	Univ. of Tokyo
S. TASAKI	Kyoto Univ.
I. YAMANE	KEK
Y. YAMAZAKI	KEK
S. YASUMI	Teikyo Univ.
H. YOSHIKI	Ibaraki Univ.
A. YOSHIMI	Tokyo Inst.Tech.